NUREG/CR-2911
ORNL/TM-8485

ornl

OAK RIDGE NATIONAL LABORATORY

UNION CARBIDE

Multirod Burst Test Program Progress Report for January–June 1982

Final Report

R. H. Chapman

Prepared for the U.S. Nuclear Regulatory Commission
Office of Nuclear Regulatory Research
Under Interagency Agreements DOE 40-551-75 and 40-552-75

OPERATED BY
UNION CARBIDE CORPORATION
FOR THE UNITED STATES
DEPARTMENT OF ENERGY

Printed in the United States of America. Available from
National Technical Information Service
U.S. Department of Commerce
5285 Port Royal Road, Springfield, Virginia 22161

Available from

GPO Sales Program
Division of Technical Information and Document Control
U.S. Nuclear Regulatory Commission
Washington, D.C. 20555

NUREG/CR-2911
ORNL/TM-8485
Dist. Category R3

Contract No. W-7405-eng-26

Engineering Technology Division

MULTIROD BURST TEST PROGRAM PROGRESS REPORT FOR JANUARY-JUNE 1982

Final Report

R. H. Chapman

Manuscript Completed - October 29, 1982
Date Published - December 1982

Prepared for the
U.S. Nuclear Regulatory Commission
Office of Nuclear Regulatory Research
Under Interagency Agreement DOE 40-551-75 and 40-552-75

NRC FIN No. B0120

Prepared by the
OAK RIDGE NATIONAL LABORATORY
Oak Ridge, Tennessee 37830
operated by
UNION CARBIDE CORPORATION
for the
DEPARTMENT OF ENERGY

CONTENTS

FOREWORD

This report summarizes progress and preliminary results of the Multirod Burst Test (MRBT) Program (sponsored by the Division of Accident Evaluation of the Nuclear Regulatory Commission) for the period January–June 1982.

Previous MRBT progress reports are:

NUREG Report No.	ORNL Report No.	Period covered
	ORNL/TM-4729	July–September 1974
	ORNL/TM-4805	October–December 1974
	ORNL/TM-4914	January–March 1975
	ORNL/TM-5021	April–June 1975
	ORNL/TM-5154	July–September 1975
	ORNL/NUREG/TM-10	October–December 1975
	ORNL/NUREG/TM-36	January–March 1976
	ORNL/NUREG/TM-74	April–June 1976
	ORNL/NUREG/TM-77	July–September 1976
	ORNL/NUREG/TM-95	October–December 1976
	ORNL/NUREG/TM-108	January–March 1977
	ORNL/NUREG/TM-135	April–June 1977
NUREG/CR-0103	ORNL/NUREG/TM-200	July–December 1977
NUREG/CR-0225	ORNL/NUREG/TM-217	January–March 1978
NUREG/CR-0398	ORNL/NUREG/TM-243	April–June 1978
NUREG/CR-0655	ORNL/NUREG/TM-297	July–December 1978
NUREG/CR-0817	ORNL/NUREG/TM-323	January–March 1979
NUREG/CR-1023	ORNL/NUREG/TM-351	April–June 1979
NUREG/CR-1450	ORNL/NUREG/TM-392	July–December 1979
NUREG/CR-1883	ORNL/NUREG/TM-426	January–June 1980
NUREG/CR-1919	ORNL/NUREG/TM-436	July–December 1980
NUREG/CR-2366, Vol. 1	ORNL/TM-8058	January–June 1981
NUREG/CR-2366, Vol. 2	ORNL/TM-8190	July–December 1981

Topical reports and papers pertaining to research and development carried out by this program are:

1. R. H. Chapman (comp.), *Characterization of Zircaloy-4 Tubing Procured for Fuel Cladding Research Programs*, ORNL/NUREG/TM-29 (July 1976).

2. W. E. Baucum and R. E. Dial, *An Apparatus for Spot Welding Sheathed Thermocouples to the Inside of Small-Diameter Tubes at Precise Locations*, ORNL/NUREG/TM-33 (August 1976).

3. W. A. Simpson, Jr., et al., *Infrared Inspection and Characterization of Fuel-Pin Simulators*, ORNL/NUREG/TM-55 (November 1976).

4. R. H. Chapman et al., *Effect of Creep Time and Heating Rate on Deformation of Zircaloy-4 Tubes Tested in Steam with Internal Heaters*, NUREG/CR-0343 (ORNL/NUREG/TM-245) (October 1978).

5. J. F. Mincey, *Steady-State Axial Pressure Losses Along the Exterior of Deformed Fuel Cladding: Multirod Burst Test (MRBT) Bundles B-1 and B-2*, NUREG/CR-1011 (ORNL/NUREG/TM-350) (January 1980).

6. R. W. McCulloch, P. T. Jacobs, and D. L. Clark, *Development of a Fabrication Procedure for the MRBT Fuel Simulator Based on the Use of Cold-Pressed Boron Nitride Preforms*, NUREG/CR-1111 (ORNL/NUREG/TM-362) (March 1980).

7. R. H. Chapman, J. V. Cathcart, and D. O. Hobson, "Status of Zircaloy Deformation and Oxidation Research at Oak Ridge National Laboratory," in *Proceedings of Specialists Meeting on the Behavior of Water Reactor Fuel Elements Under Accident Conditions, Spatind, Norway, September 13-16, 1976*, CSNI Report No. 13 (1977).

8. R. H. Chapman et al., "Zircaloy Cladding Deformation in a Steam Environment with Transient Heating," in *Proceedings of Fourth International Conference on Zirconium in the Nuclear Industry, Stratford-on-Avon, England, June 26-29, 1978*, ASTM STP 681 (1979).

9. R. T. Bailey, *Steady-State Pressure Losses for Multirod Burst Test (MRBT) Bundle B-5*, NUREG/CR-2597 (ORNL/Sub/80-40441/1) (April 1982).

10. R. L. Anderson, K. R. Carr, and T. G. Kollie, *Thermometry in the Multirod Burst Test Program*, NUREG/CR-2470 (ORNL/TM-8024) (March 1982).

11. A. W. Longest, J. L. Crowley, and R. H. Chapman, *Variations in Zircaloy-4 Cladding Deformation in Replicate LOCA Simulation Tests*, NUREG/CR-2810 (ORNL/TM-8413) (September 1982).

12. A. W. Longest, R. H. Chapman, and J. L. Crowley, "Boundary Effects on Zircaloy-4 Cladding Deformation in LOCA Simulation Tests," in *Trans. Am. Nucl. Soc.* 41, 383 (1982).

13. R. H. Chapman, J. L. Crowley, and A. W. Longest, "Effect of Bundle Size on Cladding Deformation in LOCA Simulation Tests," presented at *Sixth International Conference on Zirconium in the Nuclear Industry*, Vancouver (B.C.), Canada, June 28-July 1, 1982.

The following limited-distribution quick-look and data reports have been issued by this program:

1. R. H. Chapman (comp.), *Quick-look Report on MRBT No. 1 4 x 4 Bundle Burst Test*, Internal Report ORNL/MRBT-2 (September 1977).

2. R. H. Chapman (comp.), *Quick-look Report on MRBT No. 2 4 x 4 Bundle Burst Test*, Internal Report ORNL/MRBT-3 (November 1977).

3. R. H. Chapman, *Quick-look Report on MRBT No. 3 4 x 4 Bundle Burst Test*, Internal Report ORNL/MRBT-4 (August 1978).

4. R. H. Chapman, *Quick-look Report on MRBT B-4 (6 x 6) Bundle Test*, Internal Report, ORNL/MRBT-6 (February 1981).

5. R. H. Chapman et al., *Quick-look Report on MRBT B-5 (8 x 8) Bundle Test*, Internal Report ORNL/MRBT-5 (July 1980).

6. R. H. Chapman et al., *Quick-look Report on MRBT B-6 (8 x 8) Bundle Test*, Internal Report ORNL/MRBT-7 (January 1982).

7. R. H. Chapman et al., *Bundle B-1 Test Data*, ORNL/NUREG/TM-322 (June 1979).

8. R. H. Chapman et al., *Bundle B-2 Test Data*, ORNL/NUREG/TM-337 (August 1979).

9. R. H. Chapman et al., *Bundle B-3 Test Data*, ORNL/NUREG/TM-360 (January 1980).

SUMMARY

Major activities during this report period included the B-6 burst test and posttest examination of the test array, additional analysis of the B-5 test results, and reporting.

The primary objective of the B-6 test, the last test that will be conducted by this research program, was to investigate deformation behavior in a large test array in the alpha-plus-beta temperature range. Because the B-5 test, which was conducted under conditions conducive to large deformation and rod-to-rod interactions in the high-alpha temperature range, showed that both temperature uniformity and mechanical interactions have a significant effect on deformation behavior in large arrays, a secondary objective of the B-6 test was to determine, if possible, the relative importance of these two parameters. Also, because test conditions used in this program are generally considered to be conservative, the B-6 test results should provide an overestimate (larger magnitude) of the deformation that can be anticipated in most accidents with failures in the two-phase temperature range. Similarly, the B-5 results are believed to represent conservative (upper limit) deformation levels that can be expected for failures in the high-alpha temperature range. Consistent with these objectives, target test conditions of ~925°C burst temperature with a heating rate of 3 to 4°C/s were selected for the B-6 test.

The test was performed successfully on December 3, 1981. All 64 simulators were pressurized to the same initial level, heated at the same nominal rate, and burst. The bursts occurred in an extremely orderly manner (i.e., starting with the center simulators and progressing radially outward with time) because of the unusually uniform temperature conditions. The first burst occurred ~133.1 s after power-on, and the last one (a corner simulator) was ~58.9 s later. Electrical power was terminated 141.7 s after power-on or 8.6 s after the first tube burst; all 36 interior simulators burst before power was terminated. With respect to the 58.9-s time interval during which bursts were taking place, the last 43.5 s were associated with the last four (i.e., the four outside corner) bursts. Because of their higher heat losses, these simulators failed much later under near-isothermal creep conditions. The average burst temperature was ~931°C, and the bundle average heating rate during the time of deformation was 3.5°C/s.

Following posttest dimensional checks and photography to document the appearance, the array was cast in an epoxy matrix (flow characterization tests were not conducted) and sectioned at ~60 axial nodes. Enlarged (3X) photographs of the sections were digitized and processed to obtain detailed deformation data. Although final reduction of the digitized data is not yet complete, preliminary results are available. The burst strains ranged from 22 to 56% with an average of 30%, consistent with an average of 36% for three single-rod tests conducted earlier to aid definition of the B-6 test conditions. Volumetric expansion ranged from 17 to 33%, with an average of 24%.

Coolant channel flow area reduction was modest, with a maximum of ~39% for the entire 8 x 8 array, ~44% if based on the inner 6 x 6 array, and ~46% if based on the central 4 x 4 array.

Analysis of the B-5 test data continued during this report period. While this is a tedious process, it provides insight to and understanding of the data. In particular, the analysis indicated that (1) burst temperatures reported earlier were sometimes inconsistent with the observed deformation profiles and (2) some of the burst temperatures should be revised.

Previously, we assumed that the burst temperature must be equal to or greater than the maximum measured value at the time of burst. Our evaluation of the data indicates that this is not necessarily true in a bundle with extensive rod-to-rod interactions. The temperature distribution prior to and during the early phase of deformation may be more important in determining the burst location than the distribution at the time of burst. Because failure stress is a function of both local temperature and instantaneous strain (i.e., local stress), failure can occur at a site where the strain is high (because of its prior temperature history), and the temperature is lower than at another site where the temperature is higher but the strain is lower. The data were reevaluated, and the burst temperatures were revised accordingly; a new tabulation is included.

Noise spikes were noted in the thermocouple signals for a number of the sensors in the B-5 test. These spikes were caused by interference from one of the electrically heated temperature reference boxes used for cold junction compensation. Because erroneous temperatures would be obtained from these signals in computer analysis of the data, the spikes were removed, and a new engineering units data tape was produced for use in such analyses.

MULTIROD BURST TEST PROGRAM PROGRESS REPORT FOR JANUARY–JUNE 1982

Final Report

R. H. Chapman

ABSTRACT

The B-6 (8 x 8) array was tested, and posttest examination was completed; data reduction and analysis are in progress. Preliminary quick-look results are included in this report. All 64 rods were pressurized and burst. The average burst temperature was 931°C, and the bundle average heating rate was 3.5°C/s during the time of deformation. Preliminary results indicate burst strains ranged from 22 to 56%, with a bundle average of 30%.

Analysis of the B-5 test results continues to provide insight to the complexity of cladding deformation in bundles, particularly for conditions conducive to large deformation and rod-to-rod interactions. Additional analyses, including re-evaluation of burst temperatures, are included in this report.

The B-6 test concluded the experimental phase of this research program. Future activities will be concerned with analysis and evaluation of experimental data produced by this and other research programs.

---

1. INTRODUCTION

R. H. Chapman

The Multirod Burst Test (MRBT) Program was initiated in July 1974, as an experimental study to (1) delineate the deformation behavior of unirradiated Zircaloy cladding under conditions postulated for a large-break loss-of-coolant accident and (2) provide a data base for assessing the magnitude and distribution of geometric changes in the fuel rod cladding in a multirod array and the extent of flow-channel restriction that might result. Data have been obtained from single-rod and multirod experiments, both with and without electrical heating of the shroud surrounding the test arrays. The tests were designed to study possible effects of rod-to-rod interactions on ballooning and rupture behavior over a wide range of conditions. Program objectives have been realized, and no further tests will be performed.

Approximately 110 single-rod burst tests were conducted. In ~40% of the tests, the shroud surrounding the fuel pin simulator was electrically

heated so that the temperature difference between shroud and simulator was near zero throughout the heating transients. In this mode of testing, deformation is greater than for unheated shroud tests. Also, the single-rod heated shroud results are in substantial agreement with results from bundle tests (with negligible rod-to-rod interactions) at comparable conditions.

Six bundle tests were also performed; three (B-1, B-2, and B-3) of these were with 4 x 4 arrays. Results and interpretations of these three tests were reported[1-6] as the information became available. Data reports[7-9] giving detailed results of the tests and a topical report[10] interpreting flow tests on two of the bundles have also been published. (All published reports and papers pertaining to this research program are listed in the Foreword of this report.) One test (B-4) was conducted on a 6 x 6 array, and a revised version of the quick-look report was included in a previous report.[11] Two tests (B-5 and B-6) were conducted with 8 x 8 arrays. Preliminary results of the B-5 test, which was performed under conditions conducive to large deformation and rod-to-rod mechanical interactions, have been published;[11-13] additional results are included in this report. A series of flow characterization tests was conducted on the B-5 and an undeformed reference bundle, and a data report has been published.[14] Preliminary results of the B-6 test are included in this report.

Both the single-rod and bundle tests have shown that local temperature gradients have a marked effect on the deformation behavior of alpha-phase Zircaloy; the more uniform the temperature distribution, the greater (and more uniform) is the deformation. Also, rod-to-rod mechanical interactions have a significant influence on deformation. We concluded from these tests that deformation depends not only on the inherent metallurgical properties of Zircaloy, but also on rod-to-rod mechanical interactions and all factors that determine the temperature gradients, including the method and uniformity of heating, uniformity of the initial temperature distribution, heating rate, heat losses to coolant and surroundings, and axial distribution of heat losses. Essentially all of our tests have been conducted at relatively low steam-flow rates (i.e., at a Reynolds number of $\lesssim$800), and heat losses to the steam coolant have been small but are still an important factor to consider.

During this report period, we placed special emphasis on (1) evaluation of quick-look results and posttest examination of the B-6 test and (2) further evaluation of B-5 test results. These activities and others are summarized in this report.

This is the last progress report that will be published by this program. Evaluation and publication of the data, including detailed data reports of the B-4, B-5, and B-6 tests and final interpretative reports, are planned to continue under another program.

2. PROGRAM PLANS AND ANALYSIS

2.1 Programmatic Activities

R. H. Chapman

Major activities during this report period were concerned with (1) evaluation and publication of quick-look results of the B-6 test, (2) posttest examination of the B-6 array, (3) further evaluation of the B-5 test results, and (4) preparation of reports.

The previous report period ended during final pretest checkout operations for the B-6 test. The test was successfully performed on December 3, 1981. Quick-look results were compiled and published[15] (with limited distribution) in January. Following photographic documentation, the bundle was cast in an epoxy matrix and sectioned at ~60 axial positions to obtain detailed deformation measurements. These data have been processed to obtain preliminary estimates of the strain in each tube at each axial node. A revised version of the quick-look report[15] and preliminary posttest examination results are presented in a later section.

The B-5 test continues to provide insight into the complexity of cladding deformation in bundles, particularly for conditions conducive to large deformation and rod-to-rod interactions. Further evaluation of the B-5 results has resulted in revision of the burst temperatures as will be discussed in a later section.

Reporting activities received considerable emphasis this period. The B-6 quick-look test results,[15] the B-5 flow test data,[14] and a report[16] on MRBT thermometry techniques and associated accuracies were published. A topical report[17] on statistical variations in cladding deformation, based on five replicate single-rod heated shroud tests, was prepared. Two papers[18,19] comparing different aspects of the B-3 and B-5 tests were presented at technical society meetings.

2.2 Revised Burst Temperature Correlation

In the early phase of our research, the shroud surrounding the single-rod test simulators was not electrically heated. Prior to the test transient, the entire test assembly was equilibrated at the initial temperature condition of ~340°C. The shroud remained at approximately this temperature throughout the transient and became an effective sink, causing heat losses from the fuel rod simulator to be greater than if it were surrounded by similarly heated simulators. The high heat losses enhanced azimuthal temperature gradients in the cladding. Although it was not recognized immediately, the net effect was to localize cladding strain and cause failure at a lower total circumferential elongation than would be the case for a uniform azimuthal temperature distribution. After adding a capability for electrically heating the shroud and controlling its temperature (through a feedback control loop) to essentially the same level as the cladding, the burst temperature was, in general, underpredicted by the correlation[20] derived earlier (and used by Powers and Meyer[21]) from single-rod unheated shroud test data.

Upon completion of the single-rod heated shroud tests during the previous report period, we had accumulated sufficient 10°C/s heating rate data to permit derivation of a similar correlation over a limited temperature range for these specific conditions. Preliminary data presented earlier[6,12,17,22] for these conditions were reevaluated with respect to burst temperatures and pressures to obtain a consistent data set on which to base the revised correlation. The reevaluated data, given in Tables 1 and 2, can be correlated over the limited temperature range with the equation (obtained by a nonlinear least-squares regression analysis)

$$T = 4026 - 0.02388P + \frac{10{,}000P}{97.90 + 3.296P} ,$$

where T is the cladding temperature (°C) and P is the pressure (kPa) at the time of burst. Figure 1 compares the equation with the data and with the correlation[20] derived from our unheated shroud test data. As evident, the heated shroud correlation predicts burst temperatures over the range of the data about 20 to 40°C higher than the unheated shroud correlation.

2.3 Preliminary Results of B-6 Test

Introduction

The B-6 test, the last test that will be conducted by this research program, was performed on December 3, 1981, and a quick-look report was published[15] (with limited distribution). Updated quick-look data and preliminary posttest examination results are presented in this section.

The primary objective of the B-6 test was to investigate deformation behavior in a large array in the alpha-plus-beta Zircaloy temperature range. Single-rod burst tests have shown that deformation is rather insensitive to heating rate in this temperature range and that the magnitude of the deformation is considerably less than observed in the high-alpha and low-beta temperature ranges. Consistent with the objectives and these observations, target test conditions of ~925°C burst temperature with a heating rate of 3-4°C/s were selected for the test. These conditions are representative of those frequently predicted by LOCA licensing calculations for a range of PWR accident conditions.

Because test conditions used in this program are generally considered to be conservative, the B-6 test results are believed to provide an overestimate (larger magnitude) of the deformation that can be anticipated in most accidents with failures in this temperature range. Similarly, the results of the B-5 test are believed to be a reasonable upper limit of the deformation that can be expected in the high-alpha temperature range.

Results[18,19] of the B-5 test, which was conducted under conditions conducive to large deformation, showed that temperature uniformity and rod-to-rod mechanical interactions (resulting from large deformation and lateral restraint in a large test array) have a significant effect on deformation behavior in large arrays. Therefore, a second objective was

Table 1. Test conditions of single-rod tests in steam

Test No.	Fuel simulator No.	Heating rate[a] (K/s)		Simulator linear power rating[a] (kW/m)	Inlet steam Reynolds number	Remarks
		Simulator	Shroud			
SR-50	MNL-009	10	10	3.5	760	α + β test; constant heating rate control
SR-52	MNL-085	10	10	3.4	745	High α test; constant power control
SR-59	MNL-043	10	10	4.0	340	α + β test with grids; constant heating rate control
SR-72	SEMCO-048	10	10	3.5	340	B-3 rod 6 simulation; constant power control
SR-73	SEMCO-044	10	10	3.5	350	B-3 rod 12 simulation; constant power control
SR-76	MNL-009	10	10	2.0	345	β test; constant heating rate control
SR-81	MNL-046	10	10	2.5	335	β test with grids; constant power control
SR-86	MNL-056	9.4	10	3.4	330	Replicate of B-5 test; constant power control
SR-87	MNL-056	9.8	10.1	3.7	330	Replicate of SR-86 test
SR-88	MNL-056	10.6	10.9	3.7	335	Replicate of SR-86 test
SR-89	MNL-056	10.6	10.7	3.8	320	Replicate of SR-86 test
SR-90	MNL-056	10.8	11.1	3.7	325	Replicate of SR-86

[a]Average during deformation.

Table 2. Summary of results of single-rod tests in steam

Test No.	FPS gas volume[a] (cm³)	Initial conditions		Maximum pressure (kPa)	Burst conditions				Time from power-on to burst (s)	Burst strain (%)	Tube heated length change (%)	
		Temperature (°C)	Pressure (kPa)		Pressure (kPa)	Temperature[b] (°C)	TE No.	TE position relative to tube burst			Volume	Length
SR-50	51.0	350	5,315	5,580	4,555	898	208	60 mm above, 150° around	56.70	56	40.3	0.4
SR-52	51.3	352	11,505	11,970	9,865	761	203	103 mm below, 135° around	40.90	49	37.3	−2.4
SR-59	49.0	353	2,920	3,095	2,860	961	206	22 mm above, 65° around	59.95	45	15.3	−1.6
SR-72	51.2	346	11,585	12,020	9,430	780	213	365 mm above, 10° around	42 70	57	46.1	−3.0
SR-73	49.4	349	11,590	12,020	9,940	755	203	185 mm below, 110° around	40.70	51	37.0	−2.5
SR-76	51.7	342	1,675	1,790	1,545	1,005	203	70 mm below, 45° around	65.35	81	30.8	0.4
SR-81	50.0	338	1,325	1,405	1,200	1,040	212	57 mm above, 45° around	90.40	58	30.8	0.7
SR-86	50.7	346	11,580	12,080	9,405	779	211	25 mm below, 40° around	40.02	72	51.1	−3.7
SR-87	50.9	351	11,580	12,060	9,870	767	207	26 mm above, 55° around	37.80	50	39.3	−2.3
SR-88	50.8	349	11,580	12,080	9,610	774	208	27 mm above, 65° around	37.49	89	46.2	−3.1
SR-89	50.9	351	11,550	12,030	9,560	779	211	211 mm below, 45° around	37.03	62	45.9	−3.0
SR-90	50.5	349	11,570	12,060	9,545	770	206	82 mm below, 105° around	37.18	96	47.7	−3.0

[a] Fuel pin simulator (FPS) volume measured at room temperature; includes pressure transducer and connecting tube.

[b] Maximum measured by any thermocouple at time of burst; thermocouple number and location indicating burst are listed.

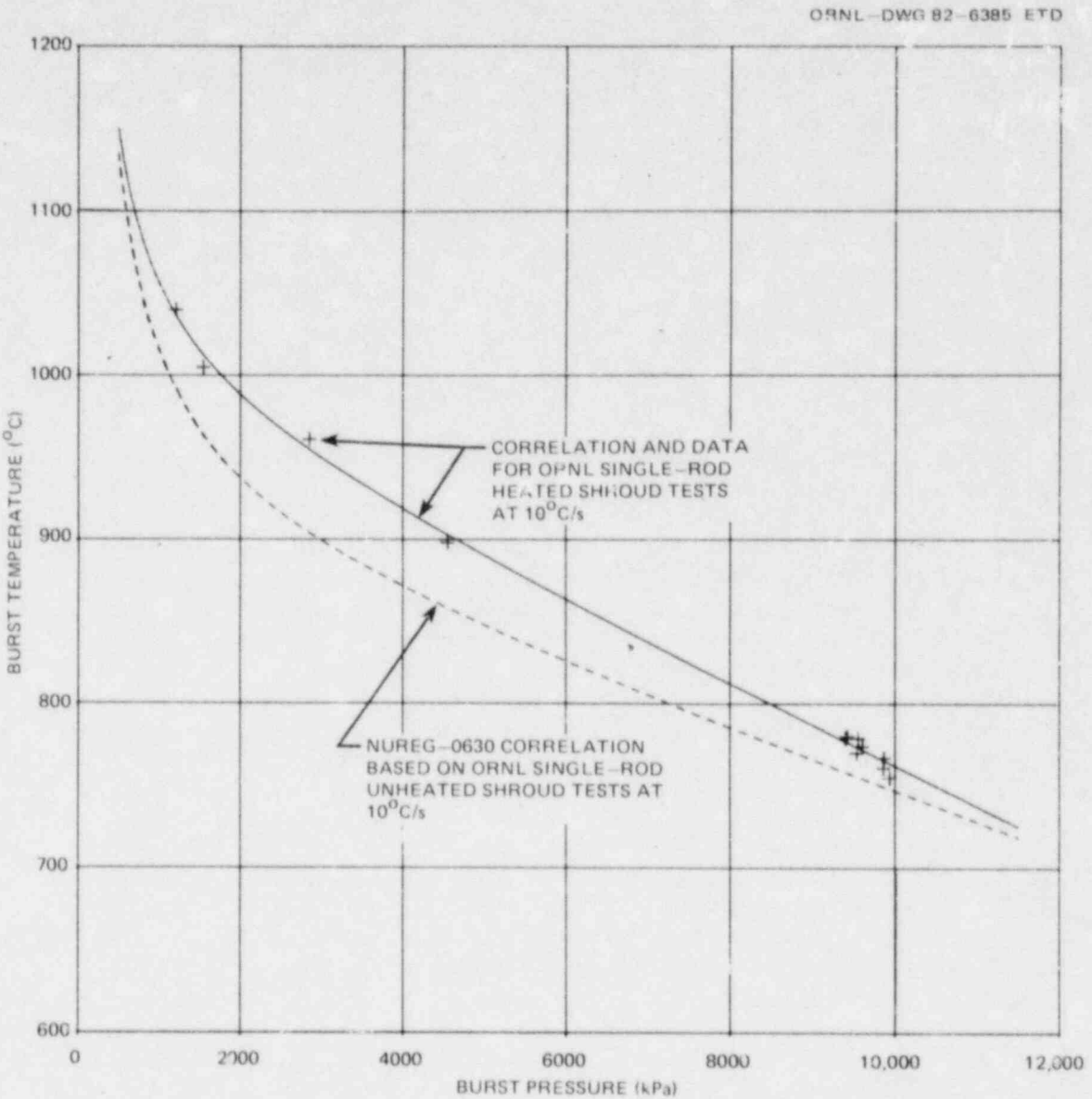

Fig. 1. Comparison of correlations based on ORNL heated and unheated shroud test data at 10°C/s.

to determine, if possible, the relative importance of these two parameters. Analysis of the test results should permit this determination because rod-to-rod interactions were relatively nonexistent in the test.

Figure 2 shows a simplified drawing of the test assembly. As indicated in Sect. A A of the figure, the shroud was constructed of thin (0.13-mm-thick) stainless steel with a highly reflective, gold-plated surface. It was backed by insulating material and strong structural supporting members to withstand radial forces during the test transient. The thin shroud was spaced one-half of a coolant channel thickness away from the outer rod surfaces; this spacing permitted some deformation of these simulators, while constraining them from moving radially outward. However, the close spacing precluded electrically heating the shroud. This design concept is the same as that used earlier in the B-4 and B-5 tests.[11,12]

The steam inlet configuration (above the upper end of the bundle heated zone) was modified from a single-entry nozzle as used in the B-5 test to a double-entry arrangement as shown in Sect. B-B of Fig. 2. This modification, combined with reduced heat losses from the top of the test vessel, eliminated the temperature gradient problems experienced in the B-5 test.

Because the B-5 test showed that the outer ring of simulators acted as deforming guard heaters and their deformation behavior was atypical, a decision was made to omit the temperature measuring instrumentation in 20 of the 28 simulators in the outer ring of B-6. However, all 28 of the simulators were provided with pressure monitoring instrumentation. Figure 3 gives pertinent details of the fully-instrumented fuel rod simulators. Tantalum wire was used for centering the fuel simulator (internal heater) in the Zircaloy tube of those simulators in the outer ring without temperature sensors. The fuel simulators were produced in our Fuel Rod Simulator Technology Development Laboratory. Fifty-three of the fuel simulators were reclaimed from the B-5 test array (the remaining 11 simulators could not be removed) and refurbished (straightened, recoated with plasma-sprayed ZrO_2, and recharacterized by infrared scanning) for use in the B-6 array. The remaining 11 B-6 simulators were previously unused. The axial heat generation profile of all the simulators, as determined by the pretest infrared characterization scans, was very uniform. The highest quality simulators were assigned to the interior positions in the array.

For those simulators provided with temperature sensors, four Inconel-sheathed (0.71-mm-diam), type K, ungrounded junction thermocouples were spot welded to the inside of the Zircaloy-4 tubes (10.9-mm O.D. x 0.635-mm wall thickness) at axial and azimuthal positions shown in Fig. 4. The figure also gives thermocouple identifications for use in subsequent figures for which the nomenclature TE 10-4 identifies the No. 4 thermocouple in the No. 10 fuel pin simulator. Figure 5 shows the axial distribution of the simulator thermocouples more clearly. As evident from the figures, the inner 6 x 6 array had 18 thermocouples (average of one for every two simulators) at each of the instrumented elevations, except for the less interesting 5 cm and the two grid elevations. The thermocouple locations for the instrumented simulators in the outer ring (see Fig. 4) were selected to provide data in the regions of most interest, with eight thermocouples located at each of four elevations.

ORNL-DWG 82-6386 ETD

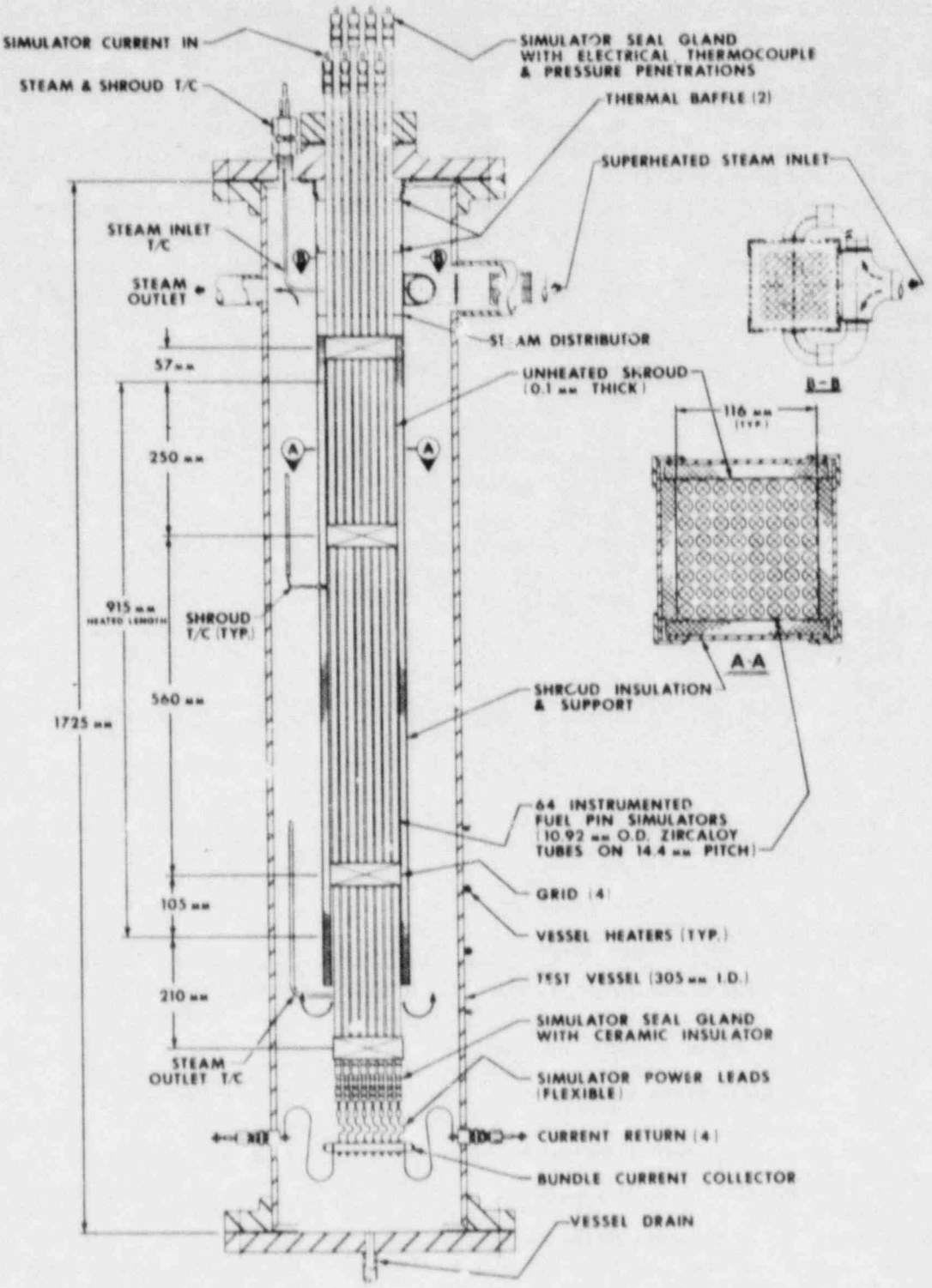

Fig. 2. Schematic of B-6 (8 x 8) bundle test assembly.

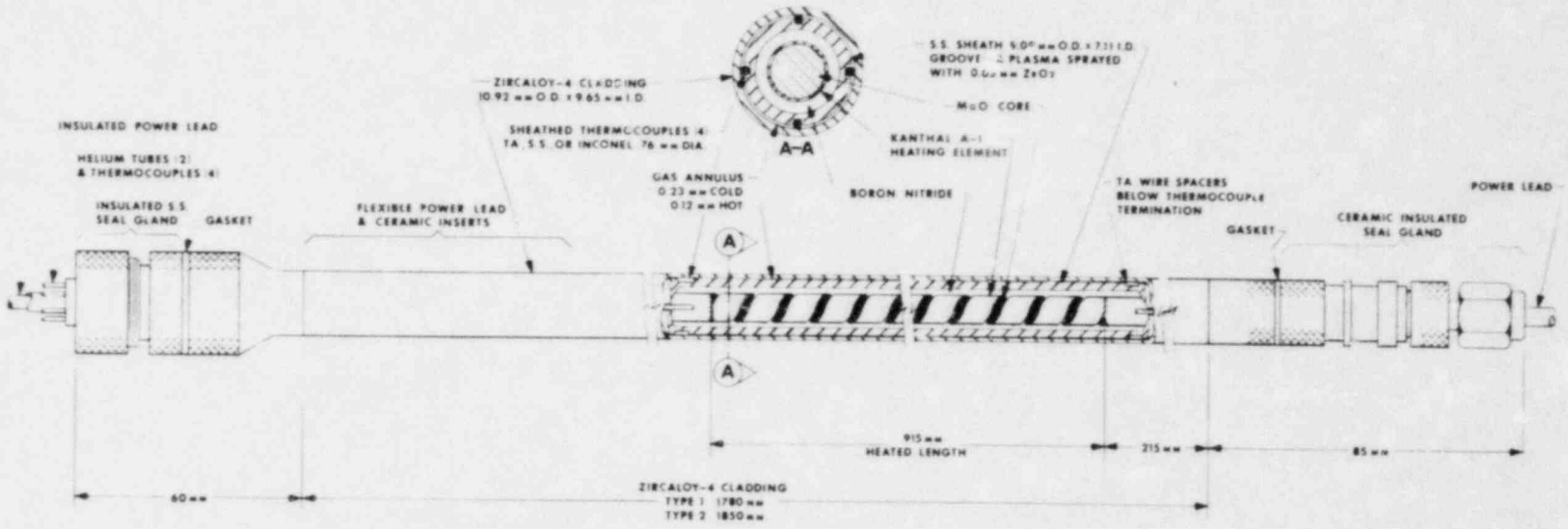

Fig. 3. MRBT fuel pin simulator.

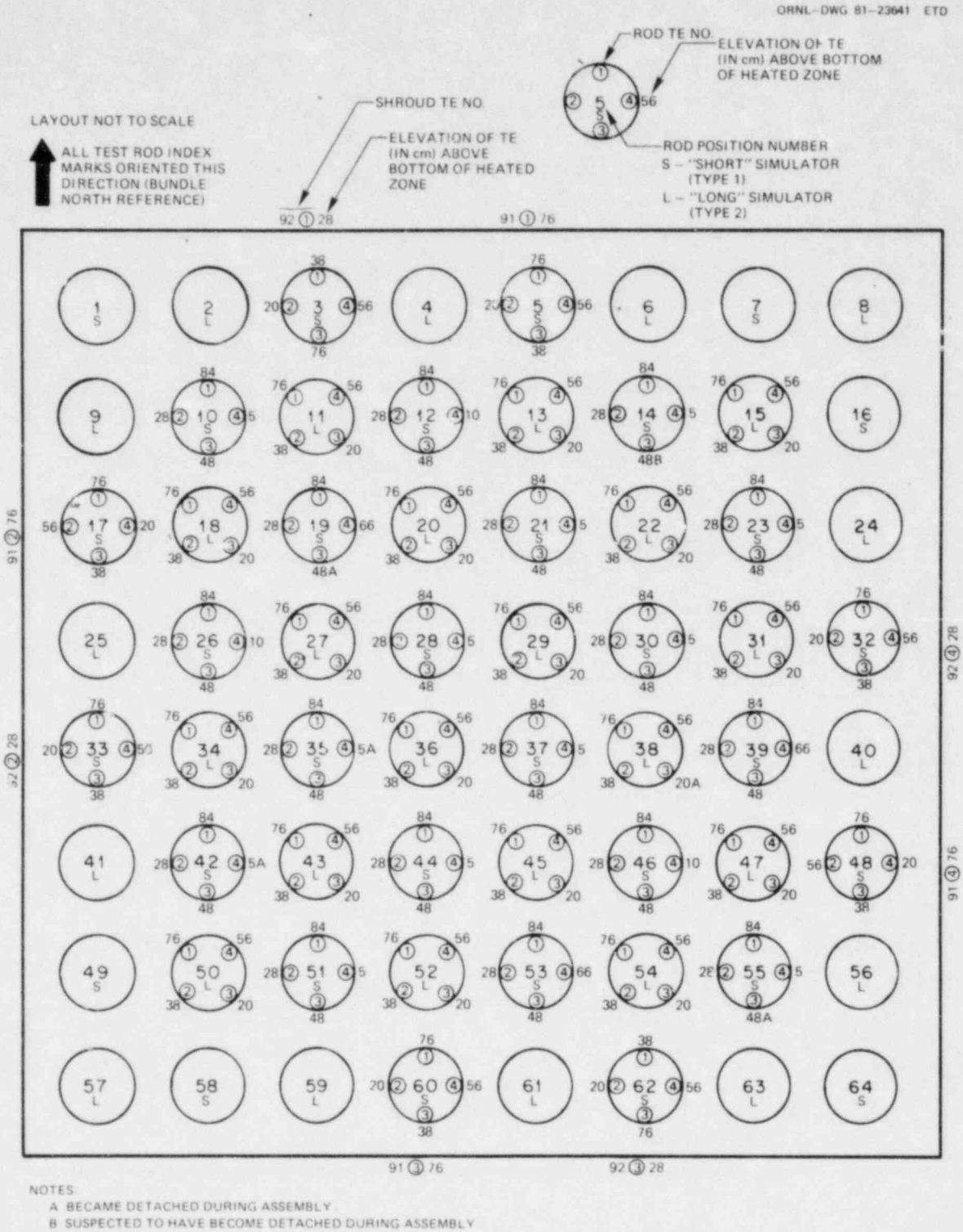

NOTES:
A. BECAME DETACHED DURING ASSEMBLY.
B. SUSPECTED TO HAVE BECOME DETACHED DURING ASSEMBLY.

Fig. 4. As-built thermocouple identifications and locations in B-6 test array (plan view).

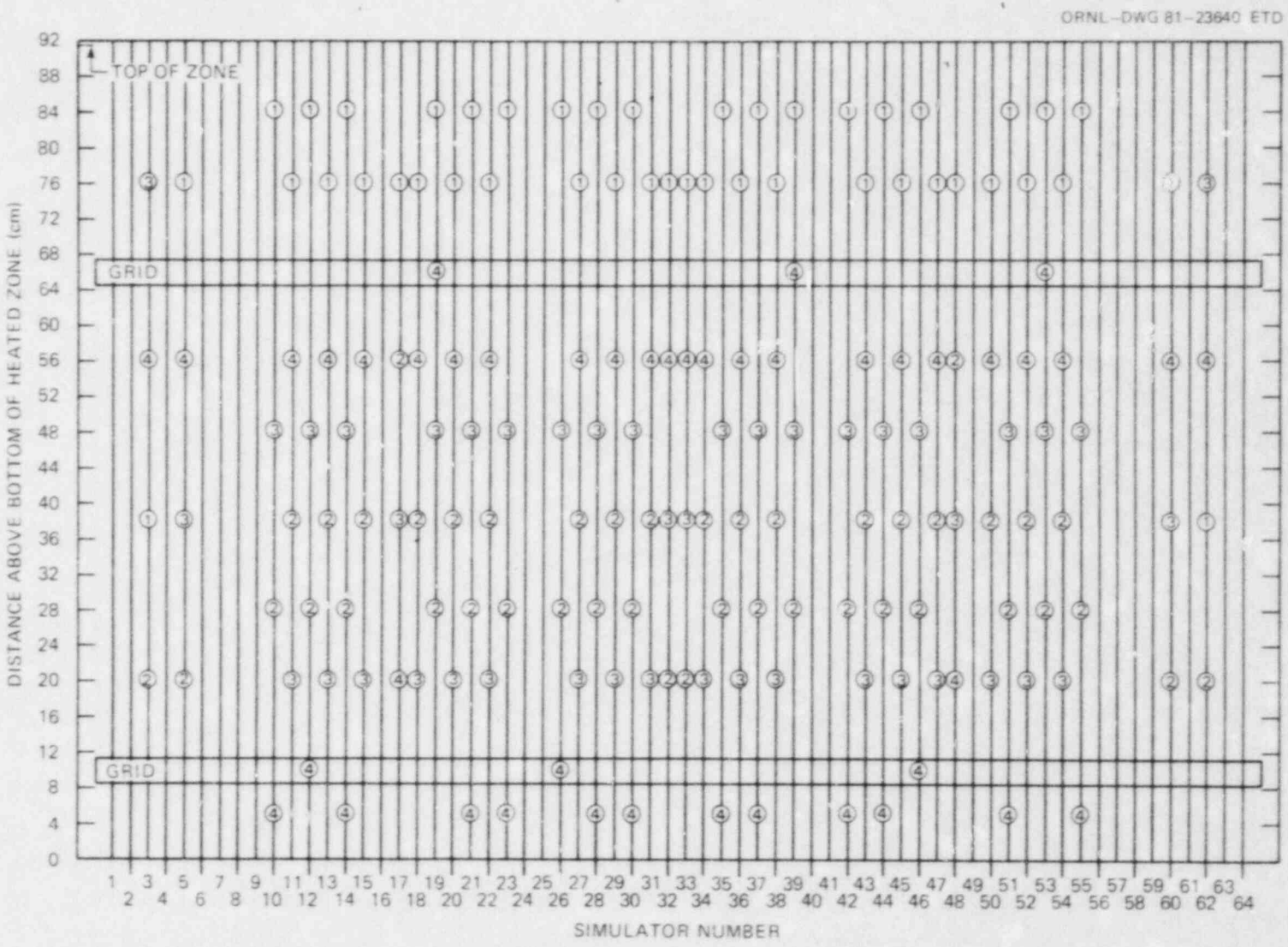

Fig. 5. As-built elevations of simulator thermocouples in B-6 test array.

As noted in Fig. 4, five thermocouples (TE 19-3, TE 35-4, TE 38-3, TE 42-4, and TE 55-3) and possibly a sixth one (TE 14-3) became detached during fabrication of the simulators. Although not apparent from the data, their readings might indicate Zircaloy temperatures slightly higher than would be the case if they had remained attached to the wall.

Eight, 0.076-mm-diam, bare wire, type S thermocouples were spot welded directly on the outside surface of the thin shroud surrounding the rod array. Two thermocouples were attached to each side at locations shown in Fig. 4 in an attempt to obtain information on both the axial and circumferential temperature distributions. The shroud thermocouple identifications are also given in the figure for use in subsequent temperature plots.

Five thermocouples (TE-320 through TE-324) were located in the inner 6 x 6 matrix at the 107-cm elevation (centerline elevation of the steam inlet nozzles) to obtain inlet steam temperature measurements across the bundle. Similarly, five thermocouples (TE-325 through TE-329) were located in the matrix near the bottom of the heated zone (3-cm elevation) to obtain outlet steam temperature measurements. Unfortunately, two of the latter group (TE-326 and TE-329) were damaged during assembly and were inoperative during the test. Figure 6 shows the respective identifications and locations. The thermocouples were 0.71-mm-diam, stainless steel sheathed, type K with ungrounded junctions.

Millivolt signals from the pressure transducers, thermocouples, and electrical power measuring instruments were recorded on magnetic tape by a computer controlled data acquisition system (CCDAS) for subsequent analysis.

Test Operations

Heatup of the test assembly was initiated early in the afternoon of December 2; the temperature was near 200°C at the end of the work shift. Power adjustments to the vessel heaters were made to maintain the temperature near this value overnight to avoid temperature cycling of the test assembly. Early on December 3, power to the vessel heaters was increased, and superheated steam was admitted to the vessel in the approach to the initial test temperature. Throughout this phase of operation, periodic leak checks indicated the simulator seals were performing very well (i.e., <1-kPa/min pressure loss at 3300 kPa and ~320°C).

After thermal equilibration (about 322°C) of the test assembly was attained, the simulators were pressurized to ~2100 kPa, and a short powered run (~13.0 s transient) was conducted to ascertain that the data acquisition system and all the instrumentation were functioning properly and that the performance of the test components was as expected. Examination and evaluation of the quick-look data from this short transient (the temperature of the simulators increased to about 380°C) indicated that minor adjustments were needed. In particular, the applied voltage setting was adjusted slightly upward in an attempt to achieve the desired heating rate.

Following restabilization of the bundle temperature at ~330°C, all the fuel pin simulators were pressurized simultaneously to ~3050 kPa (differential above the external steam pressure) and isolated individually

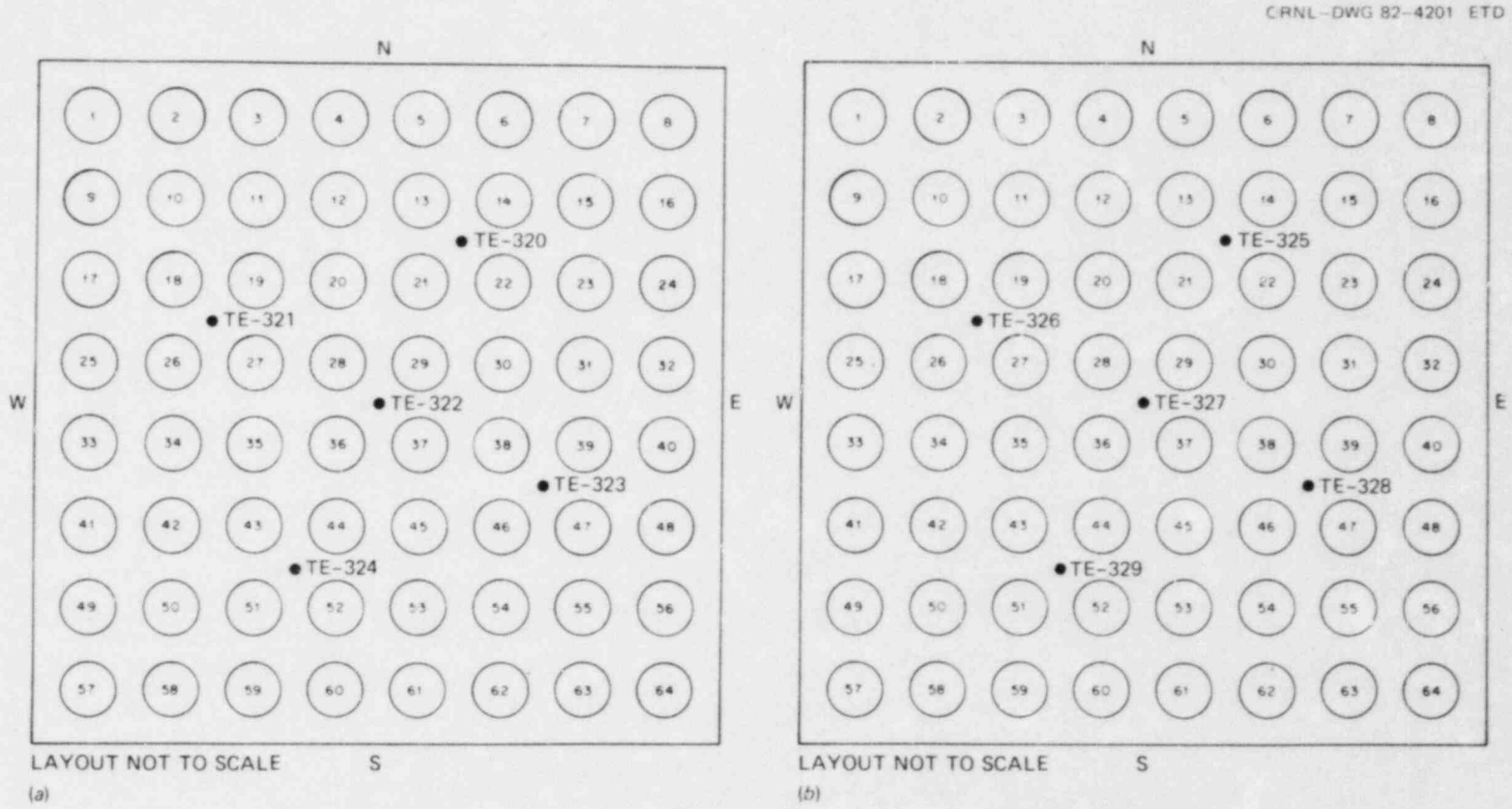

Fig. 6. Location and identification B-6 steam temperature sensors. (*a*) Inlet steam sensors at 107-cm elevation and (*b*) outlet steam sensors at 3-cm elevation. Outlet sensors TE-326 and TE-329 were inoperative during test.

from the helium supply header. The header was vented, and the leak rate of each of the 64 simulators was checked over a 2-min period, with the pressure loss being less than ~1 kPa/min. With these initial conditions established, the test transient was initiated.

Termination of the powered portion of the test could be initiated by any of four actions: (1) CCDAS action resulting from a signal that 50 of the 64 simulators had burst, (2) CCDAS action resulting from a signal that 115 simulator thermocouples had exceeded the upper temperature limit (50°C above the anticipated burst temperature) on each of three successive data scans, (3) a timer that limited the transient to ~145 s, and (4) operator override. It was decided to program criterion (1) to terminate power to the bundle after 60 bursts (with the expectation that all 64 tubes would burst) to minimize the temperature overshoot at the end of the test. Also, criterion (2), that is, the high-temperature limit, was established close to the expected burst temperature for the same reason. The test was terminated by criterion (3), and all 64 tubes burst.

Quick-look Results

Quick-look data of interest are extensive and difficult to present in concise tabular format. Instead, we have elected to display the data in a series of bundle layout diagrams and quick-look plots to facilitate visualization. Note that these results are preliminary and subject to change upon detailed analysis of the data.

Superheated steam entered the test array through two inlet nozzles located (107-cm elevation) on the east and west sides of the bundle (see Fig. 2) at an average temperature of 330°C and 309 kPa (absolute) and flowed downward through the array at a constant mass flux of 288 $g/s \cdot m^2$. With these conditions, the nominal Reynolds number at the top of the heated zone (91.5-cm elevation) was 140. These inlet conditions remained constant until disrupted by escaping helium from the bursting tubes. When power to the bundle was terminated, the steam mass flux was increased to a minimum of 2050 $g/s \cdot m^2$ for rapid cooldown. Inlet and outlet steam temperatures measured 1.0 s before power-on and 1.0 s before the first tube burst are indicated in Figs. 7 and 8, respectively.

Figures 9-18 present cladding temperatures measured at the instrumented levels 1.0 s before power-on and 1.0 s before the first tube burst. The data are presented in a format intended as a schematic layout of the thermocouple locations. If the junction is in the plane for which the particular map applies, the layout has the TE number filled in to denote the azimuthal position of a thermocouple and the temperature measurement is given. The respective row and column average temperatures for the inner 6 x 6 array are printed on the left and at the bottom of the layout. The cross section and bundle average temperatures, based on the 6 x 6 array, are also included in the format.

The overall radial temperature distribution may be visualized somewhat easier in the temperature map depicted in Fig. 19. The temperature given for each simulator is the average of the thermocouple measurements for that simulator without regard to elevation. Because every other simulator had thermocouples near the upper and lower end of the heated zone (see Figs. 4 and 5), the averages given for these simulators in Fig. 19(*b*) reflect the lower temperatures existing near the ends of the heated zone

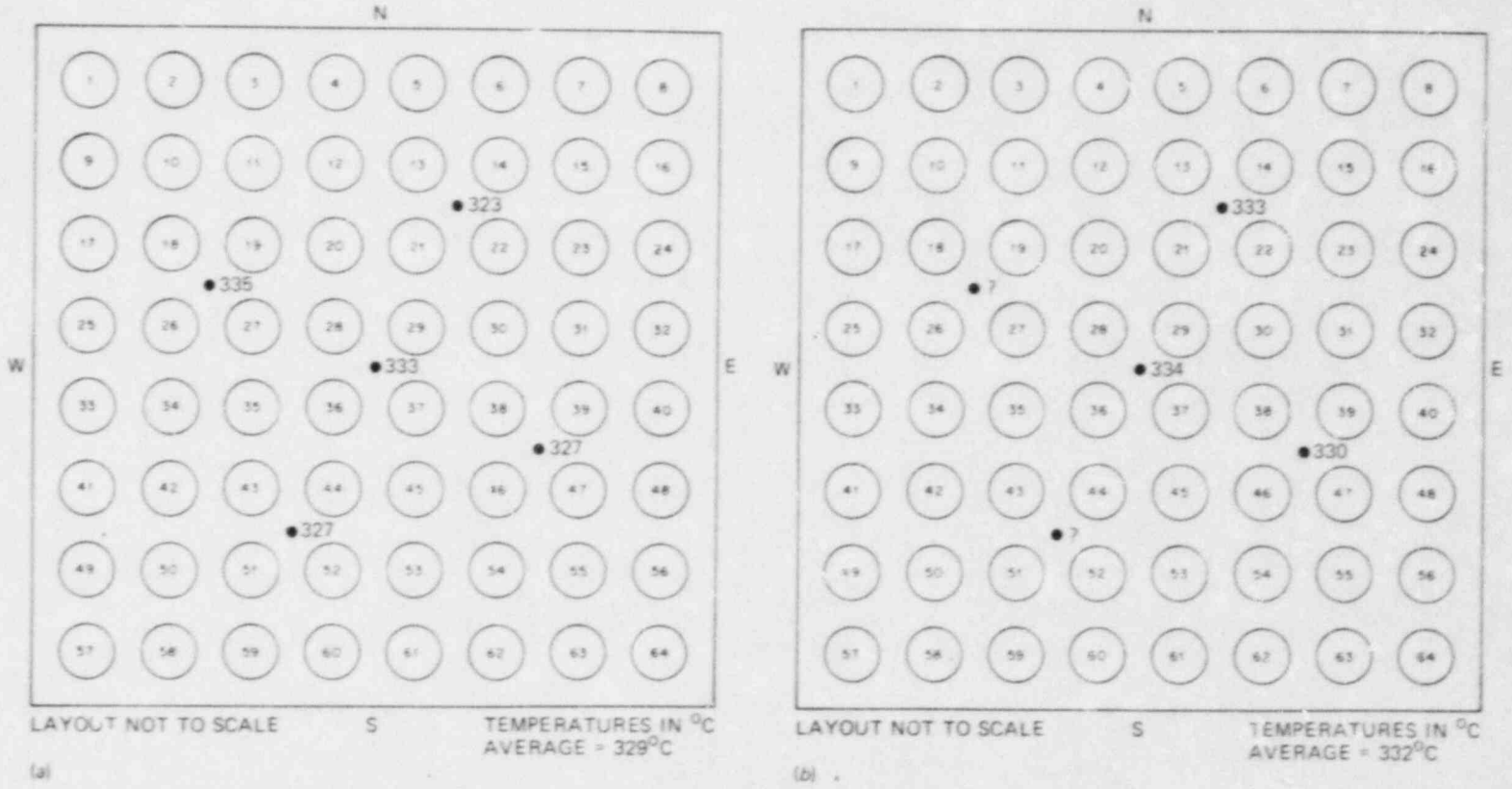

Fig. 7. Measured steam temperatures 1.0 s before power-on. (*a*) Inlet steam at 107-cm elevation and (*b*) outlet steam at 3-cm elevation.

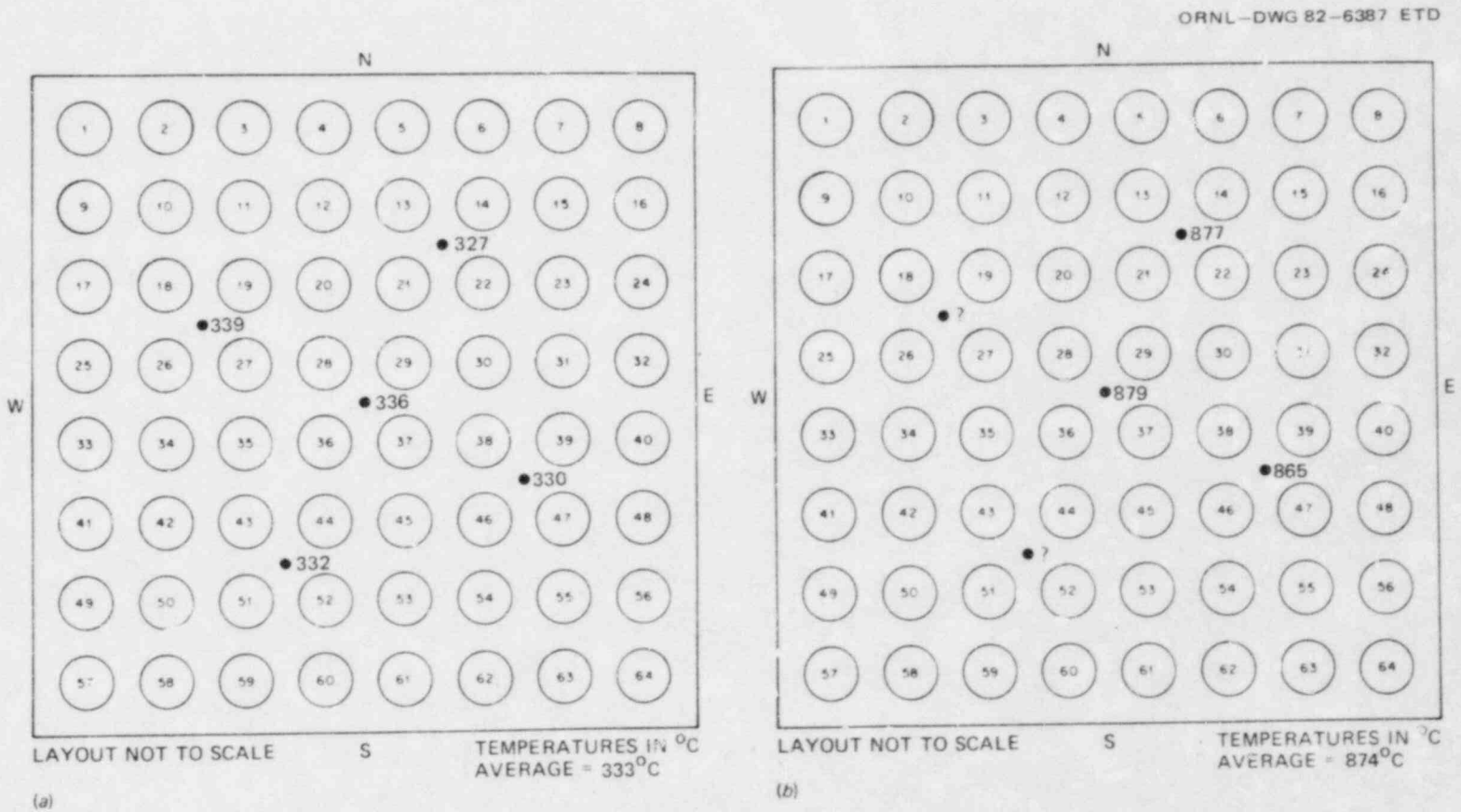

Fig. 8. Measured steam temperatures 1.0 s before the first tube burst. (*a*) Inlet steam at 107-cm elevation and (*b*) outlet steam at 3[illegible] elevation.

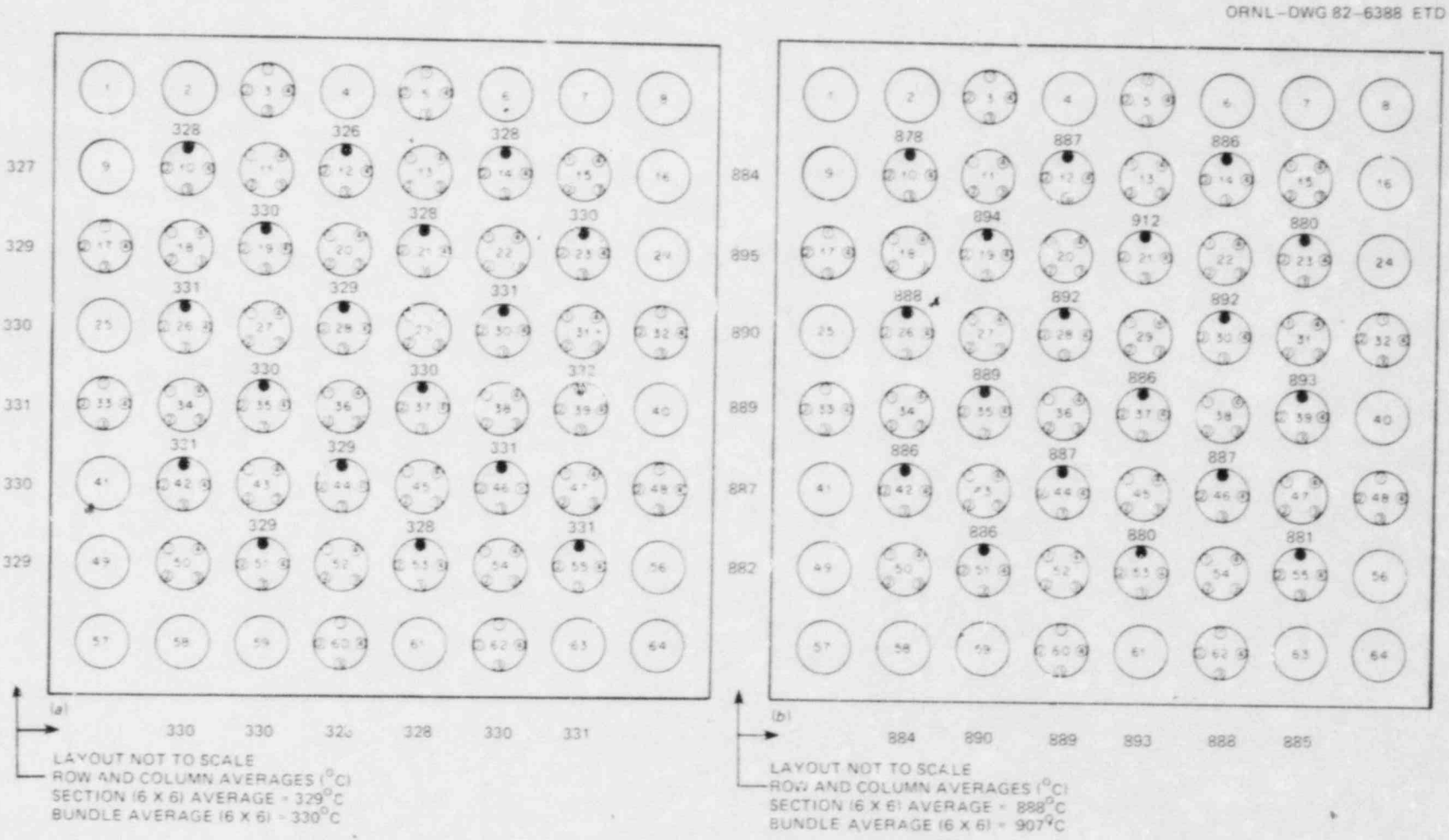

Fig. 9. Radial temperature distribution measured at 84-cm elevation (*a*) 1.0 s before power-on and (*b*) 1.0 s before first tube burst.

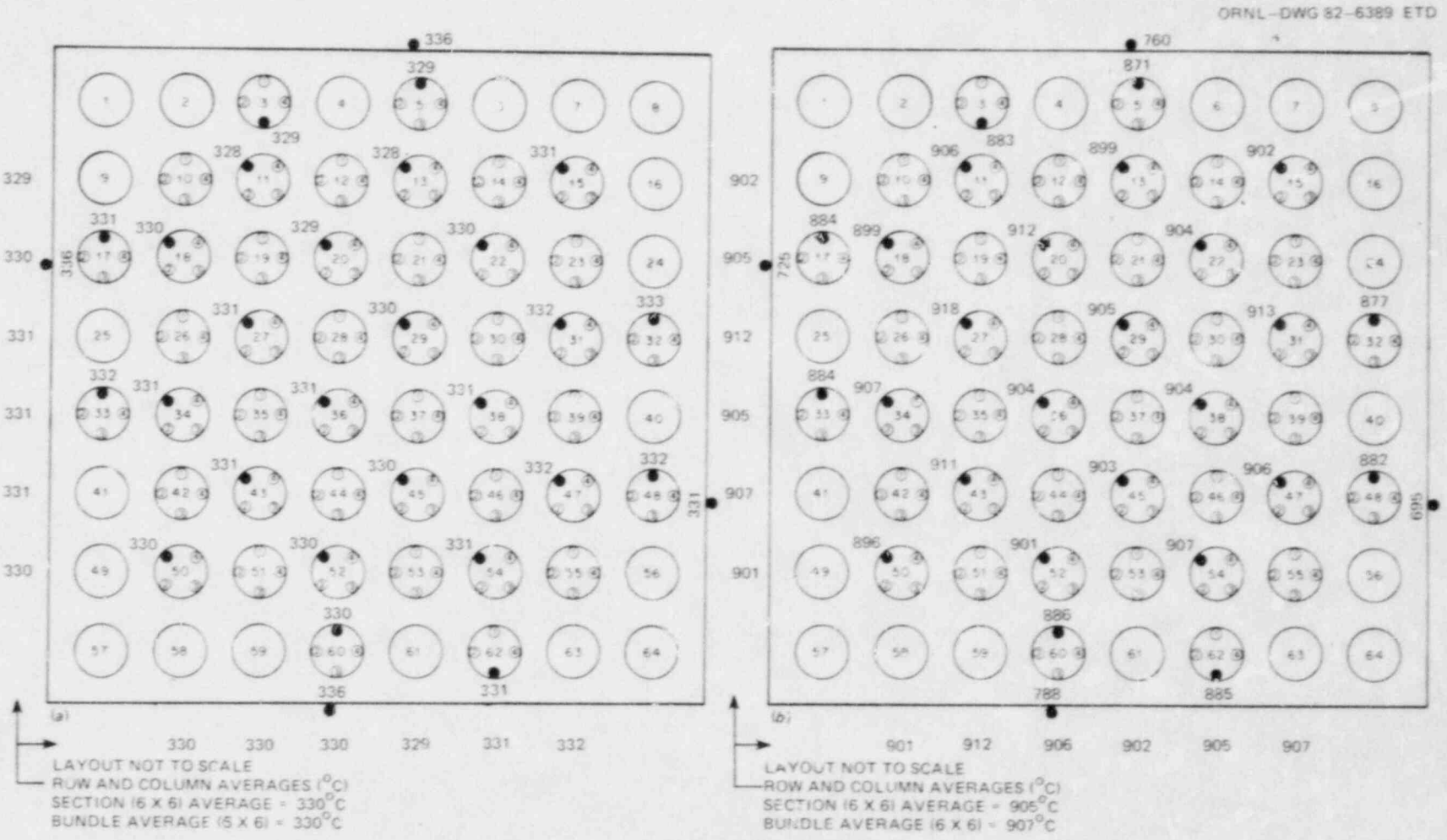

Fig. 10. Radial temperature distribution measured at 76-cm elevation (*a*) 1.0 s before power-on and (*b*) 1.0 s before first tube burst.

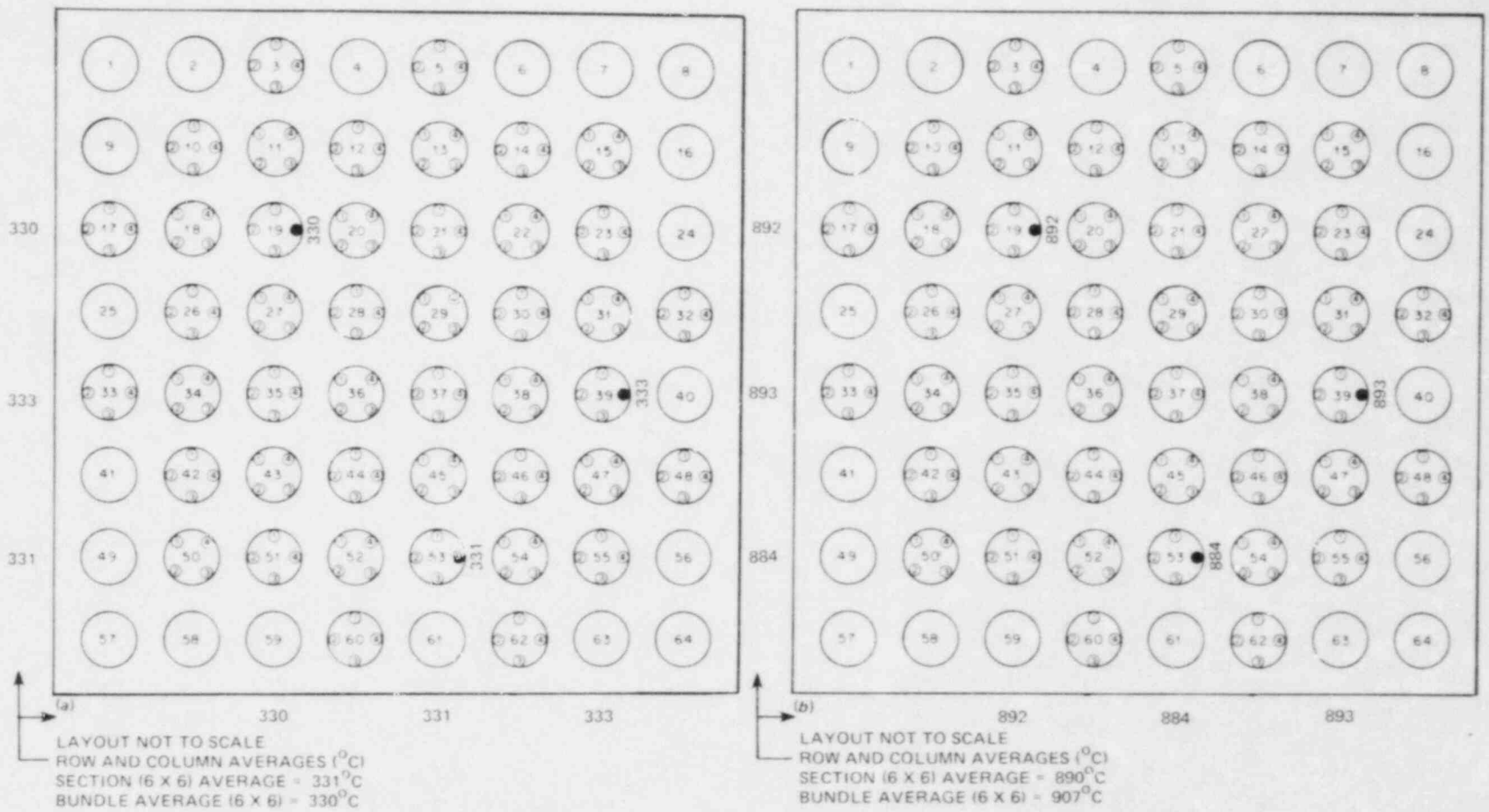

Fig. 11. Radial temperature distribution measured at upper grid (66-cm) elevation (*a*) 1.0 s before power-on and (*b*) 1.0 s before first tube burst.

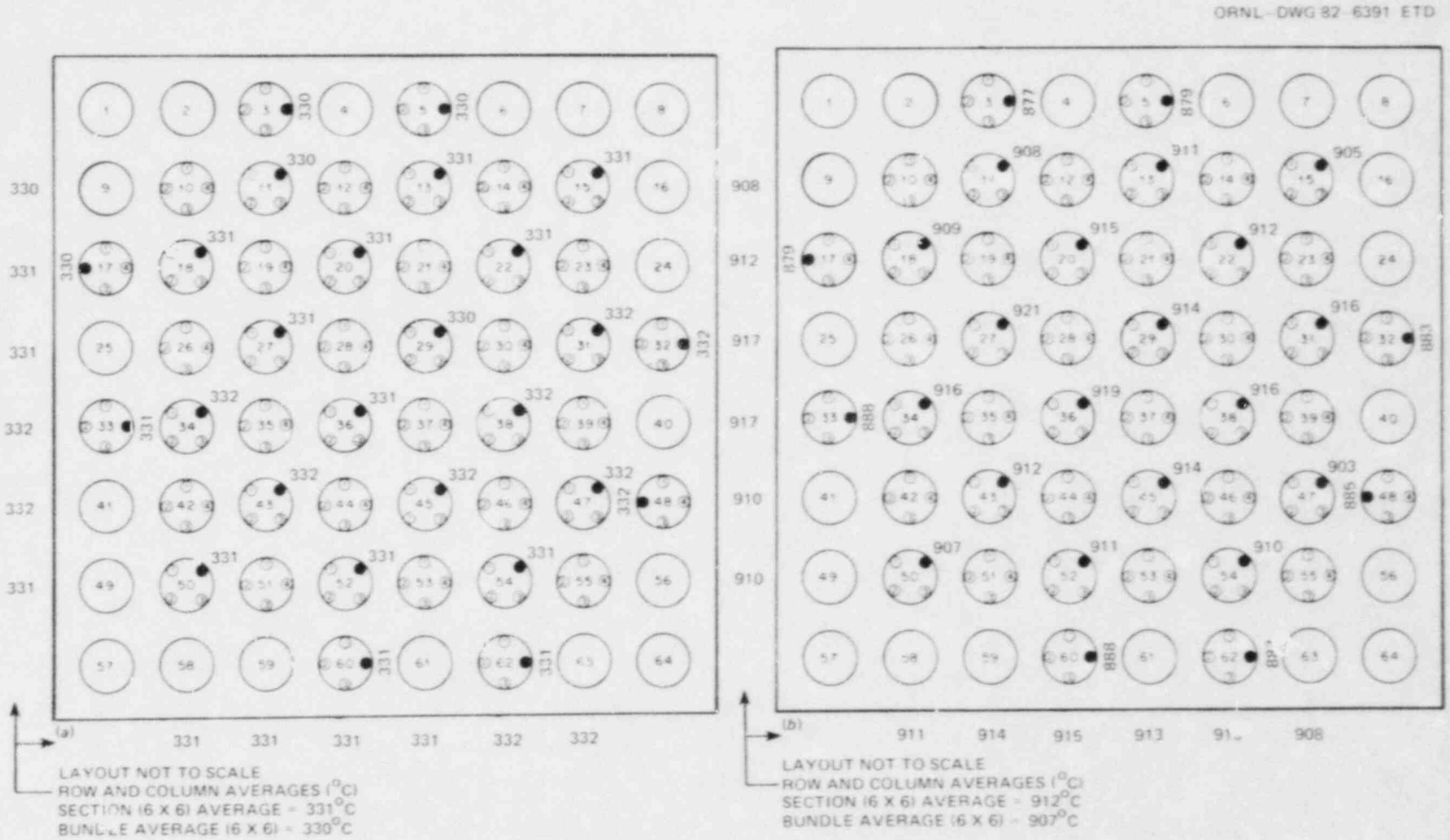

Fig. 12. Radial temperature distribution measured at 56-cm elevation (*a*) 1.0 s before power-on and (*b*) 1.0 s before first tube burst.

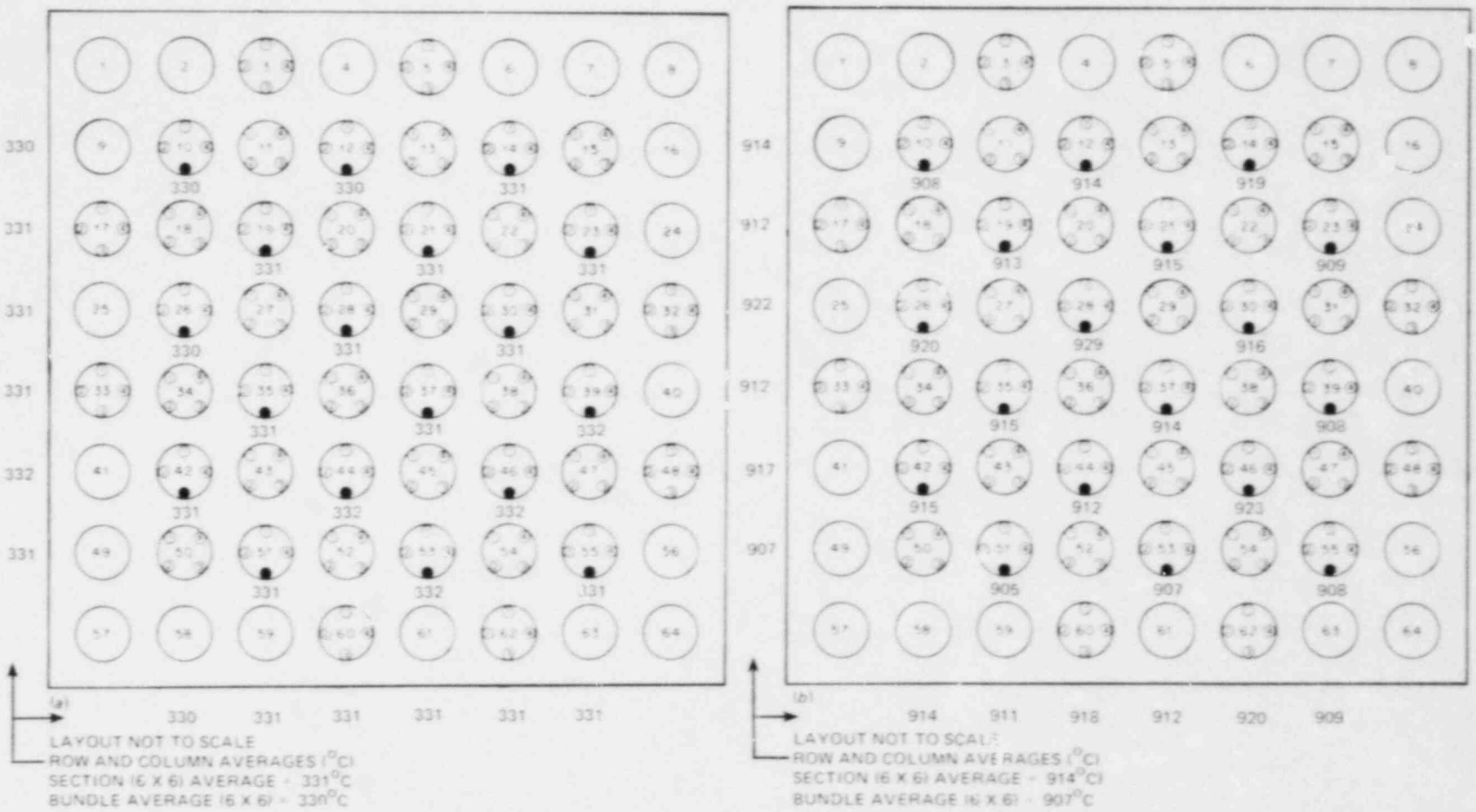

Fig. 13. Radial temperature distribution measured at 48-cm elevation (*a*) 1.0 s before power-on and (*b*) 1.0 s before first tube burst.

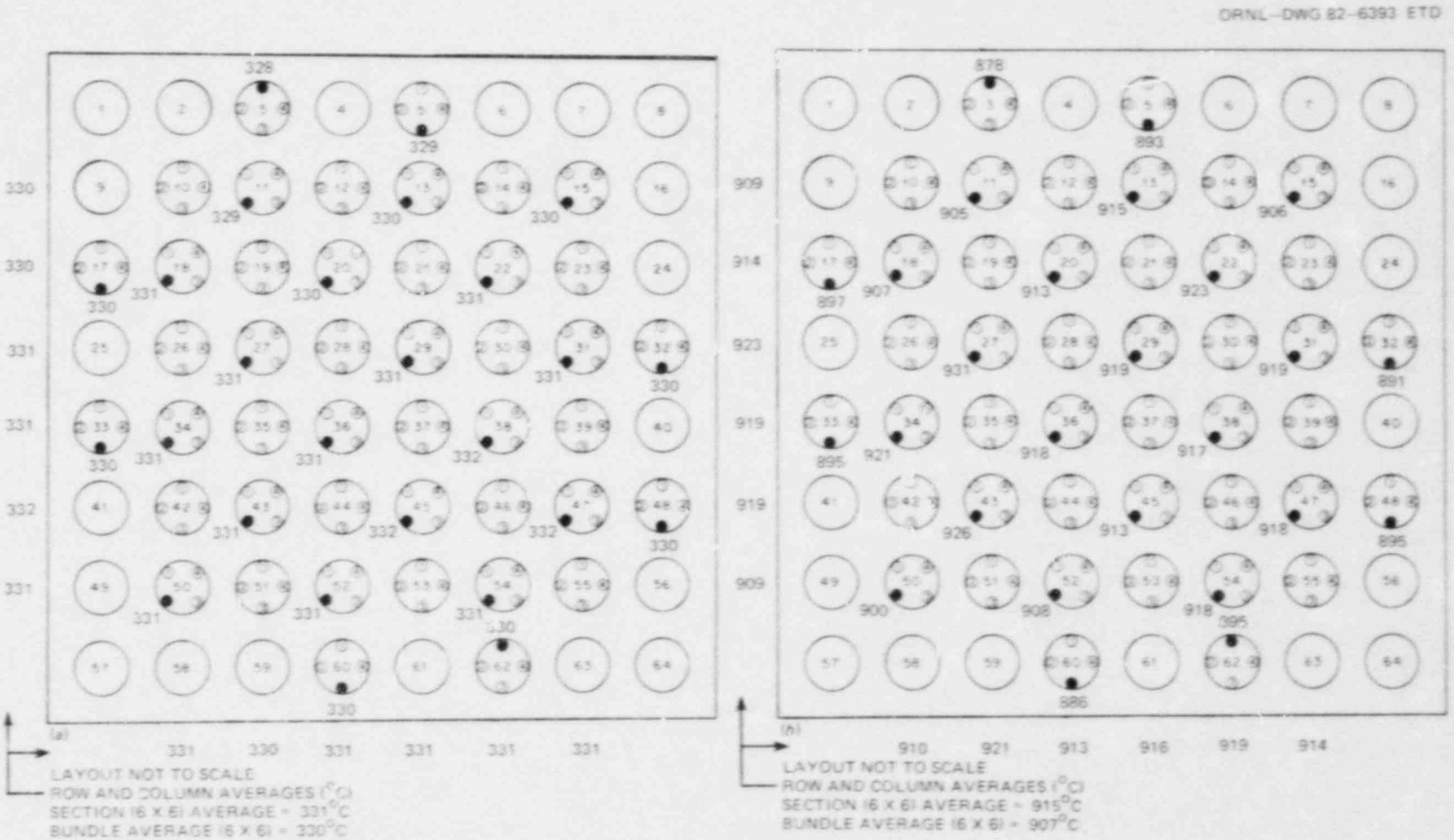

Fig. 14. Radial temperature distribution measured at 38-cm elevation (*a*) 1.0 s before power-on and (*b*) 1.0 s before first tube burst.

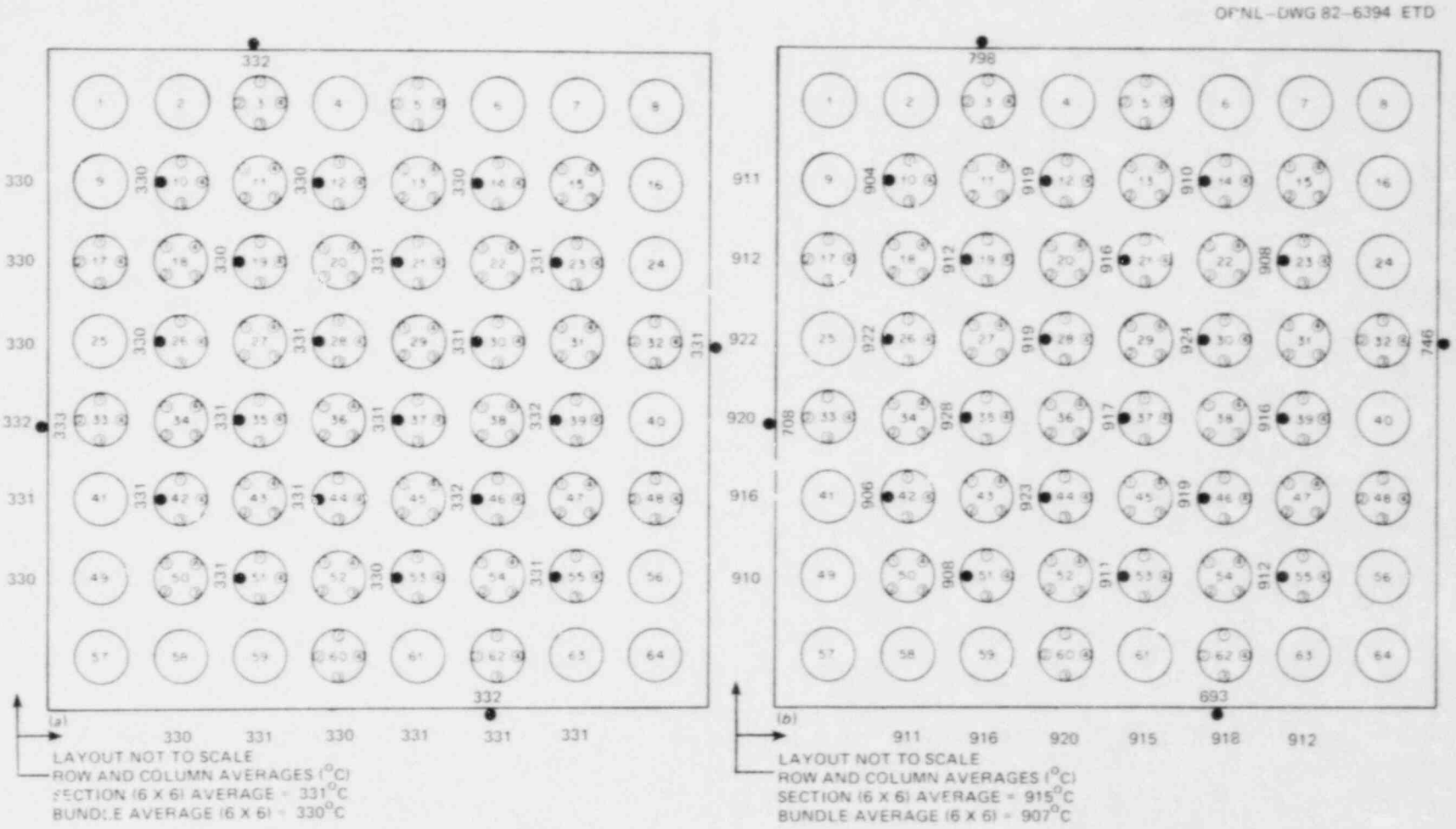

Fig. 15. Radial temperature distribution measured at 28-cm elevation (*a*) 1.0 s before power-on and (*b*) 1.0 s before first tube burst.

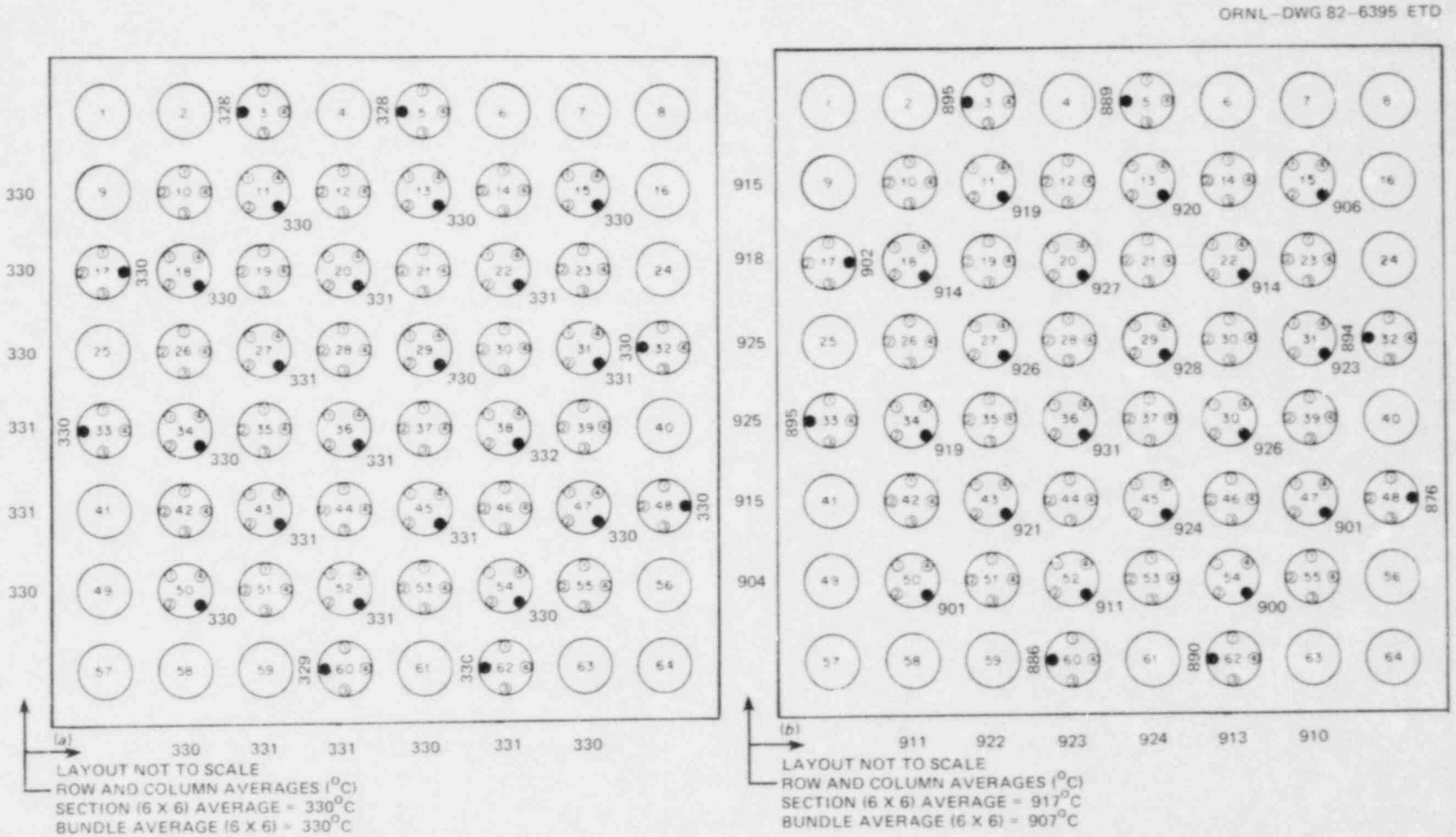

Fig. 16. Radial temperature distribution measured at 20-cm elevation (*a*) 1.0 s before power-on and (*b*) 1.0 s before first tube burst.

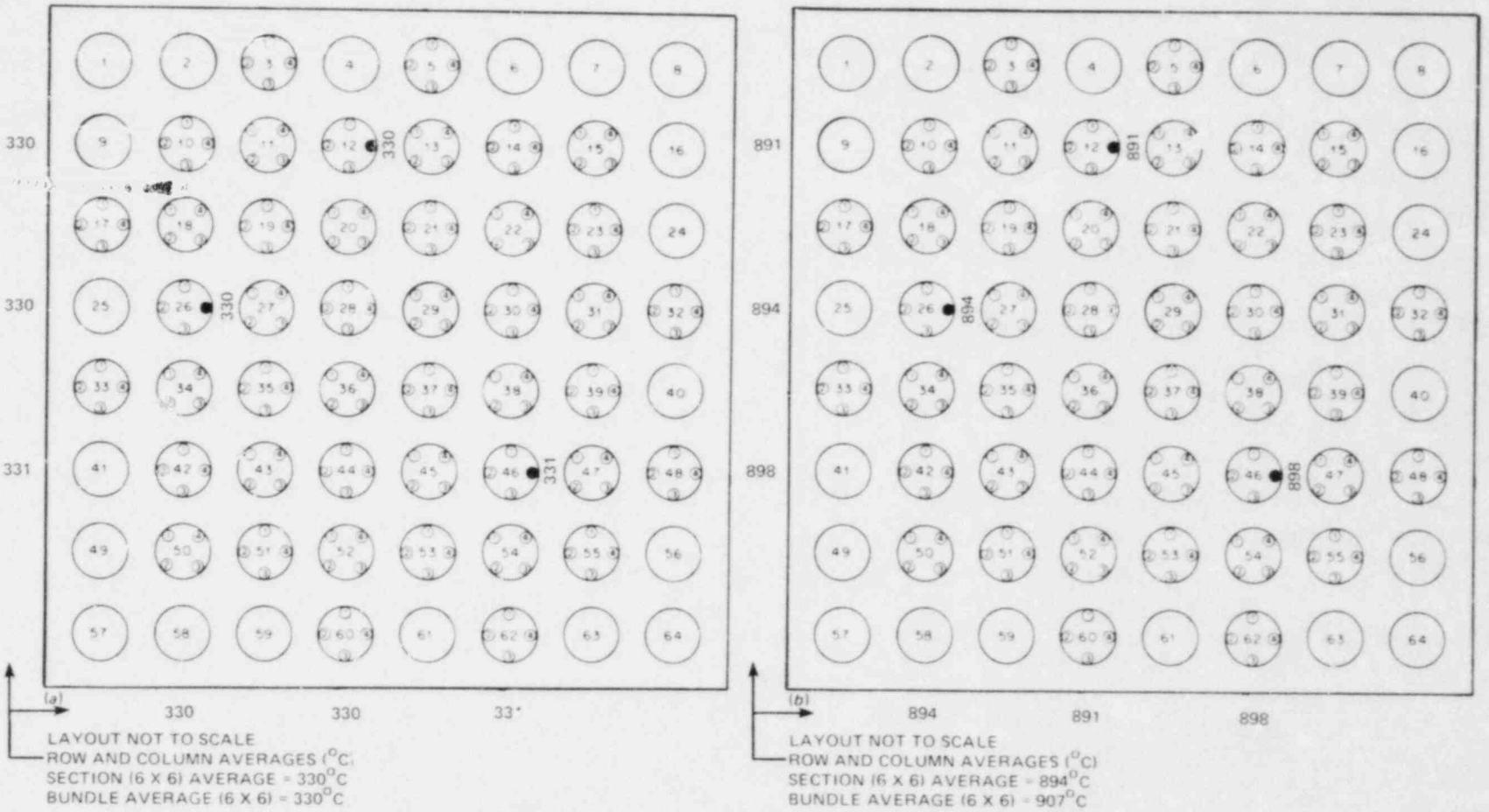

Fig. 17. Radial temperature distribution measured at lower grid (10-cm) elevation (*a*) 1.0 s before power-on and (*b*) 1.0 s before first tube burst.

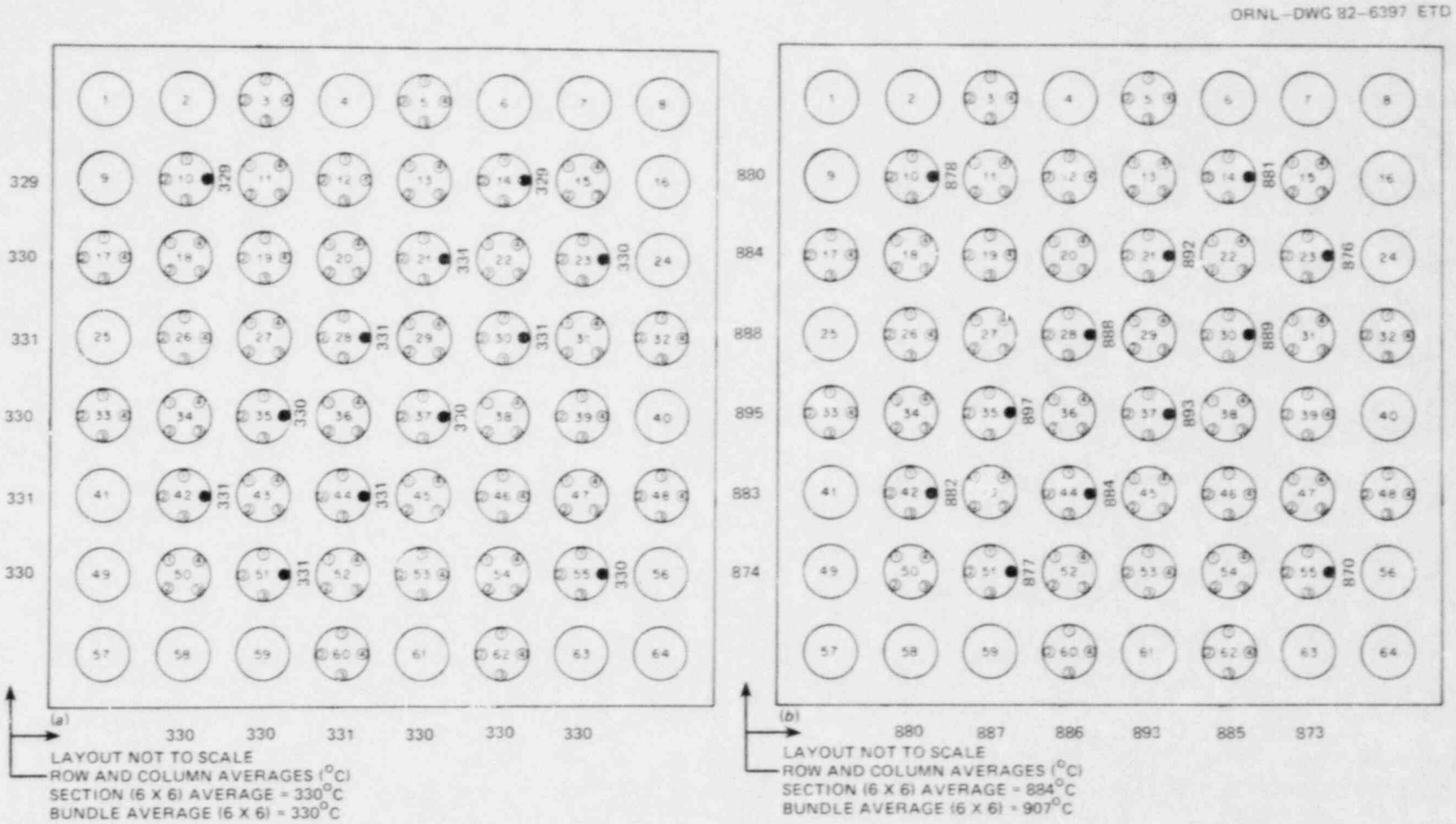

Fig. 18. Radial temperature distribution measured at 5-cm elevation (*a*) 1.0 s before power-on and (*b*) 1.0 s before first tube burst.

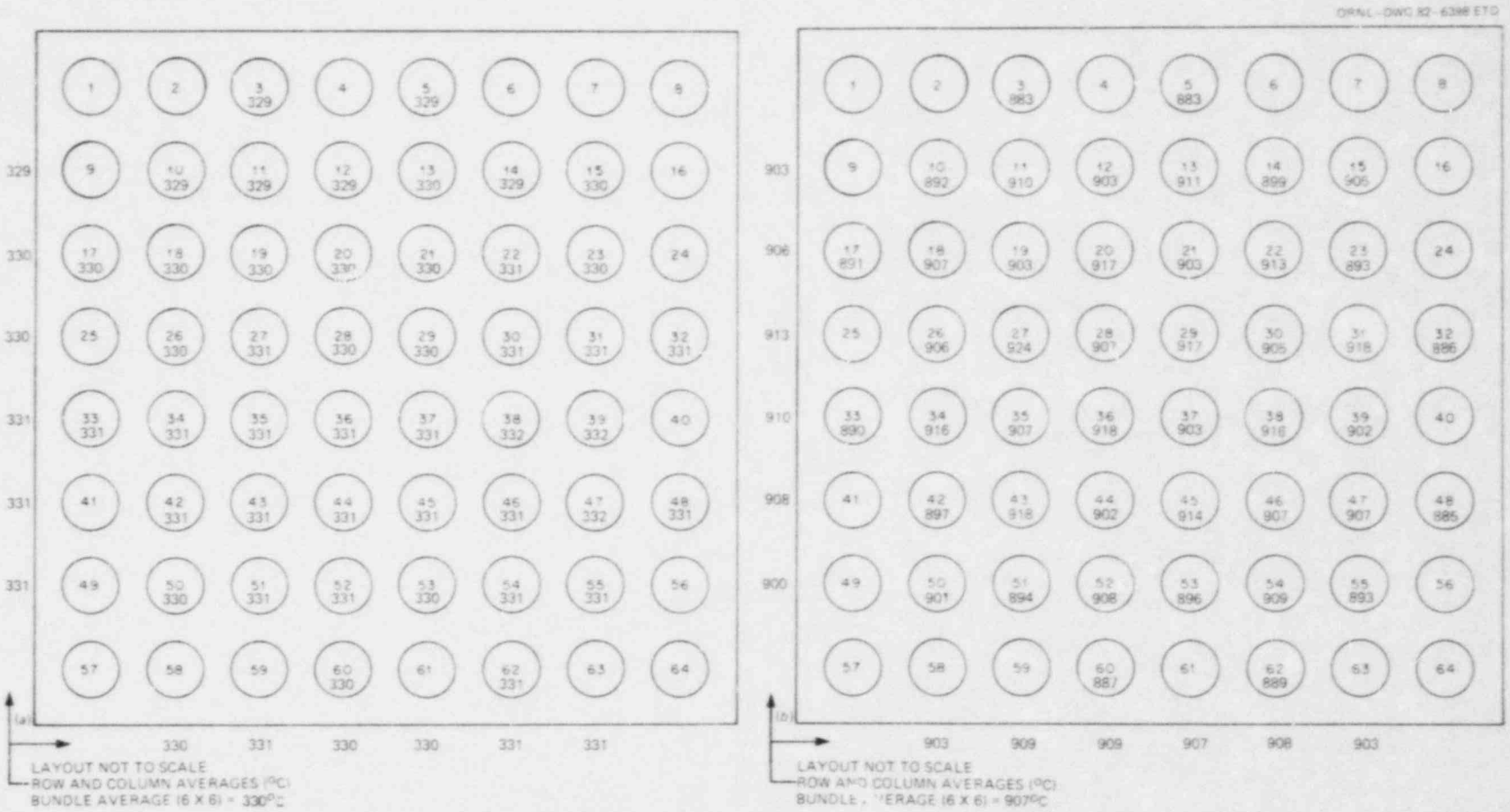

Fig. 19. Simulator-averaged temperature measurements (*a*) 1.0 s before power-on and (*b*) 1.0 s before first tube burst.

during the transient. This portion of the figure also shows that the interior simulators were a few degrees higher in temperature than the exterior ones, as would be expected from the boundary conditions.

The data given in Figs. 9–18 for the inner 6 x 6 array were averaged to obtain the axial temperature profiles plotted in Fig. 20; the average at each instrumented elevation, the range of the data, and the number of thermocouples on which the average is based are also noted in the plot. The profile 1.0 s before the first tube burst shows the end effects mentioned above; the small (~5°C) gradient between the grids reflects the slight increase in steam temperature as it flowed through the bundle.

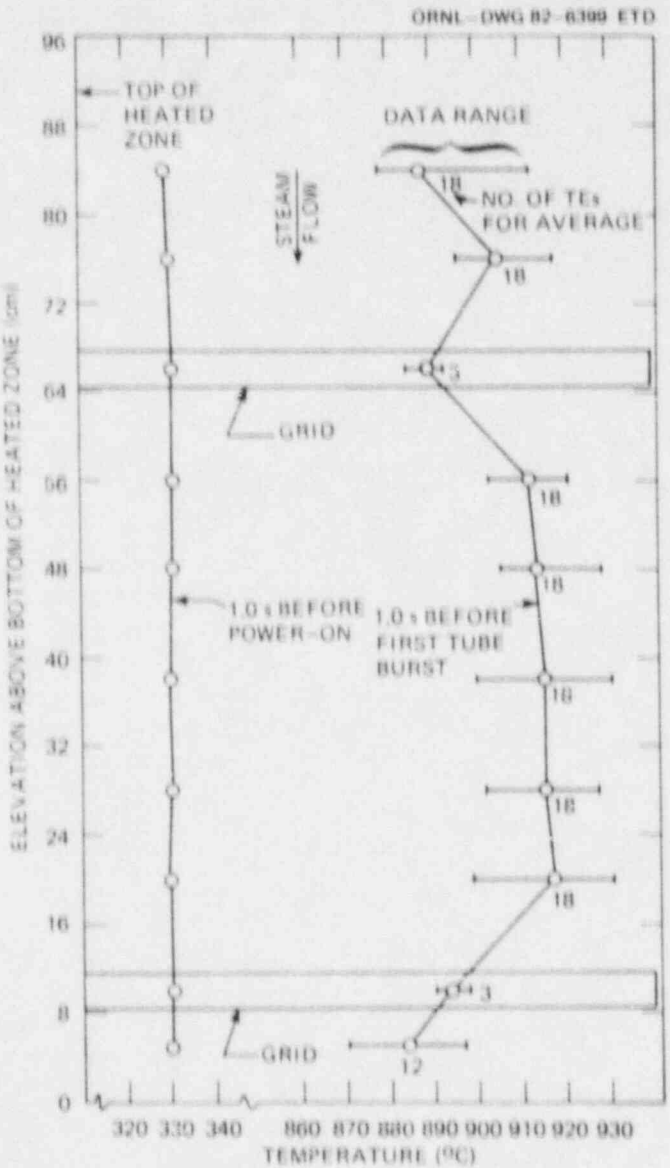

Fig. 20. Axial temperature profile of inner 6 x 6 array measured 1.0 s before power-on and 1.0 s before first tube burst.

The maps provide considerable data and greatly facilitate interpretation and quick-look evaluation of local and overall temperature distributions. As evident, the initial radial and axial temperature distributions were very uniform, indicating uniform distribution of the steam. Compare, for example, data in Fig. 9 for the 84-cm elevation with the inlet steam temperatures (at the 107-cm elevation) in Fig. 7. Also, compare Fig. 18 with Fig. 7 for the radial distributions at the lower end of the heated zone. The modifications made to the inlet steam nozzle and others made to control external heat losses effectively eliminated temperature gradients in the bundle like those experienced in the B-5 test.

Differential pressures measured 1.0 s before power-on and 1.0 s before the first tube burst are presented in a similar format in Fig. 21. Because the simulators were pressurized simultaneously from a common header and then isolated individually, the uniformity in initial pressure also indicates uniform gas volumes for the simulators and the lack of seal leaks. The data in Fig. 21(*b*) indicate, consistent with Fig. 19(*b*), that the interior simulators were hotter and had deformed more at this time than the exterior ones.

A number of quick-look plots and other data are presented below to illustrate significant features of the test as it progressed and to provide an indication of the general conditions prevailing at the times of important events. A parameter, TAV-10, is plotted in a number of these figures to represent the bundle average temperature. This parameter is in reality the average of eight thermocouples (TE 11-2, TE 20-2, TE 29-2, TE 31-2, TE 34-2, TE 38-2, TE 45-2, and TE 52-2) at the 38-cm elevation (see Fig. 4 for relative positions) that was electronically averaged and recorded during the test to facilitate characterization and visualization of the bundle temperature as a function of time.

Figure 22 shows this parameter and applied voltage plotted as a function of time after power-on. The average heating rate in the high-alpha temperature range (i.e., from about 35 to about 105 s after power-on, corresponding to TAV-10 temperatures of 498 and 813°C) was about 4.5°C/s. As the temperature increased into the two-phase range, the heating rate decreased because of greater losses and the higher heat capacity of the two-phase material and, perhaps, the effects of deformation. The average heating rate from 115 to 141.7 s after power-on (i.e., to the power-off time) was about 3.5°C/s, in good agreement with the desired rate. Because maximum pressure (indicating the onset of deformation) was encountered in all the interior simulators in the latter time interval, the lower heating rate (i.e., 3.5°C/s) is considered to be the appropriate rate for characterizing the deformation behavior.

As indicated by the applied voltage, power was on for 141.7 s; this point is noted in the figure (and in subsequent plots) by an arrow on the time axis of the plot. The average temperature, ~948°C when power was terminated, continued to increase, attaining a maximum of ~958°C several seconds later, and then started decreasing.

Figure 23 depicts the bundle characteristic temperature (TAV-10) and several pertinent pressures. In particular, vessel gage pressure is shown by PE-301, and differential pressures are shown by (1) PE-29 for simulator 20 (one of the four central simulators and the first simulator to burst), (2) PE-55 for simulator 55 (one of the corner simulators in the inner 6 x 6 array and the last simulator of the inner 6 x 6 array to burst), and

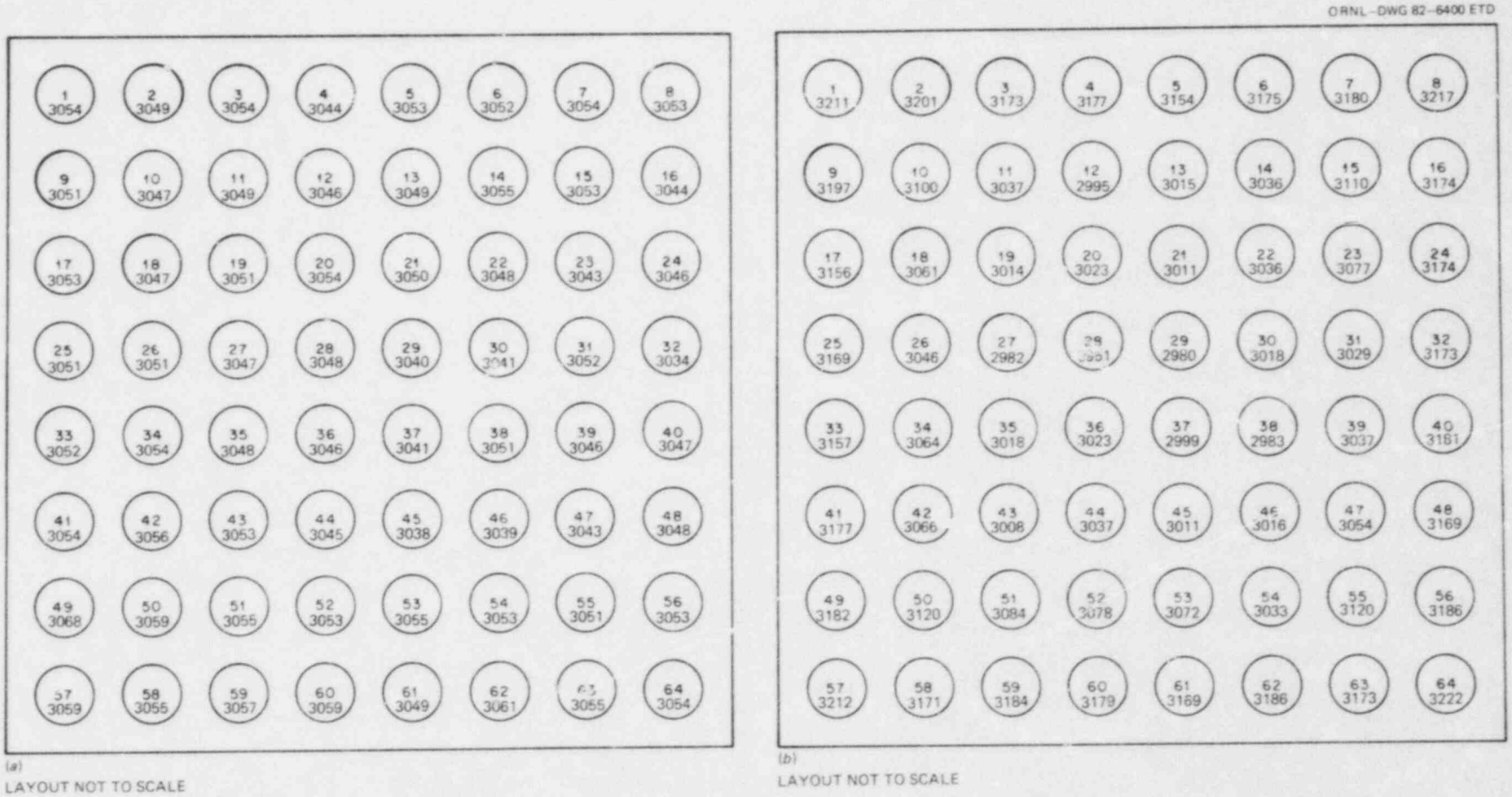

Fig. 21. Differential pressures (kPa) measured (*a*) 1.0 s before power-on and (*b*) 1.0 s before first tube burst.

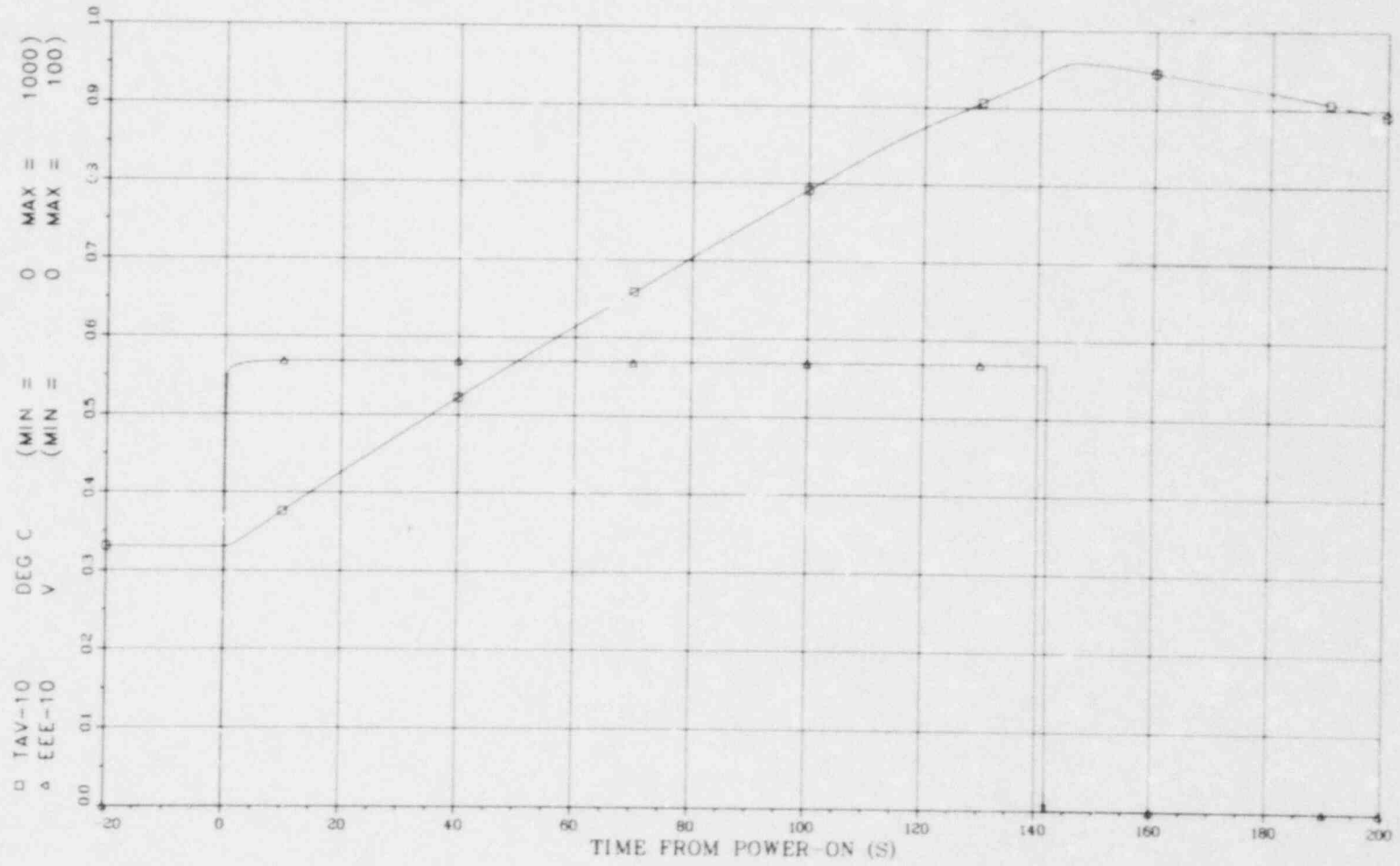

Fig. 22. Bundle average temperature and applied voltage during B-6 test.

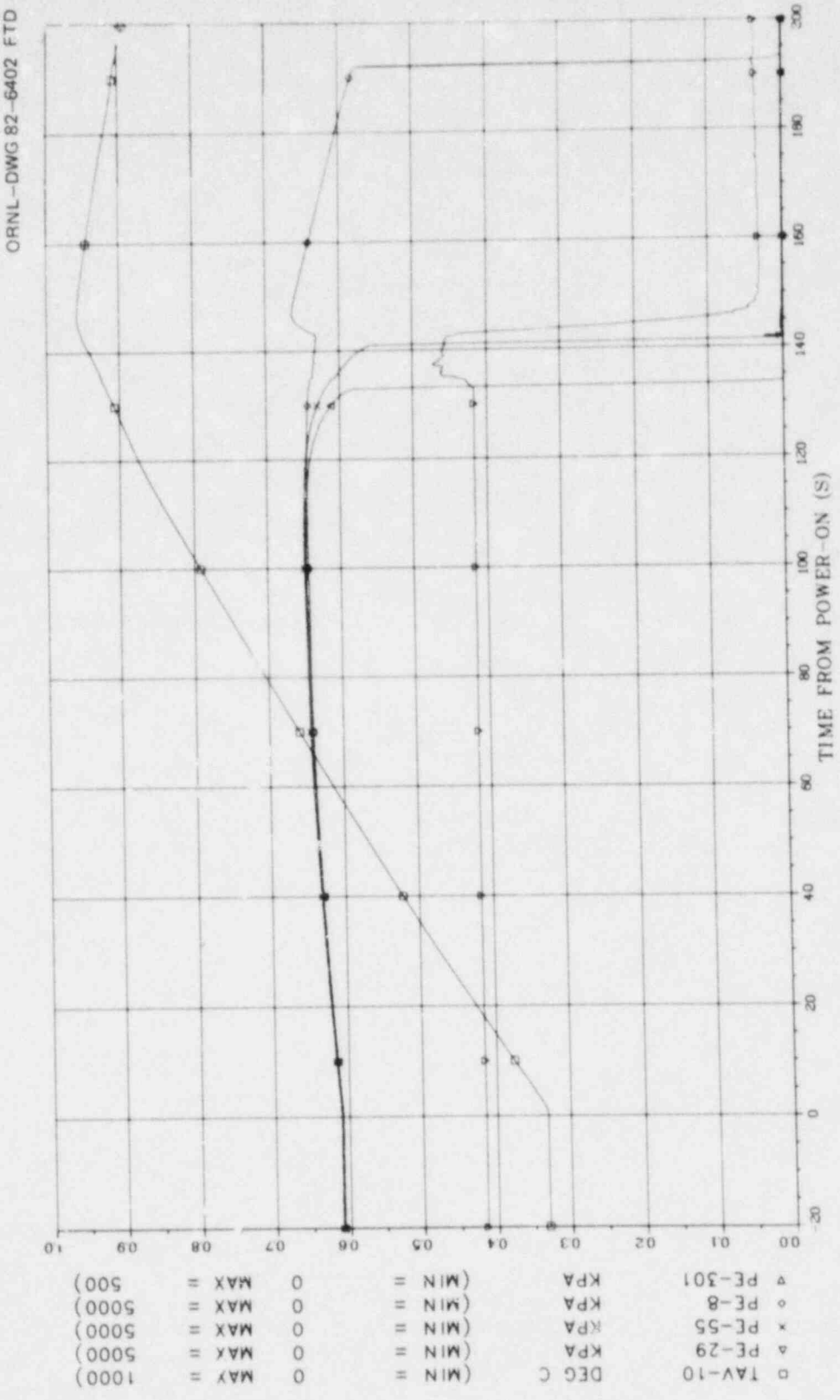

Fig. 23. Typical temperature and pressure behavior during B-6 test.

(3) PE-8 for simulator 8 (an outside corner simulator and the last simulator to burst). The vessel pressure remained constant until the first burst, at which time it increased because of the release of the hot, high-pressure gas from the ruptured simulators. About 3 s after power-off, the steam control valves opened to reduce the vessel pressure and to permit increased steam cooling; at this time the pressure decreased rapidly to atmospheric. The sudden decrease in the external pressure caused a small increase in the differential pressure of those simulators (in the outer ring of the array) not yet burst, as typified by the PE-8 pressure trace in the figure.

Temperature [Figs. 9(b)–19(b)] and pressure [Fig. 21(b)] measurements showed that conditions in the bundle 1.0 s before the first tube burst were very uniform, considering the fact that external heat losses caused the exterior simulators to be 10 to 20°C colder (at this time) than the interior simulators. As a consequence, the exterior simulators were at a slightly higher pressure because of their lower deformation level at this time.

The bursts occurred in an unusually orderly manner, as indicated in Fig. 24, because of the uniform conditions. The data are plotted in three groups to indicate radial positions in the bundle. As is evident in the figure, all the simulators in the inner 4 x 4 array except one burst before any bursts occurred in the next outer row (i.e., the outer ring of the inner 6 x 6 array). The 16 simulators of the inner 4 x 4 array burst in a 2.25-s time interval. All the simulators in the next ring (i.e., the outer ring of the inner 6 x 6 array) burst in a 6.00-s time interval, with the four corner simulators of this subarray bursting last. Power was terminated 0.60 s later; however, the temperature continued to increase (Fig. 22) for several seconds and then turned around and slowly decreased. The first simulator in the outer ring burst 0.40 s after power-off; all the simulators in the outer ring except the four corner ones burst by the time the average temperature reached its maximum value. The corner simulators, with the greatest external heat losses, were subjected to near-isothermal creep conditions and failed 25 to 50 s later as indicated in Fig. 24.

Tables 3 and 4 give computer output summaries of the important parameters recorded on magnetic tape during the test. There are no temperature entries in the tables for those simulators that were not instrumented with temperature sensors; however, measured pressure data are included for these simulators. Following our customary practice, the maximum measured temperature at the time of burst is selected as the burst temperature; these can be identified in Table 3 by the reader, and the measurement locations can be determined from Figs. 4 and 5.

The burst data are plotted in Fig. 25, using different symbols for the three radial zones indicated in the figure. As evident, data for the inner 4 x 4 array overlay the data for the outer ring of the inner 6 x 6; the respective average burst temperature and average burst pressure for these two zones were 933°C and 2800 kPa and 932°C and 2800 kPa. As expected, burst temperature data for the eight instrumented simulators in the outer ring of the 8 x 8 array were somewhat lower (average burst temperature of 924°C and average burst pressure of 3000 kPa) than data for the interior 6 x 6 array. The curve labeled "B-6 LSF" is a linear least-squares fit to all the B-6 data points. The range of the burst pressures for the remainder of the exterior simulators excluding the four corners is

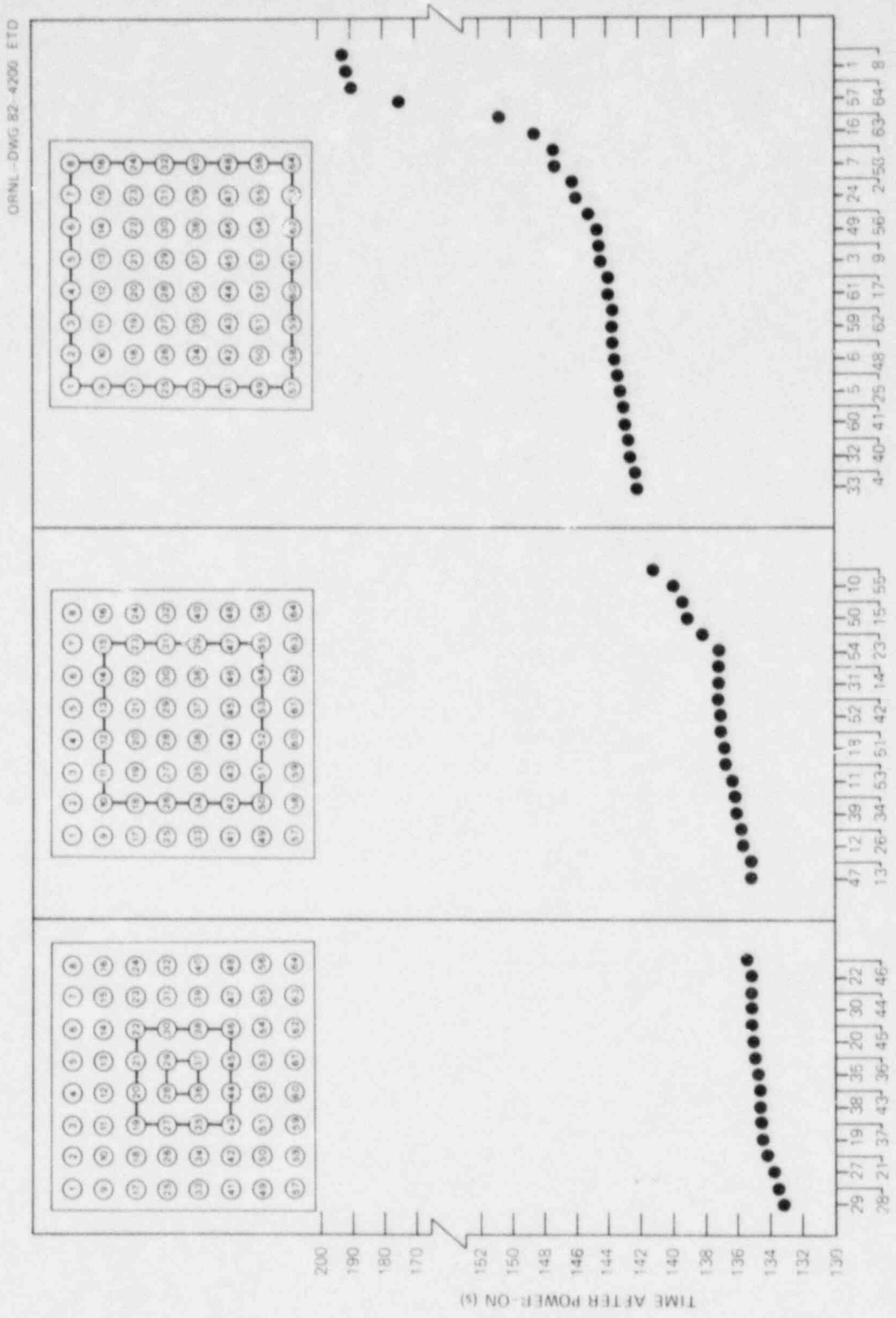

Fig. 24. Simulator burst times in B-6 test.

Table 3. B-6 Quick-look initial and burst conditions

MRBT BUNDLE B-6 ARRAY SIZE 8X8 TEST DATE DECEMBER 3, 1981

POWER-ON TIME 15:31: 0.0 RECORD # 249-A 24.800 SEC AFTER START OF SCAN 141.738 SEC BEFORE POWER-OFF
POWER-OFF TIME 15:33:21.74 RECORD # 1666-B 166.538 SEC AFTER START OF SCAN 141.738 SEC AFTER POWER-ON

NOTE: BURST TIMES WERE COMPUTER SELECTED (75KPA/50MS), THERMOCOUPLES WERE NOT ATTACHED TO RODS WHERE TEMPERATURES ARE OMITTED

SUMMARY OF BURST TEST RESULTS

ROD NO.	INITIAL CONDITIONS: DIFFERENTIAL PRESSURE (KPA)	INITIAL CONDITIONS: TEMPERATURES (DEG C) TE-1	TE-2	TE-3	TE-4	AVG	MAXIMUM PRESSURE DIFFERENTIAL (KPA)	APPROXIMATE BURST CONDITIONS: DIFFERENTIAL PRESSURE (KPA)	TEMPERATURES (DEG C) TE-1	TE-2	TE-3	TE-4	AVG	BURST TIME (SEC)	BURST RECORD NO.
1	3052						3308	2826						141.43	2163-B
2	3050						3250	3128						146.14	1710-B
3	3051	327	328	329	329	328	3236	3015	905	923	909	905	911	144.39	1693-A
4	3046						3235	2987						142.24	1671-B
5	3053	328	328	329	329	328	3241	2882	895	917	924	912	912	143.09	1680-A
6	3051						3235	2997						143.54	1684-B
7	3053						3227	3046						147.19	1721-A
8	3052						3324	2861						192.08	2170-A
9	3053						3253	3059						144.44	1693-B
10	3048	327	329	329	329	328	3235	2785	901	924	929	898	913	139.94	1648-B
11	3047	328	328	329	329	329	3240	2813	921	919	934	923	924	136.19	1611-A
12	3048	326	329	329	329	329	3249	2744	894	932	927	901	913	135.59	1605-A
13	3048	327	330	330	330	329	3229	2856	912	928	929	921	922	135.14	1600-B
14	3053	328	330	330	328	329	3236	2748	903	924	938	894	914	137.14	1620-B
15	3052	330	329	329	330	330	3244	2822	926	932	923	917	924	139.34	1642-B
16	3046						3219	3079						146.54	1734-B
17	3052	330	329	329	330	330	3234	2941	911	903	920	931	916	143.94	1688-B
18	3046	329	330	329	330	330	3238	2797	911	919	929	927	922	136.84	1617-B
19	3047	329	329	330	329	329	3253	2826	901	919	922	900	910	134.44	1593-B
20	3050	328	329	330	330	329	3240	2759	923	927	934	929	928	135.04	1599-B
21	3049	327	330	330	330	329	3245	2813	894	923	923	898	909	134.14	1590-B
22	3049	329	330	330	331	330	3234	2847	914	932	923	925	924	135.14	1600-B
23	3044	329	330	331	330	330	3244	2746	897	928	927	891	911	138.09	1630-A
24	3044						3219	3087						145.94	1708-B
25	3049						3235	2944						143.29	1682-A
26	3052	330	330	330	330	330	3256	2799	900	937	932	903	918	135.74	1606-B
27	3049	330	330	330	330	330	3249	2827	923	936	932	927	929	133.69	1586-A
28	3048	329	330	331	330	330	3253	2797	895	924	934	891	911	133.39	1583-A
29	3042	329	330	330	330	330	3242	2868	908	924	933	917	921	133.14	1580-B
30	3041	330	330	331	330	331	3229	2811	901	937	926	897	915	135.14	1600-B
31	3051	332	331	330	331	331	3230	2715	932	936	929	925	930	137.14	1620-B
32	3038	332	329	330	331	331	3245	2920	904	929	909	902	911	142.54	1674-B

Table 3 (continued)

MRBT BUNDLE B-6 ARRAY SIZE 8X8 TEST DATE DECEMBER 3, 1981

POWER-ON TIME 15:31: 0.0 RECORD # 249-A 24.600 SEC AFTER START OF SCAN 141.738 SEC BEFORE POWER-OFF
POWER-OFF TIME 15:33:21.74 RECORD # 1666-B 166.538 SEC AFTER START OF SCAN 141.738 SEC AFTER POWER-ON

NOTE: BURST TIMES WERE COMPUTER SELECTED (75KPA/50MS). THERMOCOUPLES WERE NOT ATTACHED TO RODS WHERE TEMPERATURES ARE OMITTED

SUMMARY OF BURST TEST RESULTS

ROD NO.	INITIAL CONDITIONS: DIFFERENTIAL PRESSURE (KPA)	INITIAL CONDITIONS: TEMPERATURES (DEG C) TE-1	TE-2	TE-3	TE-4	AVG	MAXIMUM PRESSURE DIFFERENTIAL (KPA)	APPROXIMATE BURST CONDITIONS: DIFFERENTIAL PRESSURE (KPA)	TEMPERATURES (DEG C) TE-1	TE-2	TE-3	TE-4	AVG	BURST TIME (SEC)	BURST RECORD NO.
33	3051	331	330	329	330	330	3227	2941	910	908	921	919	914	142.14	1670-B
34	3054	330	330	330	331	330	3239	2835	919	928	936	931	928	136.14	1610-B
35	3046	330	331	330	329	330	3238	2816	897	936	929	906	916	134.74	1596-B
36	3046	330	331	330	331	330	3231	2731	912	929	939	930	927	134.94	1598-B
37	3044	329	331	331	329	330	3248	2803	893	926	929	900	911	134.49	1594-A
38	3049	331	331	331	332	331	3251	2720	912	927	939	926	926	134.59	1595-A
39	3046	332	331	332	332	332	3241	2805	904	929	921	904	914	135.99	1609-A
40	3051						3252	2934						142.64	1675-B
41	3054						3232	2956						142.94	1678-B
42	3055	330	330	331	330	330	3234	2815	901	916	934	887	912	137.09	1626-A
43	3049	331	331	331	331	331	3242	2785	919	936	928	922	926	134.64	1595-B
44	3043	329	330	331	330	330	3245	2845	897	934	923	892	911	135.14	1600-B
45	3041	329	331	331	331	331	3230	2763	913	924	935	927	925	135.14	1600-B
46	3038	330	331	331	331	331	3240	2770	897	933	936	908	918	135.39	1603-A
47	3045	332	331	329	332	331	3244	2909	916	925	907	914	916	135.14	1600-B
48	3047	332	332	329	330	331	3236	2962	905	916	923	898	911	143.64	1685-B
49	3063						3256	2996						144.59	1695-A
50	3057	329	330	330	330	330	3251	2810	914	913	916	932	919	139.04	1639-B
51	3055	329	330	330	330	330	3259	2842	903	924	913	892	908	136.99	1619-A
52	3053	329	330	331	331	330	3248	2837	916	920	923	927	922	137.04	1619-B
53	3055	327	330	331	330	330	3248	2821	895	928	916	895	908	136.74	1616-B
54	3053	330	331	330	331	330	3245	2710	923	934	911	926	924	137.14	1620-B
55	3049	330	330	331	330	330	3252	2759	912	941	941	890	921	141.14	1660-B
56	3052						3231	3127						145.79	1707-A
57	3059						3299	2975						174.64	1995-B
58	3054						3231	3014						147.29	1722-A
59	3056						3241	2977						143.64	1685-B
60	3058	330	329	329	330	329	3255	2933	918	907	903	913	910	142.84	1677-B
61	3047						3225	3012						143.94	1688-B
62	3058	329	329	330	331	330	3249	2995	925	915	903	912	914	143.64	1685-B
63	3054						3213	3043						150.64	1755-B
64	3054						3327	2865						189.23	2141-B

Table 4. B-6 Quick-look initial and maximum pressure conditions

MRBT BUNDLE B-6 ARRAY SIZE 8X8 TEST DATE DECEMBER 3, 1981

POWER-ON TIME 15:31: 0.0 RECORD # 249-A 24.800 SEC AFTER START OF SCAN 141.738 SEC BEFORE POWER-OFF
POWER-OFF TIME 15:33:21.74 RECORD # 1666-B 166.538 SEC AFTER START OF SCAN 141.738 SEC AFTER POWER-ON

NOTE: THERMOCOUPLES WERE NOT ATTACHED TO RODS WHERE TEMPERATURES ARE OMITTED

SUMMARY OF MAXIMUM PRESSURES

ROD NO.	INITIAL CONDITIONS DIFFERENTIAL PRESSURE (KPA)	INITIAL CONDITIONS TEMPERATURES (DEG C) TE-1	TE-2	TE-3	TE-4	AVG	CONDITIONS AT TIME OF MAXIMUM PRESSURES DIFFERENTIAL PRESSURE (KPA)	TEMPERATURES (DEG C) TE-1	TE-2	TE-3	TE-4	AVG	TIME (SEC)	RECORD NO.
1	3052						3308						147.09	1720-A
2	3050						3250						114.34	1342-B
3	3051	327	328	329	329	328	3236	821	836	824	821	826	115.64	1405-B
4	3046						3235						110.09	1350-A
5	3053	328	328	329	329	328	3241	796	810	811	801	804	110.04	1349-B
6	3051						3235						110.39	1353-A
7	3053						3227						115.19	1401-A
8	3052						3324						146.84	1717-B
9	3053						3253						115.19	1401-A
10	3048	327	329	329	329	328	3235	796	816	819	798	806	108.54	1334-B
11	3047	328	328	329	329	329	3240	814	821	829	820	821	108.34	1332-B
12	3048	326	329	329	329	329	3249	791	824	820	798	808	105.99	1309-A
13	3048	327	330	330	330	329	3229	814	830	833	826	826	108.94	1338-B
14	3053	328	330	330	328	329	3236	809	834	834	804	820	110.24	1351-B
15	3052	330	329	329	330	330	3244	823	829	832	827	828	110.64	1355-B
16	3046						3219						115.09	1400-A
17	3052	330	329	329	330	330	3234	817	814	828	833	823	113.24	1381-B
18	3046	329	330	329	330	330	3238	822	830	832	828	828	110.64	1349-B
19	3047	329	329	330	329	329	3253	806	827	827	801	815	108.49	1334-A
20	3050	328	329	330	330	329	3240	827	834	840	832	833	110.19	1351-A
21	3049	327	330	330	330	329	3245	799	829	825	803	814	107.79	1327-A
22	3049	329	330	330	331	330	3234	817	828	829	823	824	108.44	1333-B
23	3044	329	330	331	330	330	3244	784	812	814	783	798	105.54	1304-B
24	3044						3219						116.04	1409-B
25	3049						3235						114.24	1391-B
26	3052	330	330	330	330	330	3256	808	831	830	807	819	109.09	1340-A
27	3049	330	330	330	330	330	3249	812	821	822	816	818	103.74	1306-B
28	3048	329	330	331	330	330	3253	778	802	804	777	790	101.64	1265-B
29	3042	329	330	330	330	330	3242	809	820	822	813	816	106.29	1312-A
30	3041	330	330	331	330	331	3229	808	833	830	806	819	108.69	1336-A
31	3051	332	331	330	331	331	3230	818	828	825	820	823	107.49	1324-A
32	3038	332	329	330	331	331	3245	819	838	834	825	829	115.24	1401-B

Table 4 (continued)

MRBT BUNDLE B-6 ARRAY SIZE 8X8 TEST DATE DECEMBER 3, 1981

POWER-ON TIME 15:31: 0.0 RECORD # 249-A 24.800 SEC AFTER START OF SCAN 141.738 SEC BEFORE POWER-OFF
POWER-OFF TIME 15:33:21.74 RECORD # 1666-B 166.538 SEC AFTER START OF SCAN 141.738 SEC AFTER POWER-ON

NOTE: THERMOCOUPLES WERE NOT ATTACHED TO RODS WHERE TEMPERATURES ARE OMITTED

SUMMARY OF MAXIMUM PRESSURES

ROD NO.	INITIAL CONDITIONS DIFFERENTIAL PRESSURE (KPA)	INITIAL CONDITIONS TEMPERATURES (DEG C) TE-1	TE-2	TE-3	TE-4	AVG	CONDITIONS AT TIME OF MAXIMUM PRESSURES DIFFERENTIAL PRESSURE (KPA)	TEMPERATURES (DEG C) TE-1	TE-2	TE-3	TE-4	AVG	TIME (SEC)	RECORD NO.
33	3051	331	330	329	330	330	3227	816	823	820	818	819	112.29	1372-A
34	3054	330	330	330	331	330	3239	817	823	824	822	822	107.34	1322-B
35	3046	330	331	330	329	330	3238	816	844	840	818	830	111.09	1360-A
36	3046	330	331	330	331	330	3231	801	814	816	807	809	104.59	1295-A
37	3044	329	331	331	329	330	3248	791	819	816	794	805	105.74	1306-B
38	3049	331	331	331	332	331	3251	806	817	820	812	814	105.29	1302-A
39	3046	332	331	332	332	332	3241	800	823	816	796	809	106.44	1313-B
40	3051						3252						114.89	1398-A
41	3054						3232						117.49	1424-A
42	3055	330	330	331	330	330	3234	810	834	833	805	820	110.64	1355-B
43	3049	331	331	331	331	331	3242	805	817	817	809	812	105.24	1301-B
44	3043	329	330	331	330	330	3245	796	824	822	797	810	107.54	1324-B
45	3041	329	331	331	331	331	3230	818	830	831	826	827	109.84	1337-B
46	3038	330	331	331	331	331	3240	813	843	840	817	826	111.04	1359-B
47	3045	332	331	329	332	331	3244	806	823	818	814	818	107.49	1324-A
48	3047	332	332	329	330	331	3236	818	820	827	812	819	113.74	1386-B
49	3063						3256						114.94	1398-B
50	3057	329	330	330	330	330	3251	825	831	833	832	830	111.54	1364-B
51	3055	329	330	330	330	330	3259	781	806	800	779	791	103.84	1287-B
52	3053	329	330	331	331	330	3248	830	840	841	836	837	111.59	1365-A
53	3055	327	330	331	330	330	3248	786	812	812	788	800	105.84	1307-B
54	3053	330	331	330	331	330	3245	832	837	831	834	834	111.34	1362-B
55	3049	330	330	331	330	330	3252	806	827	824	798	814	110.14	1350-B
56	3052						3231						114.04	1389-B
57	3059						3239						146.99	1719-A
58	3054						3231						115.04	1399-B
59	3056						3241						114.09	1390-A
60	3058	330	329	329	330	329	3255	796	798	800	802	800	107.59	1325-A
61	3047						3225						116.04	1409-B
62	3058	329	329	330	331	330	3249	823	836	812	817	817	111.34	1362-B
63	3054						3213						116.24	1411-B
64	3054						3327						146.79	1717-A

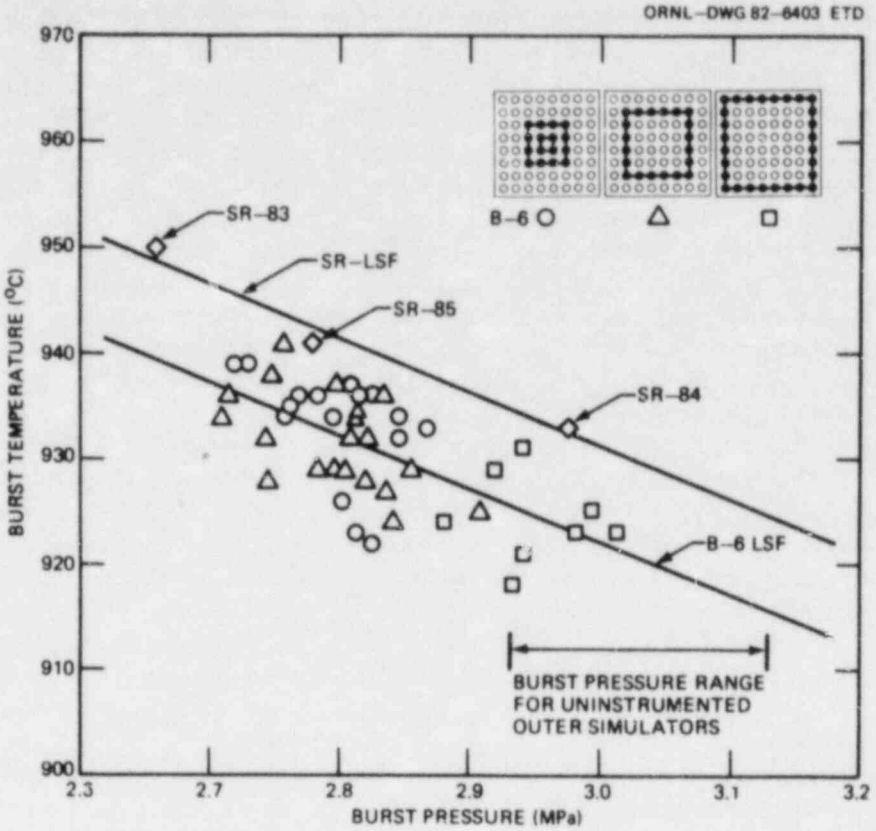

Fig. 25. Experimental burst temperature and pressure data.

noted. The corner simulators failed 25 to 50 s later in a creep mode and represent a different set of conditions. Burst temperatures for those simulators without temperature sensors will be estimated when the data are analyzed.

Although a difference can be detected between the data for the external and internal simulators, note that the pressure scale is greatly expanded to facilitate plotting of the individual data points. In reality, the difference between maximum and minimum burst pressures was only ~400 kPa. By way of comparison, the burst pressure variation in the B-5 test was about 2200 kPa, while the burst temperature variation was about the same for the two tests.

Prior to performing the B-6 test, three single-rod heated shroud tests were conducted[11] with heating rates in the range of 5 to 6°C/s to aid selection of the B-6 test parameters. The burst data for these three tests are included in the plot for comparison; the curve labeled "SR-LSF" is a linear least-squares fit of the three single-rod data points. While the two fitted curves have virtually identical slopes, the bundle curve is about 10°C lower than the single-rod curve. Some of this difference may be caused by the slightly lower heating rate in the bundle test (3.5 vs 5.5°C/s), but most of the difference is attributed to our use of fewer thermocouples to measure temperatures in bundle simulators than in single-rod simulators (i.e., 4 vs 12), and thus a greater statistical probability exists for underestimating burst temperatures in bundle tests.

Figure 26 shows initial-to-burst pressure ratios for each of the three radial zones of the array. This parameter is related to the volume change of the cladding heated length and, hence, provides a qualitative indication of simulator average deformation over this length. These data are consistent with those given in the previous figure and indicate that the inner 6 x 6 array deformed more than the external ring; there was no significant difference between the inner 4 x 4 array and the next outer ring. Again, note that the scale for the ordinate is greatly expanded to facilitate plotting. The reader should be careful to take this fact into account when comparing this figure with similar plots we have published for the B-5 test. (The B-5 initial-to-burst pressure ratios ranged from about 1.2 to 1.5, considerably greater than the B-6 data range; hence, deformation in B-6 is much less than in B-5.)

Typical measured steam temperatures (see Fig. 6 for thermocouple locations) at the inlet (TE-322) and at the outlet (TE-327) and vessel pressure (PE-301) are shown in Fig. 27; TAV-10 is included to characterize the bundle temperature. Neither the inlet nor outlet steam thermocouples indicated unstable temperatures during the time the interior simulators were bursting (i.e., before power-off as noted by the arrow on the time axis); however, the outlet steam thermocouple sensed a temperature increase after the sudden vessel pressure decrease. This temperature increase was probably an effect of increased steam flow caused by opening the large bypass valve downstream of the vessel.

As mentioned previously, the need for electrical isolation between the test array and the closely fitted shroud precluded Joule heating of the shroud. Although the shroud had a highly polished, gold-plated surface to reflect thermal radiation, the temperature of the shroud increased significantly during the test. Figure 28 compares measured shroud temperatures on each of the four sides (at the 76-cm elevation) with the characteristic bundle temperature (TAV-10). Differences of ~100°C were measured around the shroud before the first tube burst. Similar temperatures and behavior were noted for the shroud thermocouples at the 28-cm elevation. Figure 29 compares shroud temperature measurements at the two instrumented levels on the north side of the bundle with simulator temperatures measured in the vicinity (see Fig. 4). The average of the eight shroud temperature measurements was ~165°C less than the bundle average temperature during the time deformation was occurring (i.e., 1 s before the first tube burst).

Posttest Examination

Following the burst test, the test assembly was removed from the test vessel and partially disassembled for observation and examination. After performing posttest instrumentation checks, the shroud assembly was removed to permit visual observation and dimensional checks of the test array. Further disassembly (including successful removal of the internal heater from all except four of the outer ring of simulators) was then accomplished, and photographs were made to document the appearance in detail.

Figure 30 shows the west face of the assembly after removal of the shroud and internal heaters. The meter stick (suspended from the bundle

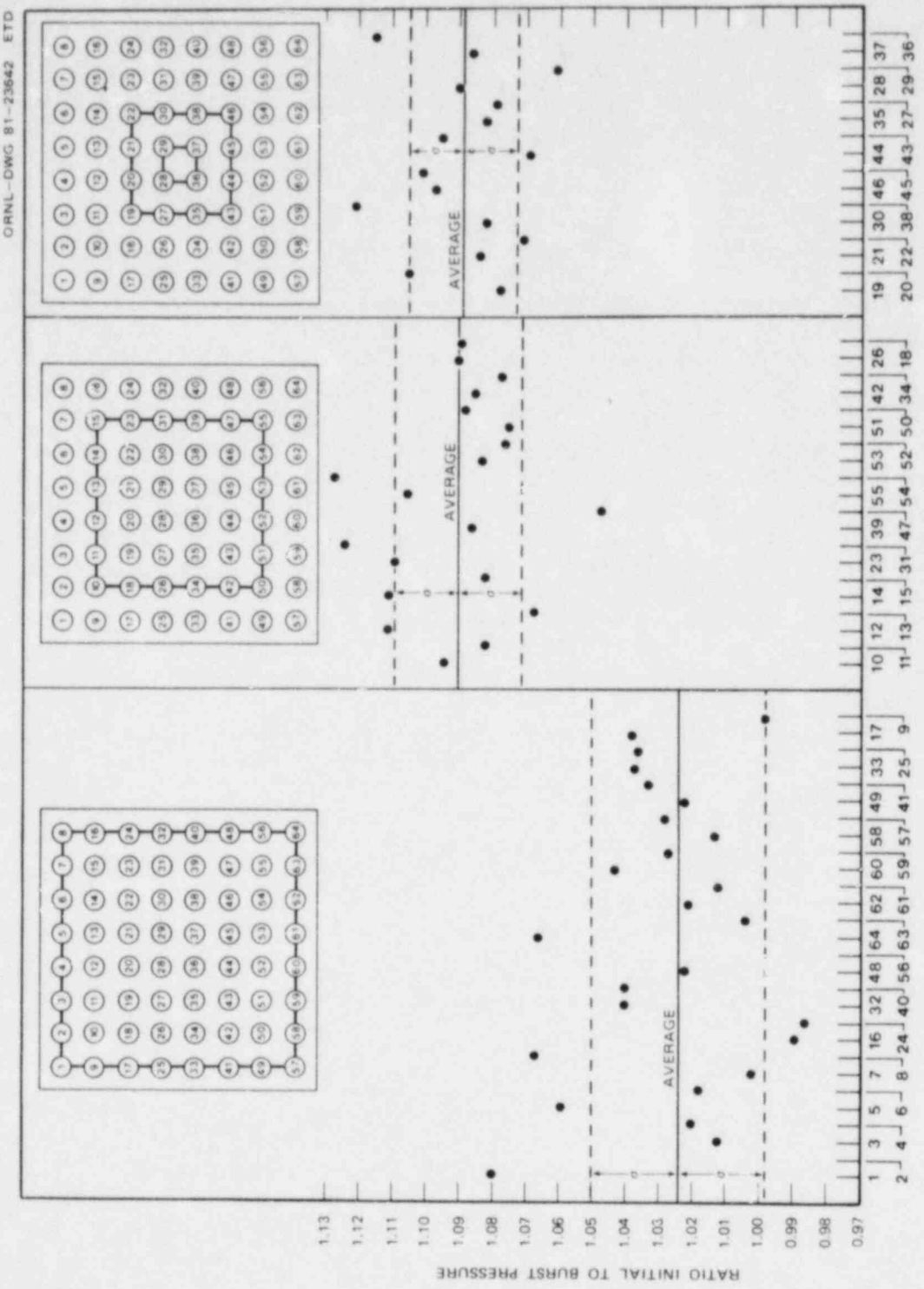

Fig. 26. Initial-to-burst pressure ratios in B-6 test.

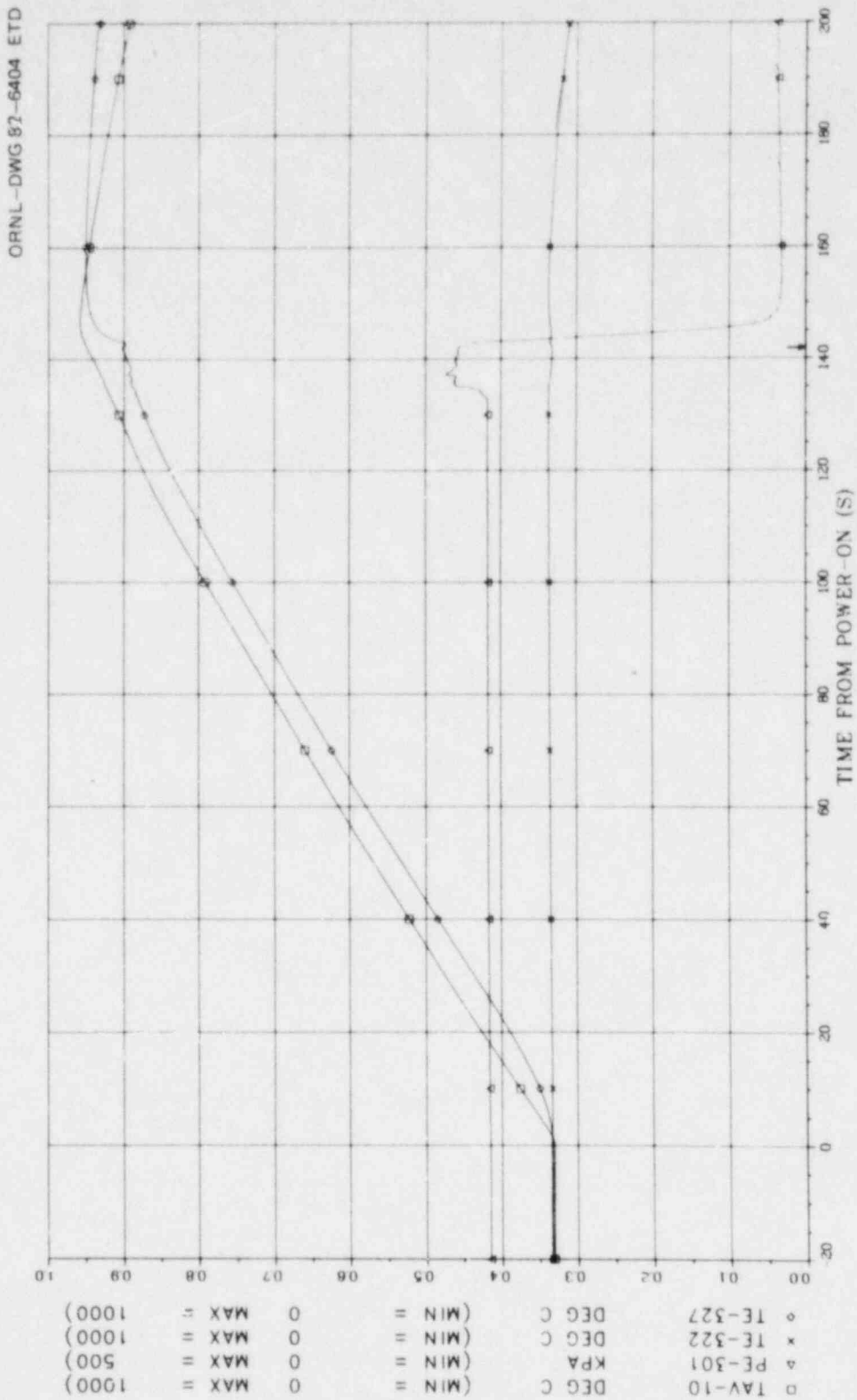

Fig. 27. Typical steam-related parameters during B-6 test.

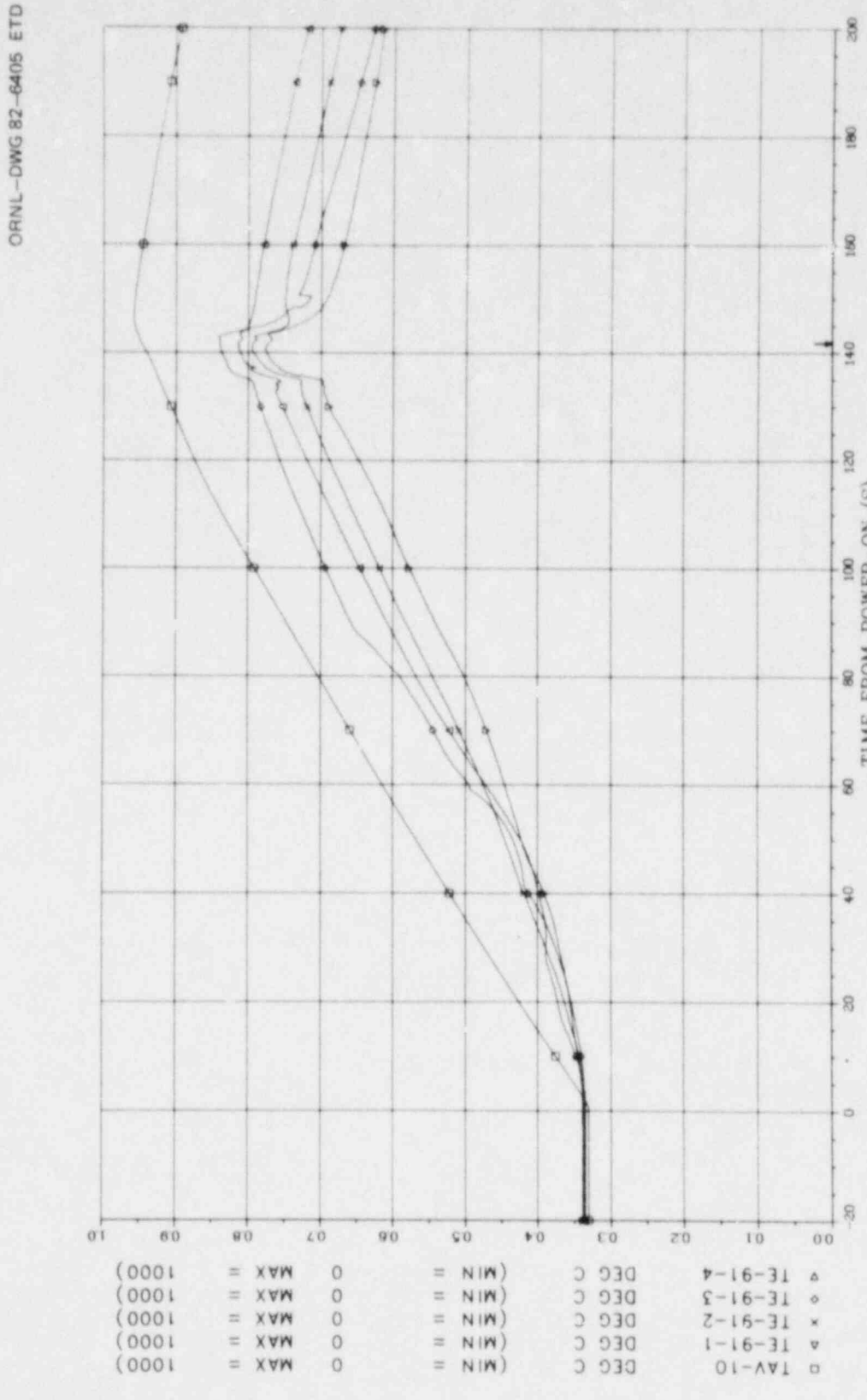

Fig. 28. Shroud temperature measurements at the 76-cm elevation.

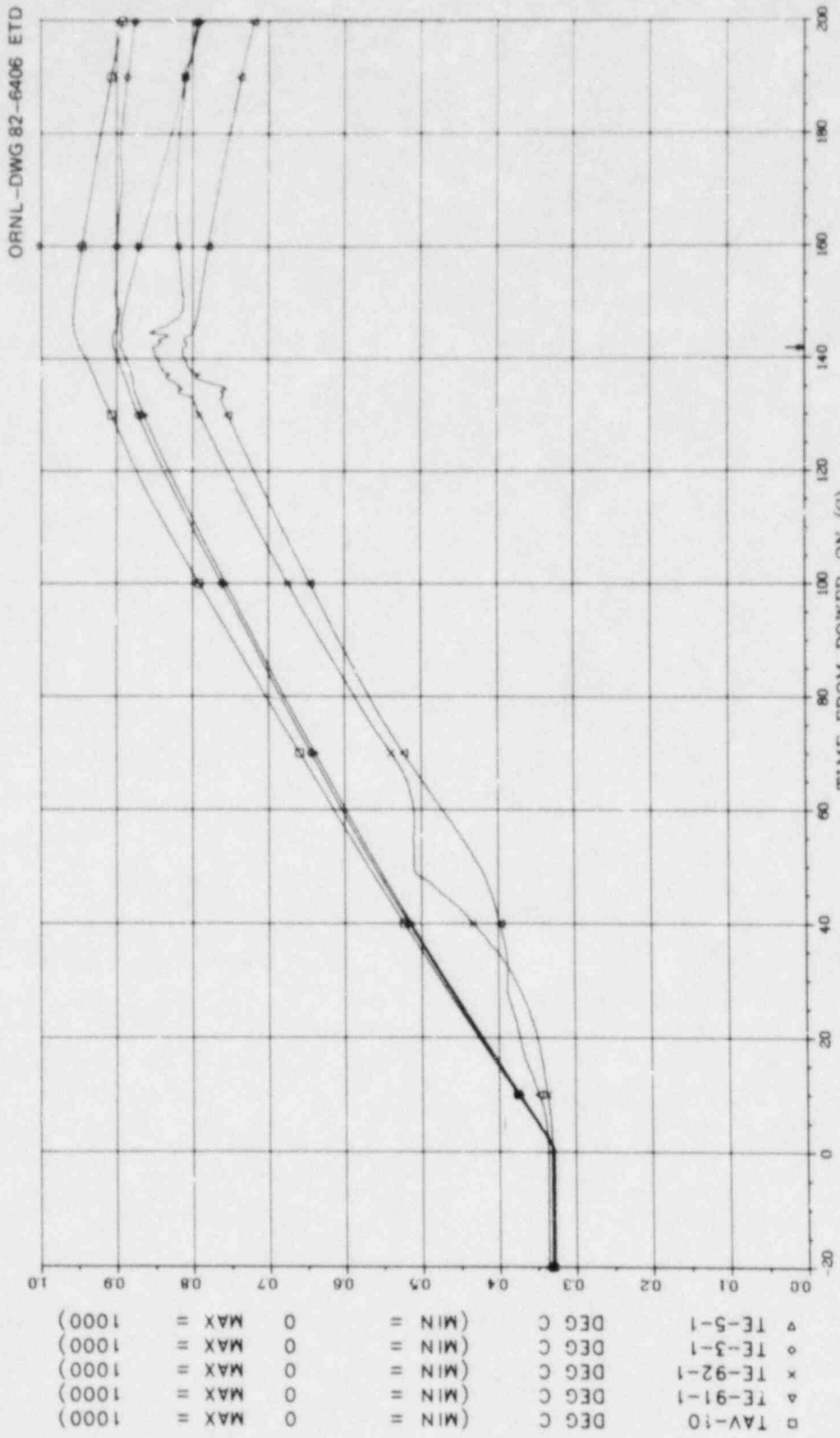

Fig. 29. Comparison of shroud and simulator temperature measurements on the north side of the array.

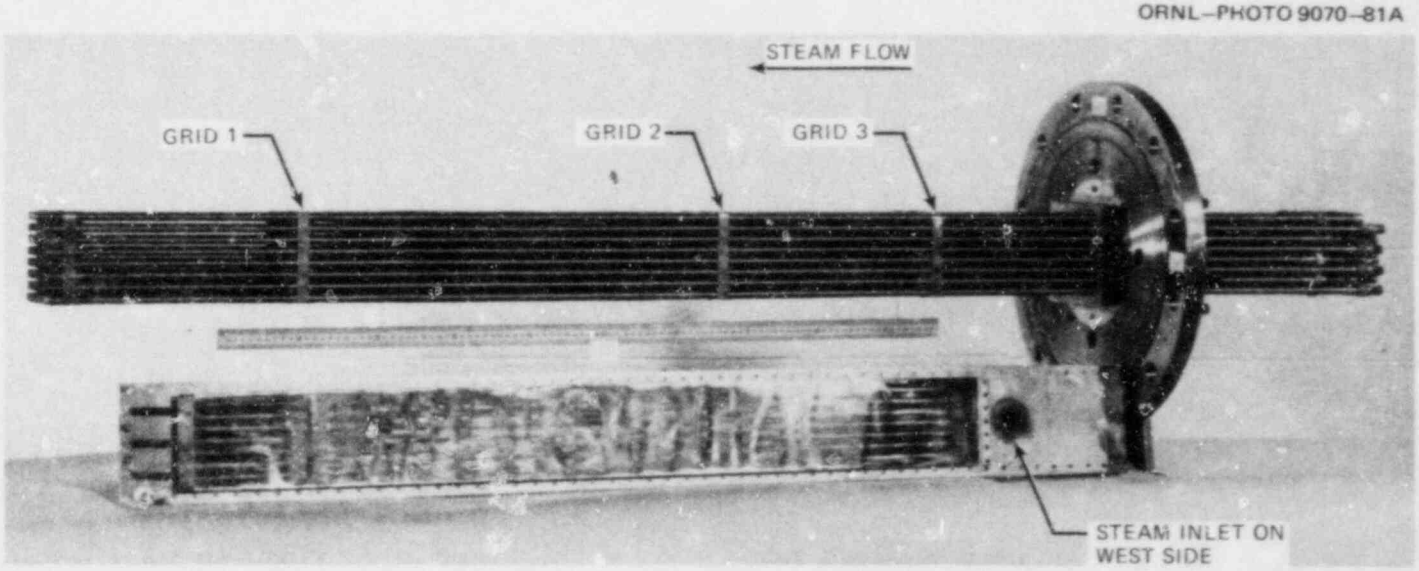

Fig. 30. Posttest view of west face of B-6 test array and shroud.

with zero at the bottom of the heated zone) serves as a convenient reference to the discussion throughout this report. The west face of the shroud box is also shown in its relative axial position; one of the two inlet steam nozzles (see Fig. 2) is noted.

The thin shroud liner shows discolorations that reflect the image of the test array. Evidence of liner distortion, indicating contact with the test array, is also present. Even though springs were attached at the lower end of the thin liner (to the left in Fig. 30) to keep it taut during the test, wrinkles appear at numerous places, indicating thermal distortion and/or restricted axial movement; this probably accounts for the unusual behavior observed in the shroud temperature plots during the first 80 s of the transient (see Figs. 28 and 29).

Close-up views of the region between the No. 1 and No. 3 grids are shown in Figs. 31–34. The west face, the same one as presented in Fig. 30, is shown in detail in Fig. 31. The pretest centerline elevation of the No. 1 grid was 10 cm and of the No. 2 grid was 66 cm. The region between the No. 2 and the No. 3 grid is the thermal entrance region.

Several noteworthy features are apparent in Fig. 30: (1) deformation is moderate and fairly uniform (except for the immediate vicinity of the bursts) over the lower half of the region between grids 1 and 2, (2) very little deformation is evident between grids 2 and 3, (3) very little length change occurred, (4) all visible bursts are directed inward, and (5) deformation of the four corner rods is atypical. This latter observation results from the fact that the corner rods, having more exposed surface area and thus greater heat losses, did not burst until 25 to 50 s after the remainder (see Fig. 24). During this delay, the tubes were subjected to near-isothermal creep conditions; as a result, their deformation behavior was different from the remainder of the tubes, which deformed under transient heating conditions.

Because flow characterization tests were not performed, the bundle was next cast into an epoxy matrix and sectioned transversely at about 60 axial locations. The sections were polished sufficiently to sharply define the tube wall boundaries and photographed to facilitate acquisition of deformation data. Burst locations are given in Table 5. The axial locations were determined by internal examination of the tubes with a borescope before encapsulation with epoxy and confirmed later from measurements of the sections; the midpoint elevations and burst lengths are considered reasonably accurate (to within 3 to 5 mm). The azimuthal orientations were determined from angle measurements made on the sections near the end of the burst opening and are probably accurate to within 5 to 10° of arc length. Burst midpoint elevations and orientations are shown schematically in Figs. 35 and 36, respectively.

As evident in Fig. 35, the bursts occurred over a length of ~28 cm in the lower portion of the region between the two interior grids (centerline elevations of 10 and 66 cm); this is consistent with the axial temperature profile shown in Fig. 20. Although the steam mass flux was the same as in the previous tests, the very low cladding heating rate, in effect, caused this steam flow to have a relatively greater cooling effect and displaced the deformation downward (i.e., in the direction of steam flow).

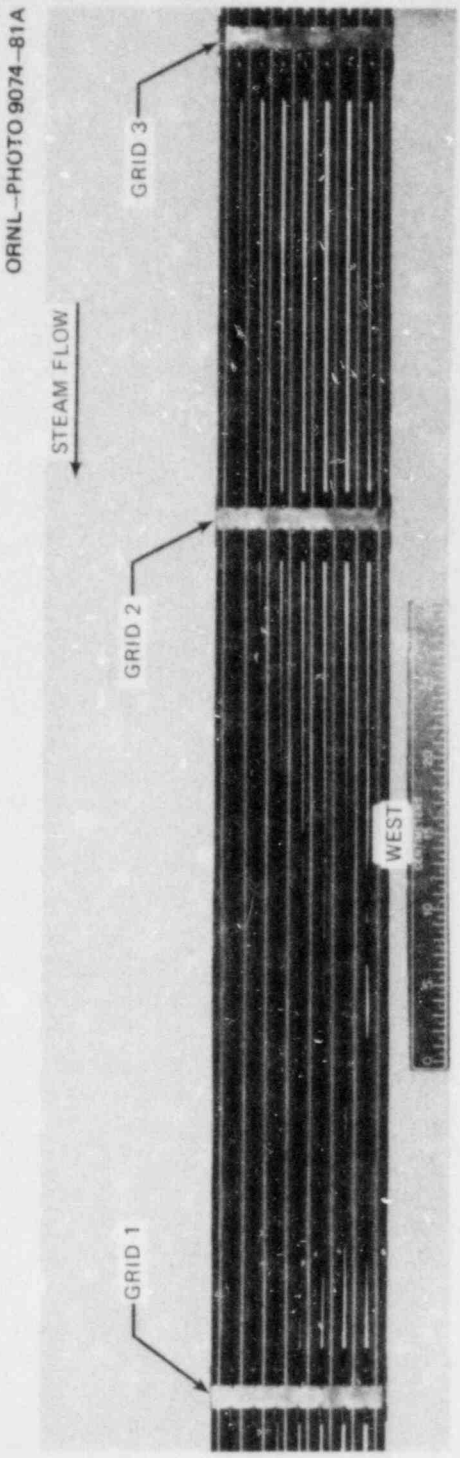

Fig. 31. Close-up view of west face of B-6 test array.

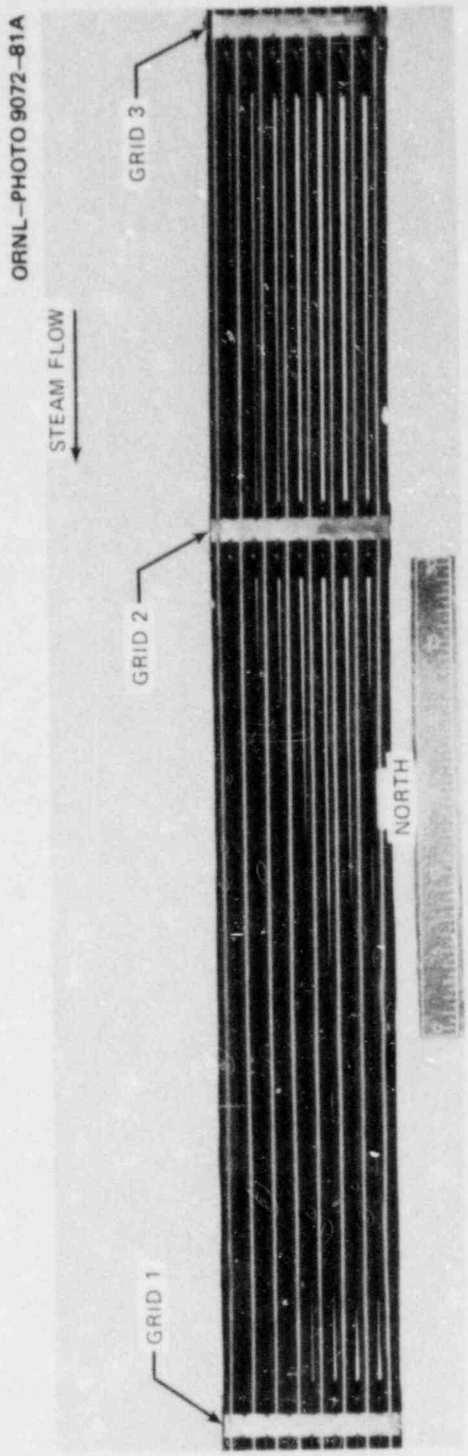

Fig. 32. Close-up view of north face of B-6 test array.

ORNL–PHOTO 9071–81A

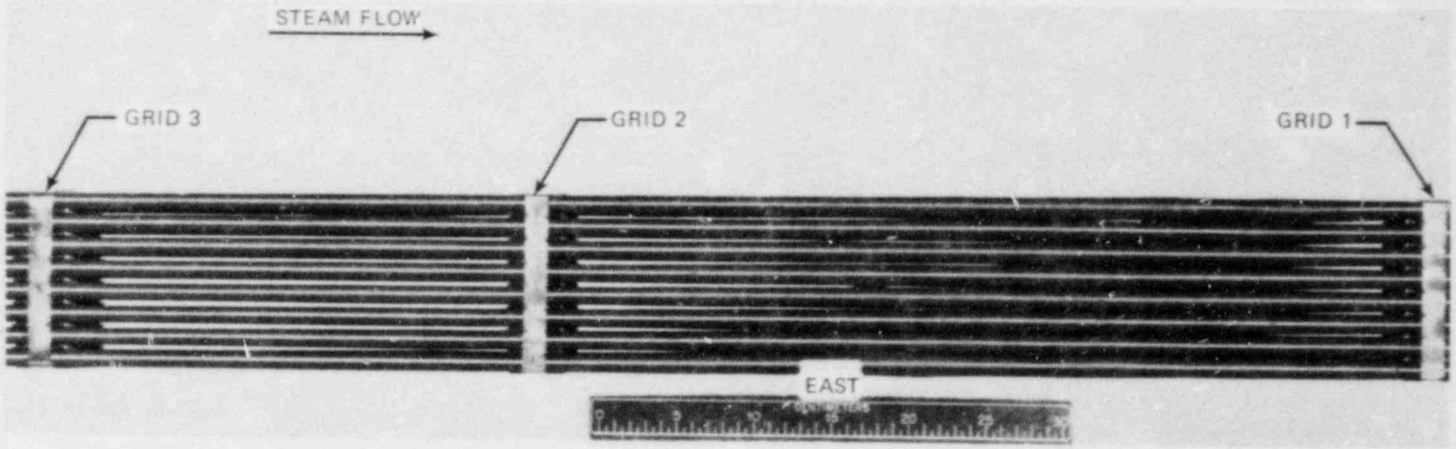

Fig. 33. Close-up view of east face of B-6 test array.

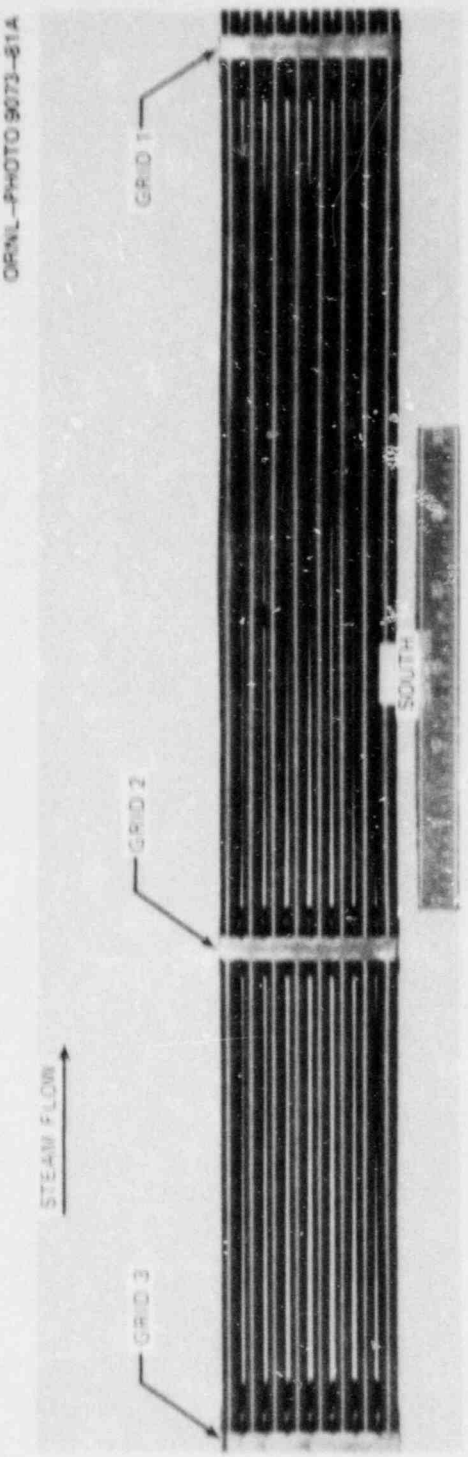

Fig. 34. Close-up view of south face of B-6 test array.

Table 5. Burst locations in B-6 test array

Simulator No.	Burst location		Burst length (mm)	Simulator No.	Burst location		Burst length (mm)
	Axial[a] (mm)	Angle[b] (deg)			Axial[a] (mm)	Angle[b] (deg)	
1	374	115	14	33	213	100	25
2	179	158	12	34	243	55	19
3	343	200	26	35	225	350	31
4	337	180	23	36	200	305	17
5	338	190	23	37	269	0	36
6	266	180	24	38	456	45	21
7	268	180	21	39	219	290	29
8	189	238	8	40	383	295	21
9	190	120	13	41	217	102	24
10	329	173	22	42	208	100	31
11	203[c]	144[c]	6[c]	43	247	40	18
12	259	100	36	44	193	45	14
13	204[c]	152[c]	9[c]	45	296	145	13
14	332	113	19	46	199	62	19
15	218	240	20	47	381	317	23
16	388	260	18	48	383	270	32
17	205[c]	90[c]	14[c]	49	236	50	14
18	202[c]	135[c]	6[c]	50	213	45	14
19	346	80	24	51	235	57	14
20	349	318	16	52	391	45	14
21	302	95	37	53	238	355	38
22	304	315	17	54	301	315	21
23	278	5	40	55	322	333	17
24	328	275	23	56	401	310	18
25	313	90	25	57	234	45	7
26	259	60	13	58	317	0	27
27	256	45	20	59	392	350	25
28	227	75	30	60	387	350	22
29	389	45	24	61	389	315	15
30	285[c]	270[c]	16[c]	62	385[c]	0[c]	16[c]
31	264	320	25	63	314	350	26
32	329	265	22	64	423	277	15

[a]Posttest midpoint elevation above bottom of heated zone. The bottom of heated zone of the bundle (zero elevation) represents an average of all rods.

[b]Clockwise rotation looking down on top of bundle. Estimated angle of rupture initiation.

[c]Burst probably initiated at thermocouple attachment.

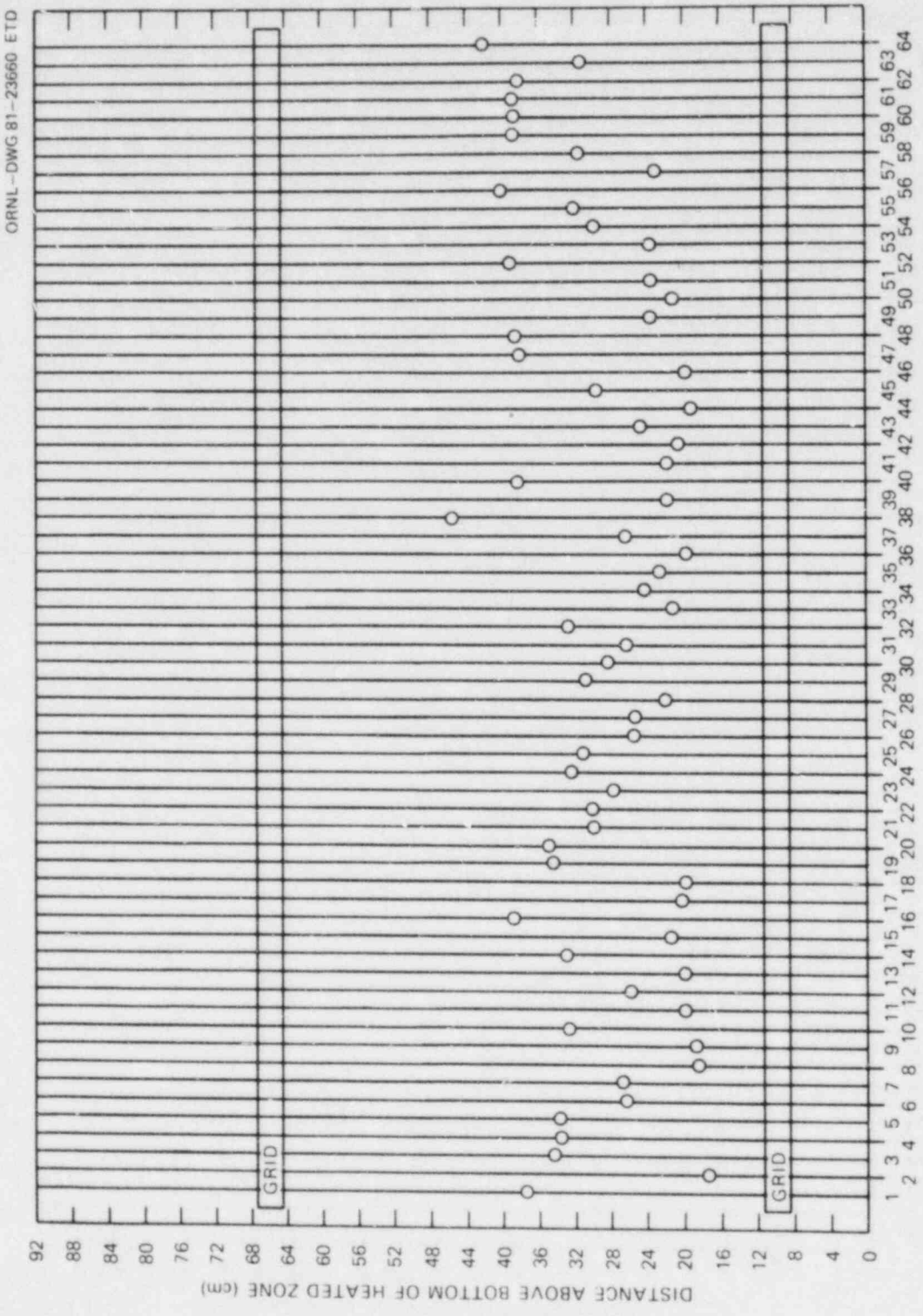

Fig. 35. Approximate burst midpoint elevations.

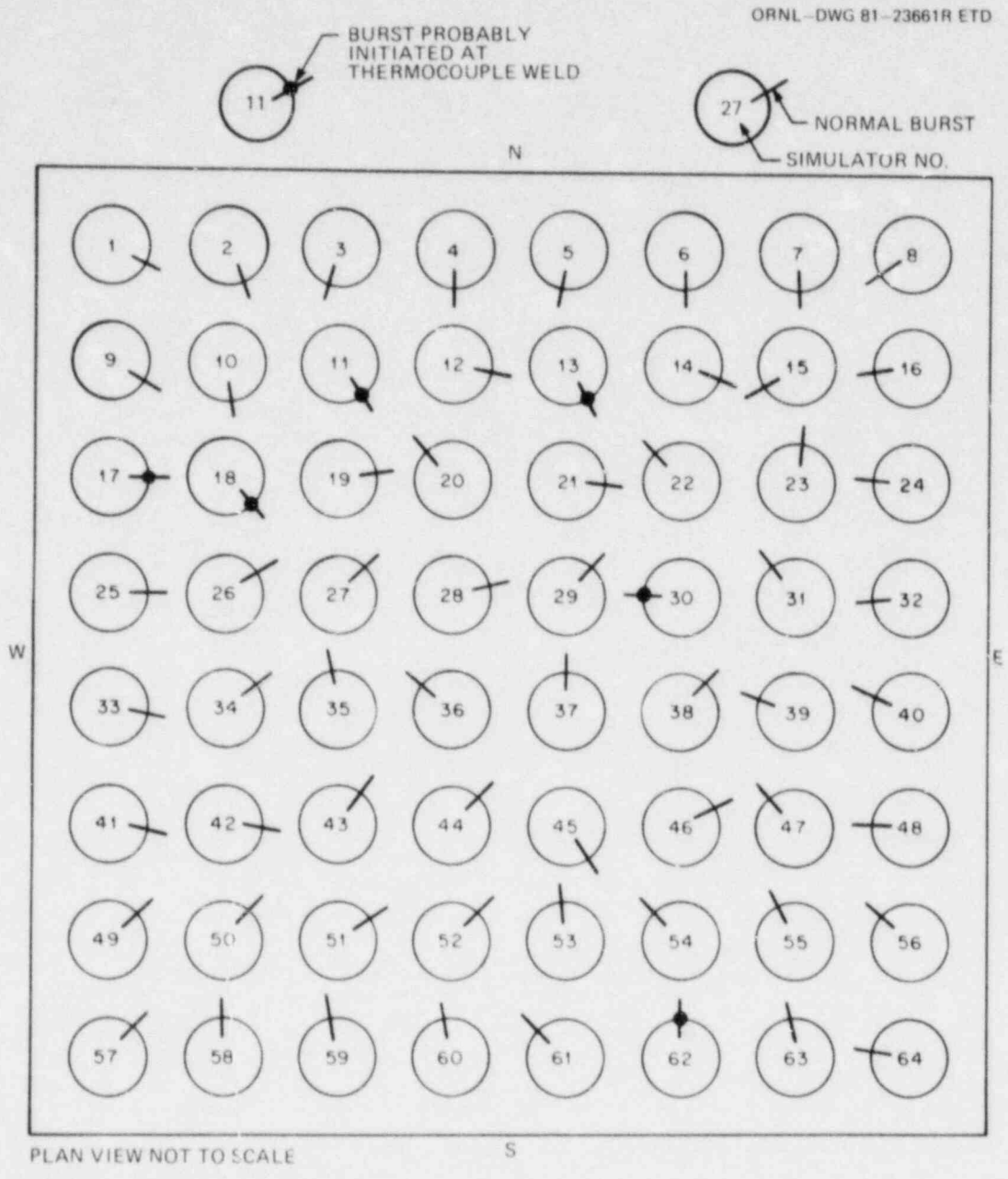

Fig. 36. Approximate burst midpoint orientations.

As evident in Fig. 36, burst orientations in the two outer rings of simulators had a preferred (and rather uniform) direction toward the center of the bundle, indicating the influence of azimuthal temperature gradients (and an unusually high sensitivity of the creep rate equation to temperature in the alpha-plus-beta phase temperature range[23]) in each ring superimposed on the uniform radial distribution. Burst directions for the inner 4 x 4 array were more randomly distributed, indicating negligible azimuthal gradients. As noted in the figure, six bursts probably initiated at thermocouple spot welds. However, the unusual consistency in

burst times, temperatures, pressures, and deformation profiles indicate that the bursts were not premature. Also, the burst opening shapes and lengths (Table 5) suggested nothing unusual about these failures. (In previous bundle tests, failures at thermocouple spot welds resulted in very small pinholes.)

A selection of section photographs is presented in Figs. 37–42 to show interesting deformation features. Each photograph was taken looking down on top of the bundle, with the two arrow points and the scale being on the north side (i.e., the northwest corner tube is No. 1), so that the tube numbering system conforms to that of Fig. 4. Figure 37 shows the section at the 20.3-cm elevation. Four failures (tubes 11, 13, 17, and 18) that probably initiated at thermocouple spot welds occurred at this elevation. Although the failure angles for tubes 11 and 13 (see Fig. 4) are slightly different from the specified thermocouple location, there is physical evidence the failures were at the spot welds.

Localized wall thinning at other than the immediate vicinity of the tube failures was observed at a number of locations; typical examples are noted by tube 42 in Fig. 37, tube 35 in Fig. 38, tube 54 in Fig. 39, tube 46 in Fig. 40 [incipient failure (?), although the failure was at a much lower elevation (Fig. 37)], tube 20 in Fig. 41 (at two places), and tube 38 in Fig. 42. While some of the locally thinned areas (at least before the burst) were opposite neighboring tubes (tube 42 in Fig. 37 is an example), a number of the thinned areas were located ~$\pi/4$ rad around (tube 20 in Fig. 41, for example) from neighboring tubes. Presumably, very small azimuthal temperature gradients, combined with the high sensitivity of the creep rate equation to temperature in the alpha-plus-beta phase region,[23] were responsible for the localized thinning.

Enlarged photographs of the sections were digitized to facilitate reduction of the geometrical data to strains, areas, and volumes. Although reduction of the digitized data is not complete, it has progressed sufficiently to provide quick-look estimates of the important parameters. Preliminary burst strain data are plotted (by zones) in Fig. 43; the average and one standard deviation (σ) values are noted for each of the radial zones. As mentioned earlier, the four corner simulators deformed and failed under near-isothermal creep conditions much later (see Fig. 24) than the other simulators. As a result, deformation of these simulators was greater and atypical, as indicated by the large burst strains (relative to the other simulators in the outer ring). For this reason, they were excluded from the average of this zone. The figure shows that burst strain was not strongly dependent on position, although the data for the outer ring does reflect a small effect of azimuthal temperature gradients.

As mentioned earlier, three single-rod heated shroud tests were conducted prior to the bundle test to aid definition of bundle test conditions. Burst strains[11] for the three tests (36, 36, and 37%) were consistent with the results of this test.

The quick-look strain matrix was used to calculate the volumetric expanse of each tube over the heated length. These data are shown in Fig. 44 for each of the three radial zones of the bundle. The figure shows also that the volumetric expansion, like burst strain, was not strongly dependent on position, although the data for the outer ring of simulator does reflect a small effect of azimuthal temperature gradients.

ORNL–PHOTO 3497–82

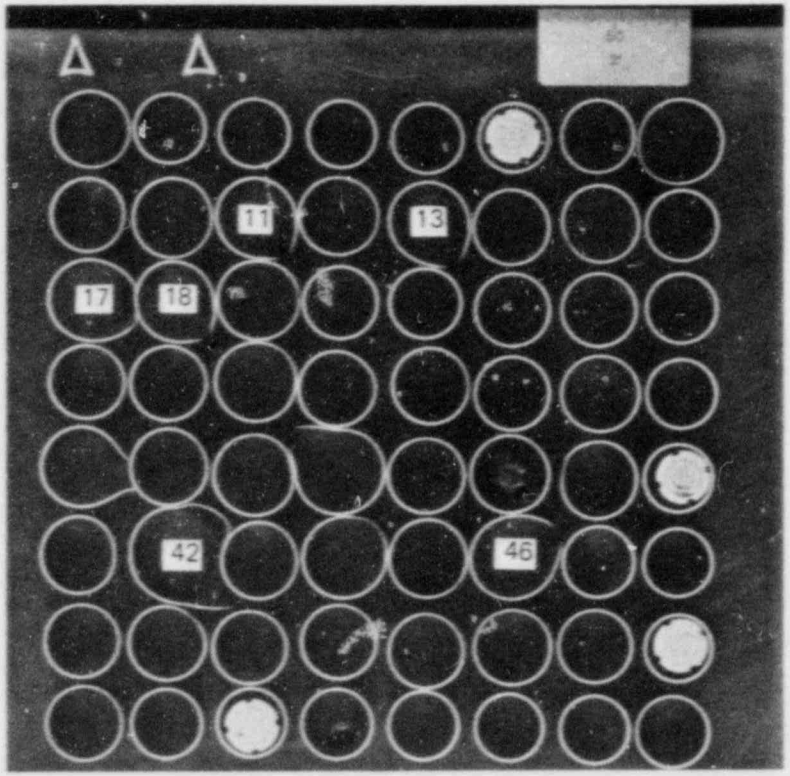

Fig. 37. Section through B-6 bundle at 20.3-cm elevation.

ORNL–PHOTO 3498–82

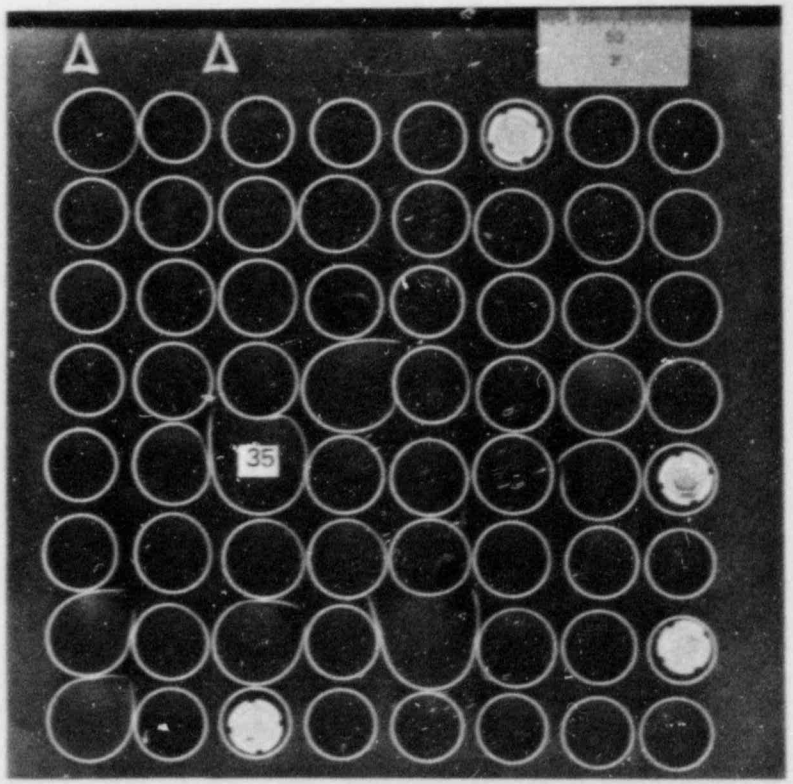

Fig. 38. Section through B-6 bundle at 23.2-cm elevation.

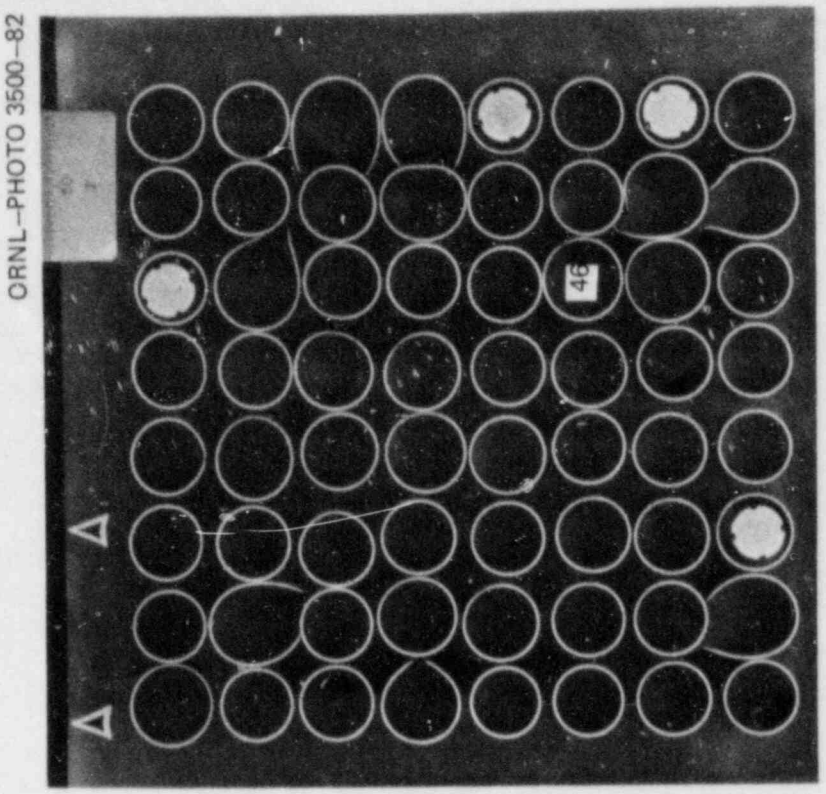

Fig. 40. Section through B-6 bundle at 32.4-cm elevation.

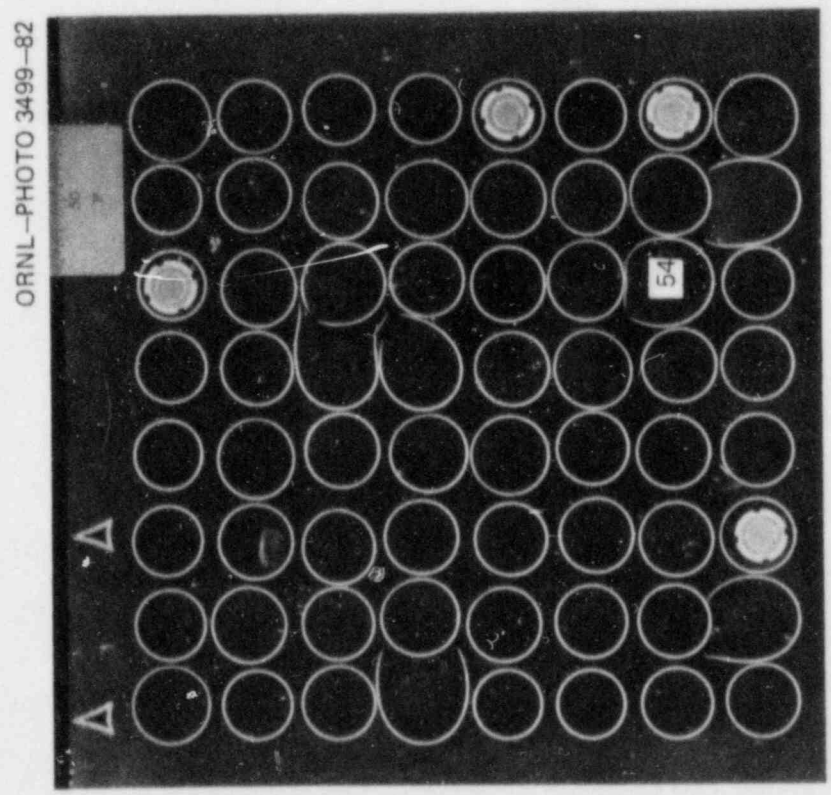

Fig. 39. Section through B-6 bundle at 31.0-cm elevation.

ORNL–PHOTO 3501–82

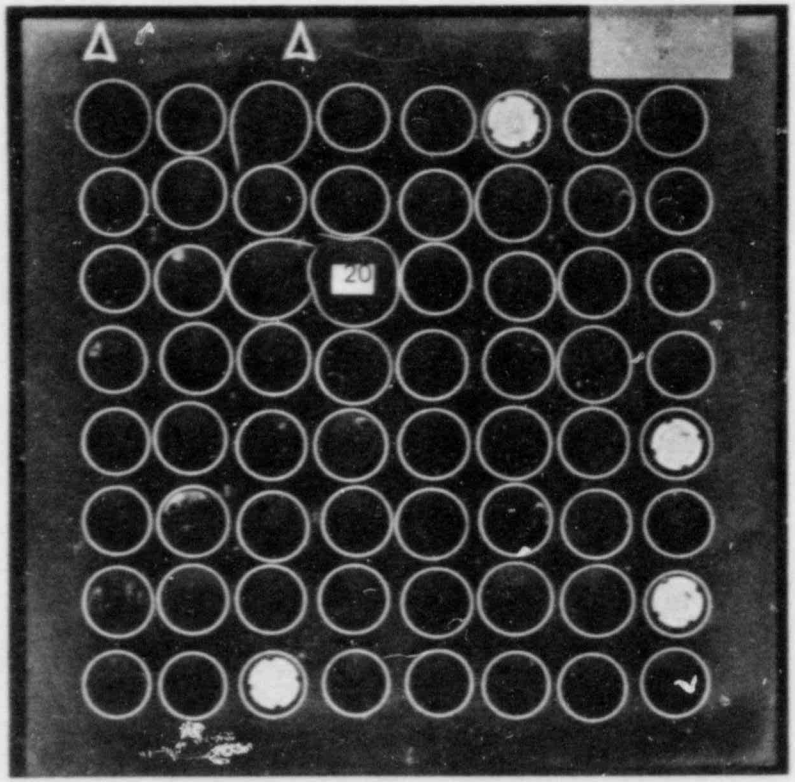

Fig. 41. Section through B-6 bundle at 35.2-cm elevation.

ORNL–PHOTO 3502–82

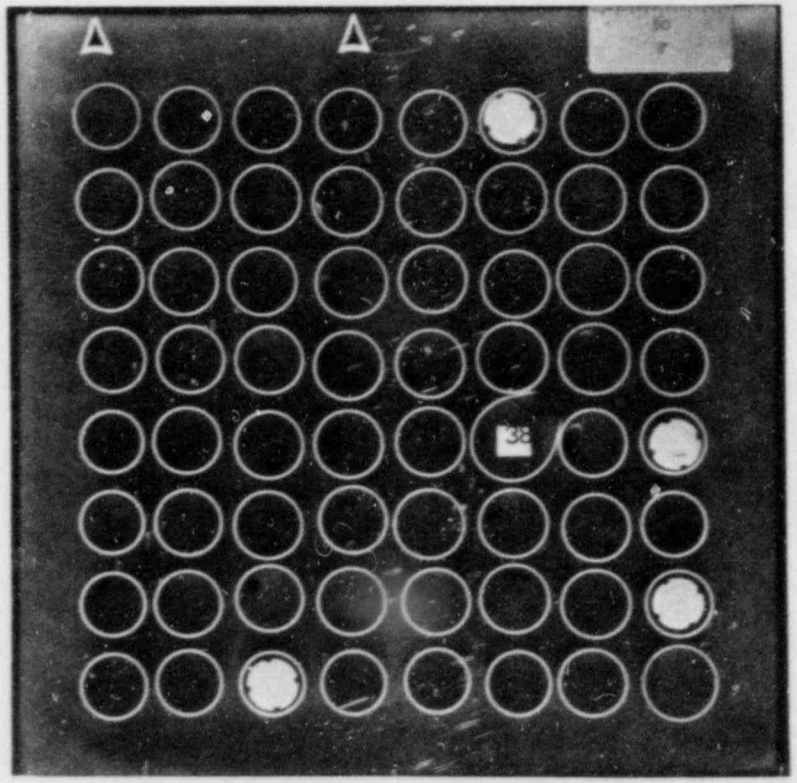

Fig. 42. Section through B-6 bundle at 45.3-cm elevation.

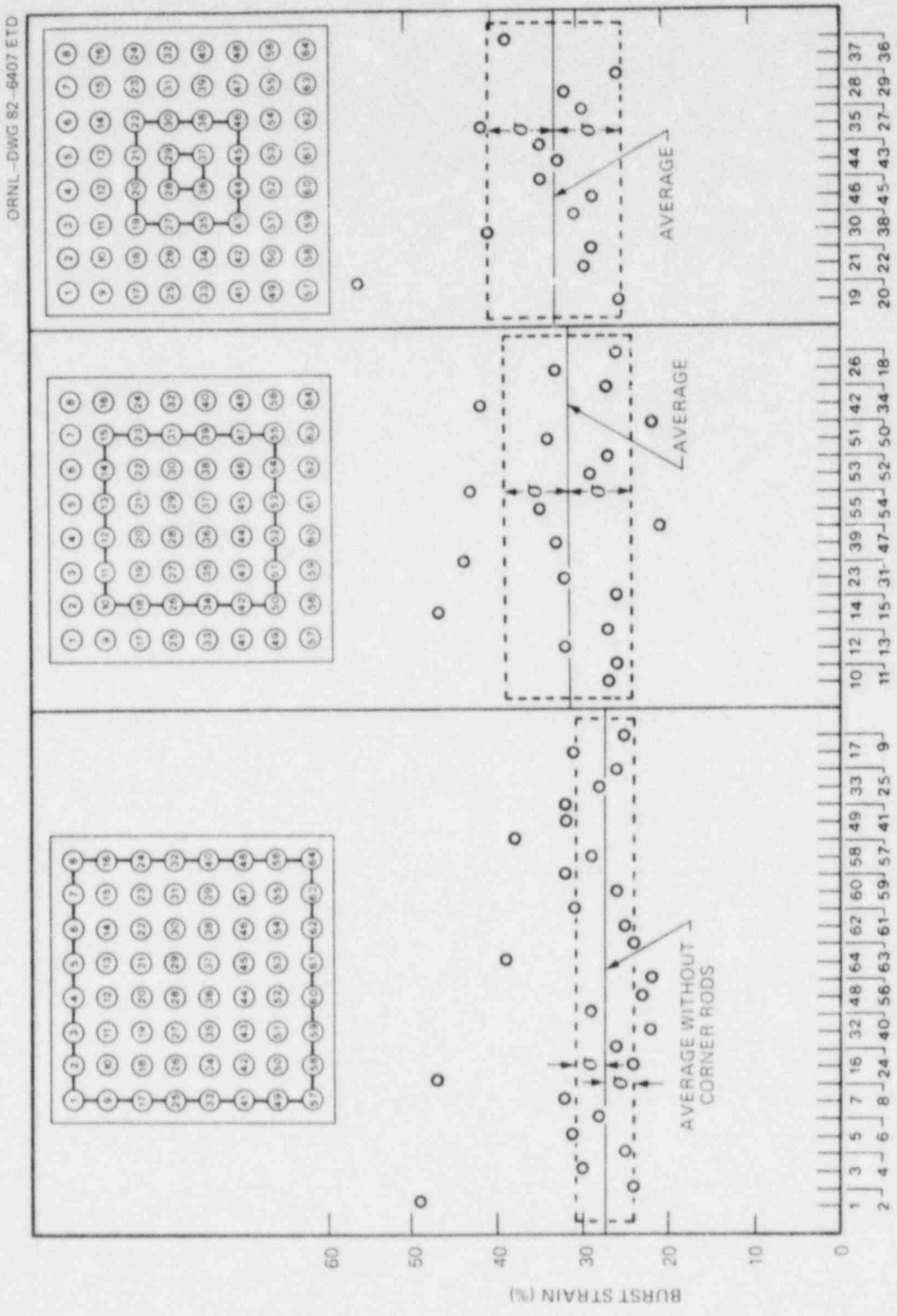

Fig. 43. Preliminary burst strain data for B-6 test.

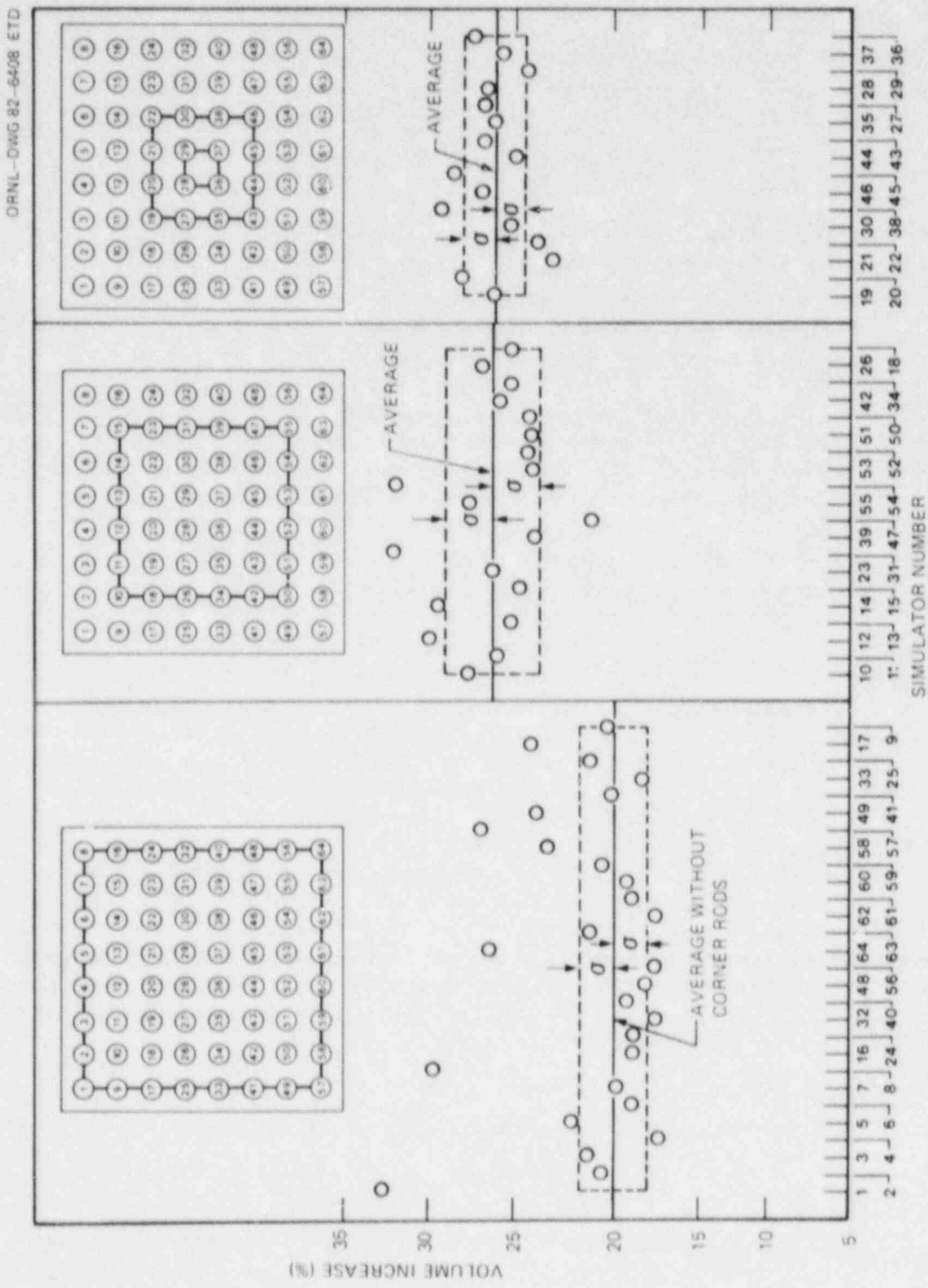

Fig. 44. Preliminary volumetric expansion data for B-6 test.

The coolant channel flow area restriction was also calculated, based on the rod-centered unit cell method, using the equation

$$B = 100 \times \frac{\sum_{n=N} (A_{d,n} - A_o)}{N (p^2 - A_o)} ,$$

where

B = percentage restriction in coolant channel flow area,
$A_{d,n}$ = outside area of deformed tube (mm²),
A_o = outside area of original tube (mm²),
p = tube-to-tube pitch in square array (mm),
N = number of tubes in square array.

With this definition, B is 0% for no deformation and 100% if all the tubes deform into a square with sides of length p (completely filling the open area). For the case of uniform ballooning such that the tubes just come into contact (i.e., 32% strain for the dimensions appropriate to this test), B is 61%.

The quick-look strain data were used to calculate the value of $A_{d,n}$ in this equation for each tube at each axial node, assuming the tubes had circular cross sections. For those axial nodes containing tube bursts, a fictitious value of $A_{d,n}$ was constructed by converting the perimeter of the burst tube into a closed circle of the same perimeter. This definition gives a reasonable lower limit for the flow area restriction and corresponds to the one used in NUREG-0630 (Ref. 21). The calculations were performed for the entire 8 x 8 array, for the inner 6 x 6 array, and for the central 4 x 4 array. Results of the calculations are shown graphically in Fig. 45. The cross-sectional area occupied by grids (~200 mm²) was not included in the calculation; including this area slightly increases the restriction at the grid locations centered about elevations 10.0 and 66.0 cm. As evident, deformation was skewed in the direction of the steam flow (although the flow was very low); this is consistent with the small axial temperature profile shown in Fig. 20. The maximum loss in flow area in the entire 8 x 8 array was ~39% at the 34.4-cm elevation, ~44% at the 20.3-cm elevation in the inner 6 x 6 array, and ~46% at the same elevation in the central 4 x 4 array.

2.4 Additional Analysis of B-5 Test Results

J. L. Crowley

Revised burst temperatures

Analysis of the B-5 cross sections and the strain profiles continued during this report period and provided additional insight to and understanding of the data. In particular, the analysis indicated that the

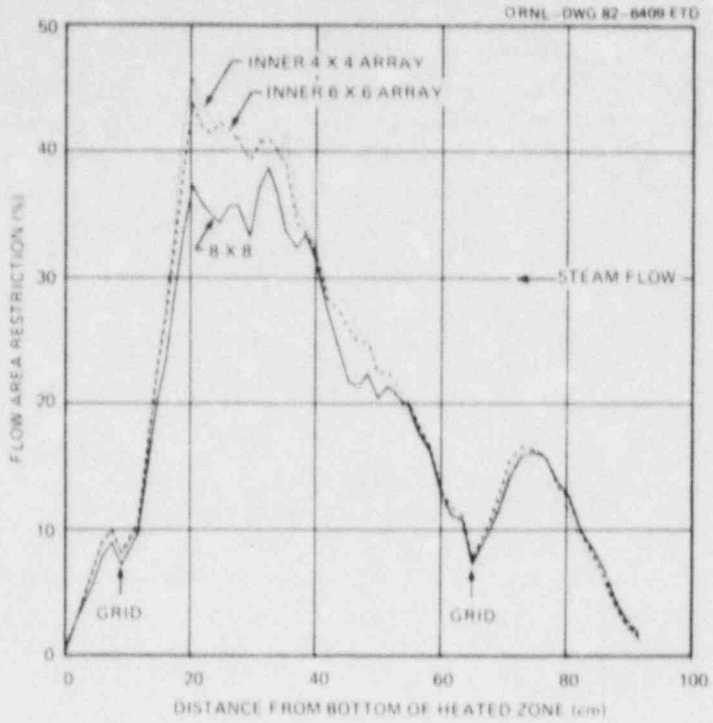

Fig. 45. Preliminary coolant flow area restriction data for B-6 test.

burst temperatures reported earlier[11] were sometimes inconsistent with deformation observations and that some should be revised.

In the earlier data tabulation,[11] "observed" and "corrected" burst temperatures were given. Consistent with our past practice, the observed burst temperature for a simulator was defined as the maximum temperature indicated by any of the thermocouples at the time of burst without regard to location of the thermocouple with respect to the burst. During the last few seconds of the transient, the traces of some thermocouples that had indicated the highest temperature (for a given simulator) throughout most of the transient showed what was assumed to be erratic behavior, (i.e., a reduction of temperature). In these cases, the traces were extrapolated to give a best estimate of the temperature that would have been measured by that thermocouple if the earlier trend had continued until the tube burst. Thus, the higher of maximum measured value or extrapolated value at the time of burst was reported as the "corrected" burst temperature. Justification for this approach assumed that (1) the true burst temperature was at least as high as the maximum value recorded on that simulator regardless of location and (2) the erratic behavior observed near the end of the transient was caused by malfunctioning of the thermocouples.

Analysis of the data indicates that both of these assumptions may be incorrect in a bundle test with extensive rod-to-rod interactions (such as B-5). This derives from observations that (1) interaction of the outside ring of simulators with the thin reflective shroud could be correlated with thermocouple response and (2) maximum temperatures, whether recorded or extrapolated, at the time of burst did not correspond in a consistent

manner with posttest strain measurements at the thermocouple locations. In particular, for 46 of the 63 (73%) pressurized tubes, larger-than-average deformation was noted at axial locations of those thermocouples that had indicated maximum temperatures at the onset of deformation (about 32 to 38 s after power-on). However, at the time of burst, the temperature at these axial locations was not necessarily the highest recorded in a given simulator. This indicates that the temperature distribution prior to the onset (and during the early phase) of deformation may be more important in determining the burst location than the distribution at the time of burst. Because failure stress is a function of both local temperature and instantaneous wall thickness (i.e., local strain), failure can occur at a site where the strain is high (due to its prior temperature history) but the temperature is lower (due to greater cooling and/or interaction with adjacent tubes) than at another site where the temperature is higher but the strain is lower.

For this reason, we reevaluated the temperature measurements and correlated the data with the deformation profiles and the burst locations. Based on this evaluation, the extrapolated temperatures are not, in general, representative of the temperature at the burst site at the time of failure. Instead, we believe the thermocouples measured the correct temperature, and we have revised about 60% of the "corrected" values accordingly. The new data are tabulated in Table 6. As in the previous tabulations,[11] the data include (1) the maximum recorded temperature and the thermocouple indicating this temperature, (2) the temperature "selected" as being the best estimate of the burst temperature and the thermocouple indicating this temperature, and (3) the thermocouple nearest the burst. In the absence of more definitive data and analysis, we believe the "selected" temperature is the best estimate of the burst temperature.

Table 6 also gives revised volumetric expansion data for each of the tubes. While the previous tabulation provided expansion data predicted by a model[11] derived specifically for MRBT application, the revised data were obtained (and reported[13] earlier in graphical format) by integration of the deformation profiles.

Removal of noise spikes from temperature data

As reported previously,[12] noise spikes were observed in about 30% of the thermocouple response signals in the B-5 test. The magnitude and polarity of the spikes depended on the particular signal multiplexer and the thermocouple reference furnace used for each signal, and the sequence and time of occurrence depended on the order of the sensors in the CCDAS scan list. The noise spikes were caused by interference from the electrically heated furnaces that were used for cold junction compensation. Figure 46 shows an example of the noise spikes in the temperature data.

Because erroneous temperatures would be used in computer analysis of the data if the temperature were sampled at the time of a spike, the spikes have been removed from the data from the time of power-on to the time of burst for each simulator exhibiting such behavior. However, if a spike was superposed on another event that caused a rapid change in the indicated temperature, the spike was not removed. A new engineering units data tape without the noise was generated for use in subsequent analyses. Figure 47 shows the data of the previous figure without the spikes.

Table 6. Updated summary of B-5 burst test results

Rod No.	Initial conditions		Burst conditions							
				Observed		Selected		Number of TE nearest to failure[c]	Tube heated length volume change (%)	Burst time (s)
	Pressure (kPa)	Temperature (°C)	Pressure (kPa)	Temperature[a] (°C)	TE No.	Temperature[b] (°C)	TE No.			
1	11,650	340	9,685	776	3	776	3	2	35	49.60
2	11,645	342	9,160	770	3	765	1	2	46	45.65
3	11,620	341	9,240	755	3	762	4	1	42	46.90
4	11,645	343	9,560	769	1	769	1	2	39	44.85
5	11,660	341	8,750	778	4	778	4	4	50	47.50
6	11,635	343	9,290	778	3	778	3	1	47	46.40
7	11,645	342	9,485	766	4	773	4	4	39	45.75
8	11,650	341	9,325	768	2	768	2	1	44	47.35
9	11,640	339	8,590	787	3	766	4	3	55	48.15
10	11,635	339	8,310	772	3	772	3	3	61	46.30
11	11,595	342	8,650	768	4	768	4	3	56	45.50
12	11,605	342	8,480	780	2	774	3	3	56	45.60
13	11,640	342	8,660	767	3	767	3	3	56	45.55
14	11,650	342	8,655	777	2	763	1	1	54	45.05
15	11,635	341	9,130	766	1	766	1	1	49	45.80
16	11,625	341	9,655	775	3	775	3	4	37	44.55
17	11,635	338	8,615	786	4	776	1	2	54	48.45
18	11,645	335	8,800	774	2	770	4	1	54	45.25
19	11,630	336	7,695	774	3	774	3	1	74	46.50
20	11,655	339	7,985	764	2	764	2	2	68	46.20
21	11,635	339	9,110	766	4	763	3	3	43	44.00
22	11,640	337	7,670	780	2	776	1	2	78	46.25
23	11,620	338	8,725	772	1	772	2	2	52	45.20
24	11,610	338	9,005	771	1	769	3	3	49	46.65
25	11,630	334	9,730	763	1	763	1	3	38	46.20
26	11,645	334	8,980	770	2	770	2	2	47	45.60
27	11,635	336	8,430	768	1	760	4	3	61	45.10
28	11,585	336	8,595	783	1	783	1	1	52	45.70
29	11,650	337	8,605	770	1	770	4	4	55	45.30
30	11,620	337	8,135	784	1	784	1	4	66	46.40
31	11,605	335	9,175	773	2	773	2	2	48	44.90
32	11,630	335	8,970	768	2	768	2	4	47	46.80
33	11,650	333	8,970	772	1	762	4	2	48	47.30
34	11,615	332	8,695	773	4	773	4	4	55	45.90
35	11,625	334	8,645	779	4	774	2	2	52	45.85
36	11,740	334	8,835	768	2	756	1	1	52	45.10
37	11,635	336	7,697	783	1	771	4	2	67	47.20
38	11,640	335	7,715	777	4	770	2	1	70	45.70

Table 6 (continued)

Rod No.	Initial conditions		Burst conditions							
				Observed		Selected				
	Pressure (kPa)	Temperature (°C)	Pressure (kPa)	Temperature[a] (°C)	TE No.	Temperature[b] (°C)	TE No.	Number of TE nearest to failure[c]	Tube heated length volume change (s)	Burst time (s)
39	11,635	333	8,205	773	4	773	4	4	60	46.70
40	11,615	334	8,975	782	1	773	4	2	48	46.45
41	11,685	333	9,360	769	4	769	4	2	45	46.50
42	11,650	331	8,405	773	1	773	1	1	53	46.25
43	11,630	332	9,385	775	2	775	2	2	41	44.90
44	11,645	334	8,355	763	3	763	3	3	59	46.10
45	11,630	333	7,800	769	1,3	769	1,3	3	70	46.75
46	11,625	333	8,035	762	2,4	763	4	4	60	46.25
47	11,625	332	8,975	777	1	774	2	1	49	45.50
48	11,630	332	8,775	763	3	763	3	4	50	47.80
49	11,620	331	9,720	761	4	761	4	2	35	46.90
50	11,585	328	8,900	768	2	768	2	4	47	45.70
51	11,555	328	8,135	771	1	759	3	3	60	47.05
52	11,585	330	8,630	765	4	757	3	3	53	45.20
53	11,575	330	8,935	769	2	760	4	4	46	46.30
54	11,595	331	8,770	771	1	766	4	2	51	45.90
55	11,585	330	8,785	763	2	763	2	2	49	46.35
56	11,575	331	8,985	781	1	781	1	2	48	47.05
57	11,580	331	9,530	752	3	753	2	2	40	47.90
58	11,590	331	9,125	757	1	757	1	3	45	46.45
59	11,560	331	9,470	770	4	770	4	4	40	46.30
60	11,565	332	8,800	755	2	755	2	2	48	47.20
61	11,560	332	9,285	768	1	768	1,3	1	39	46.20
62	[d]	331	[d]	[d]	[d]	[d]	[d]	[d]	[d]	[d]
63	11,585	331	8,685	775	1	775	1	1	57	47.75
64	11,580	333	9,350	743	1	756	4	4	38	48.65

[a] Maximum temperature indicated at time of rupture.

[b] Best-estimate value based on an evaluation of recorded temperature data and posttest deformation profiles.

[c] Excluding TEs located at grid elevations.

[d] Simulator unpressurized (but heated) and did not burst.

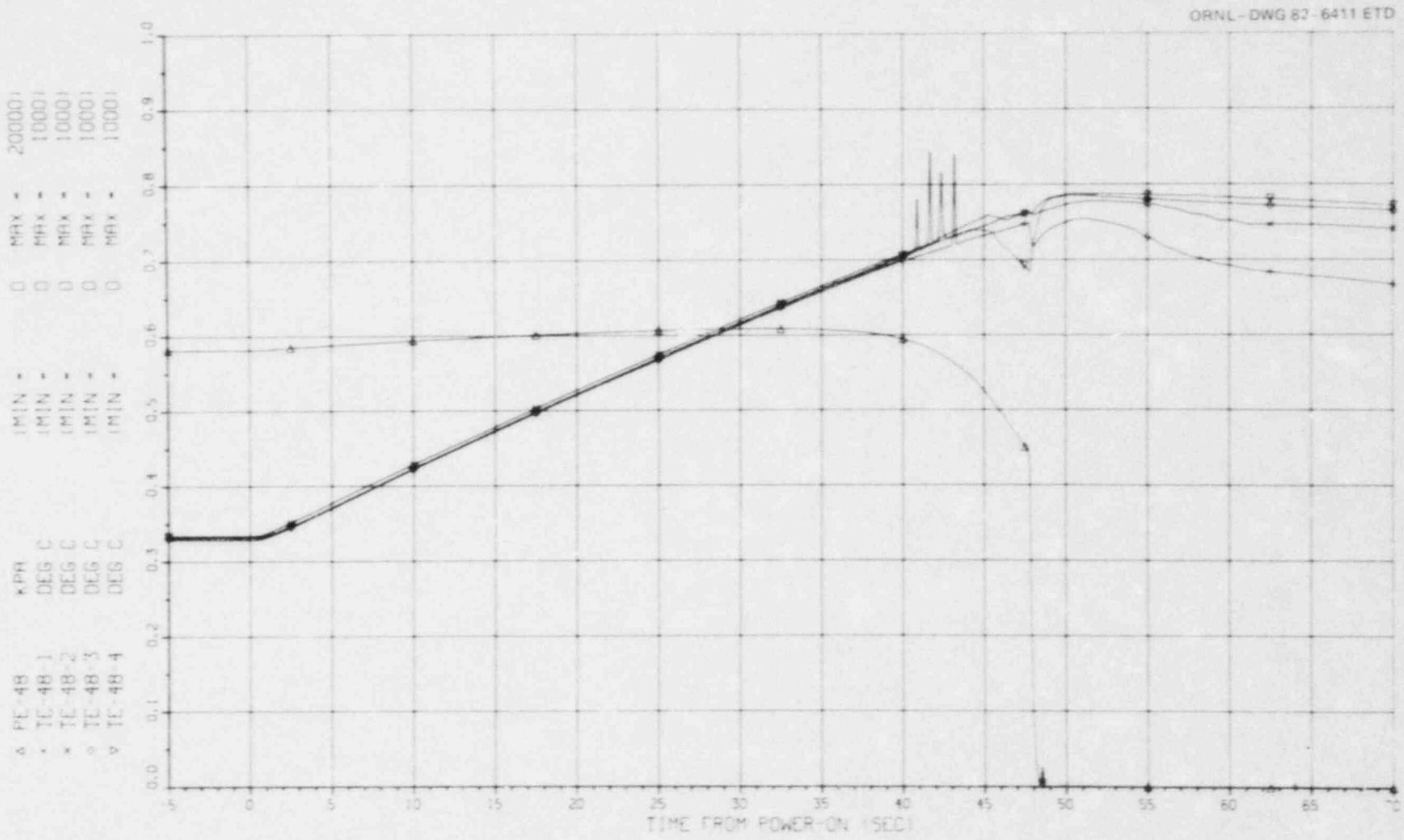

Fig. 46. Temperature (and pressure) data plot for B-5 simulator No. 48 showing noise spikes caused by thermocouple reference box.

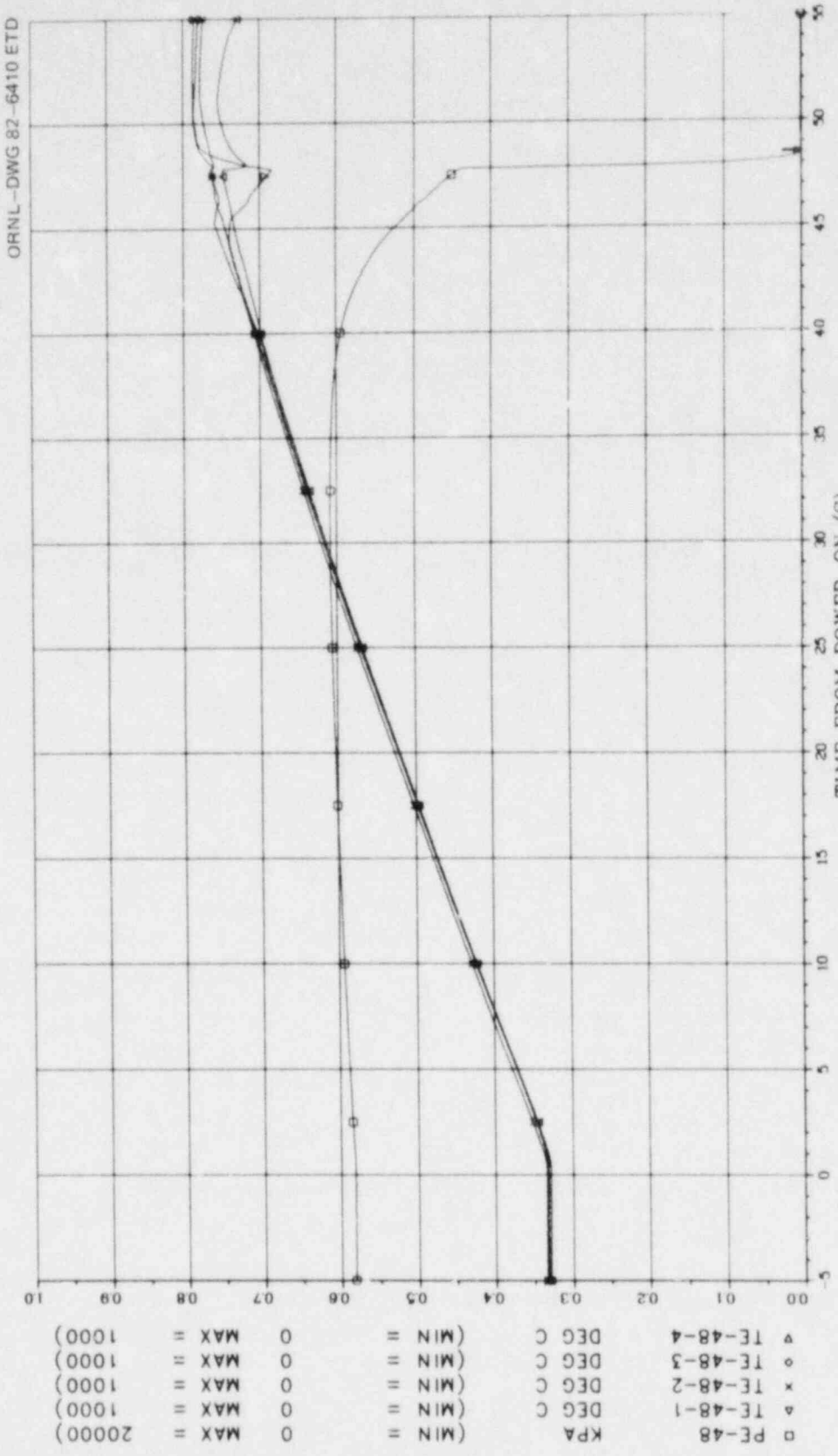

Fig. 47. Temperature (and pressure) data plot for B-5 simulator No. 48 after thermocouple noise spikes were removed.

3. OPERATIONS

3.1 B-6 Test

J. L. Crowley A. W. Longest
F. R. Gibson* W. A. Bird*

The B-6 bundle was transported from the assembly area to the test site on November 2, 1981, and was installed in the test vessel the same day. The remainder of the basic installation, consisting of electrical, instrumentation, and auxiliary connections, required about three additional weeks.

Simultaneous with the basic installation, certain portions of the data acquisition and electrical interlock systems were checked out. More extensive checkout than usual was required because equipment shared with the Thermal Hydraulic Test Facility (THTF) had been inactive for several months.

After all connections were made to the bundle, the remaining verifications and calibrations were made. Extensive check lists, previously prepared for each system and each calibration, were used to ensure that nothing of importance was overlooked. Calibration information was processed by the data system so that output in the form of printouts and graphs would contain data with calibration coefficients already applied. Two cathode-ray tube (CRT) readout devices were set up to display key test variables in real time for the benefit of the operator. One CRT displayed (in graphical form) the bundle average temperature, the applied bundle voltage, a pressure signal, and an artificial temperature ramp for comparison with the real test transient. The other CRT displayed (in bar graph form) all 64 simulator pressures and 32 of the thermocouples in the bundle. These were arranged in groups representing the three zones of the bundle consisting of the outer ring, the second ring, and the inner 4 x 4 array of fuel pin simulators. This real-time display was a definite aid to the operating personnel. With arrangement of pressure signals according to zones, it was apparent early that burst times were also grouped by zones. This information is presented in Sect. 2.2.

All check lists except those to be performed on the day of the test were completed by December 2, 1981. Heatup of the test vessel and steam lines at a low rate was initiated that afternoon so that its temperature would remain at about 200°C overnight. Early on December 3, power to the vessel and steamline heaters was increased (power was not applied to the fuel pin simulators during the heatup), and superheated steam was admitted to the vessel in an approach to the initial test temperature of about 330°C. Throughout this phase of the preparation, the data system was used to monitor leak rates and temperatures of individual fuel pin simulators. Satisfactory performance of the simulator gaskets was indicated by leak rates of <1 kPa/min loss up to the time of the test transient.

---

*Instrumentation and Controls Division.

By about 1100 h on December 3, the bundle temperatures were sufficiently close to equilibrium for a short powered run (with the fuel pin simulators at a low pressure) to ascertain that the data acquisition system and all the instrumentation were functioning properly and that the applied voltage was proper for the desired temperature ramp. Examination and evaluation of data from this short (~13 s) transient indicated that minor adjustments were needed; the temperature increased ~58°C during this pretest transient. The temperature ramp rate was slightly lower than desired, and it was decided to increase the no-load voltage setting for the burst transient from 57 to 59 V, resulting in an average rod power of about 1590 W/m.

Following reequilibration of the temperatures at the desired initial values, all 64 fuel pin simulators were pressurized simultaneously to ~3050 kPa. The test was initiated by applying power (at a rate of about 93 kW) to the bundle. Termination of the powered portion of the test could be initiated by any of four actions: (1) CCDAS action resulting from a signal that 60 of the 64 simulators had burst, (2) CCDAS action resulting from a signal that 115 simulator thermocouples had exceeded the upper temperature limit (50°C above the anticipated burst temperature) on each of three successive data scans, (3) a timer that limited the transient to ~145 s, and (4) operator override. It was decided to program criterion (1) to terminate power to the bundle after 60 bursts (with the expectation that all 64 tubes would burst) to minimize the temperature overshoot at the end of the test. Also, criterion (2), that is, the high-temperature limit, was established close to the expected burst temperature for the same reason. The test was terminated by criterion (3), and all 64 tubes burst.

Cooling steam, saturated at about 200 kPa, was then supplied to the bundle to minimize the length of time at elevated temperature. The remaining systems were shut down, and processing of the data began immediately. The bundle was removed the following day for posttest examination.

3.2 Storage of Equipment

The burst test conducted on B-6 on December 3 was the final test operation of the MRBT program. A number of very specialized pieces of equipment, required for the assembly, testing, and examination of both single-rod and multirod arrays, have been placed in storage or in standby.

The single-rod test facility remains essentially intact with its separate power supplies for shroud and rod. The temperature controllers, which were designed and built especially for the task of controlling these two power supplies, have been placed in storage.

The assembly equipment, which includes the internal thermocouple attachment device and the posttest strain measurement device, has been stored. Usable bundle parts and seals for fuel pin simulators and about 140 fuel simulators (mostly used) were also placed in storage.

The multirod burst test facility with its test vessel and superheated steam system is essentially intact. Other equipment, such as the PDP/11 data acquisition system, is shut down, and the area is secured. This area and equipment are shared with two other facilities, the Thermal Hydraulic

Test Facility (THTF) and the Instrument Development Loop (IDL), which are also in standby condition.

REFERENCES

1. R. H. Chapman, *Multirod Burst Test Program Prog. Rep. July–December 1977*, NUREG/CR-0103 (ORNL/NUREG/TM-200).

2. R. H. Chapman, *Multirod Burst Test Program Prog. Rep. January–March 1978*, NUREG/CR-0225 (ORNL/NUREG/TM-217).

3. R. H. Chapman, *Multirod Burst Test Program Prog. Rep. July–December 1978*, NUREG/CR-0655 (ORNL/NUREG/TM-297).

4. A. W. Longest, *Multirod Burst Test Program Prog. Rep. January–March 1979*, NUREG/CR-0817 (ORNL/NUREG/TM-323).

5. R. H. Chapman, *Multirod Burst Test Program Prog. Rep. April–June 1979*, NUREG/CR-1023 (ORNL/NUREG/TM-351).

6. R. H. Chapman, *Multirod Burst Test Program Prog. Rep. July–December 1979*, NUREG/CR-1450 (ORNL/NUREG/TM-392).

7. R. H. Chapman et al., *Bundle B-1 Test Data*, ORNL/NUREG/TM-322 (June 1979).

8. R. H. Chapman et al., *Bundle B-2 Test Data*, ORNL/NUREG/TM-337 (August 1979).

9. R. H. Chapman et al., *Bundle B-3 Test Data*, ORNL/NUREG/TM-360 (January 1980).

10. J. F. Mincey, *Steady-State Axial Pressure Losses Along the Exterior of Deformed Fuel Cladding: Multirod Burst Test (MRBT) Bundles B-1 and B-2*, NUREG/CR-1011 (ORNL/NUREG/TM-350) (January 1980).

11. A. W. Longest, *Multirod Burst Test Program Prog. Rep. January–June 1981*, NUREG/CR-2366, Vol. 1 (ORNL/TM-8058).

12. R. H. Chapman, *Multirod Burst Test Program Prog. Rep. January–June 1980*, NUREG/CR-1883 (ORNL/NUREG/TM-426).

13. J. L. Crowley, *Multirod Burst Test Program Prog. Rep. July–December 1981*, NUREG/CR-2366, Vol. 2 (ORNL/TM-8190).

14. R. T. Bailey, *Steady-State Pressure Losses for Multirod Burst Test (MRBT) Bundle B-5*, NUREG/CR-2597 (ORNL/Sub/80-40441/1) (April 1982).

15. R. H. Chapman et al., *Quick-look Report on MRBT B-6 (8 x 8) Bundle Test*, ORNL Internal Report ORNL/MRBT-7 (January 18, 1982).

16. R. L. Anderson et al., *Thermometry in the Multirod Burst Test Program*, NUREG/CR-2470 (ORNL/TM-8024) (March 1982).

17. A. W. Longest et al., *Variations in Zircaloy-4 Cladding Deformation in Replicate LOCA Simulation Tests*, NUREG/CR-2810 (ORNL/TM-8413) (September 1982).

18. A. W. Longest et al., *Boundary Effects on Zircaloy-4 Cladding Deformation in LOCA Simulation Tests*, presented at the American Nuclear Society Meeting in Los Angeles, June 6–11, 1982.

19. R. H. Chapman et al., *Effect of Bundle Size on Cladding Deformation in LOCA Simulation Tests*, presented at the Sixth International Conference on Zirconium in the Nuclear Industry, Vancouver (BC), Canada, June 28–July 1, 1982.

20. R. H. Chapman, *Multirod Burst Test Program Prog. Rep. April–June 1979*, NUREG/CR-1023 (ORNL/NUREG/TM-351).

21. D. A. Powers and R. O. Meyer, *Cladding Swelling and Rupture Models for LOCA Analysis*, NUREG-0630 (April 1980).

22. R. H. Chapman, *Multirod Burst Test Program Prog. Rep. July–December 1980*, NUREG/CR-1919 (ORNL/NUREG/TM-436).

23. C. A. Mann et al., *The Deformation of PWR Fuel in a LOCA*, UKAEA Report No. ND-4-701(S) (April 1982).

NUREG/CR-2911
ORNL/TM-8485
Dist. Category R3

Internal Distribution

1-5. R. H. Chapman
6. W. G. Craddick
7. J. L. Crowley
8-9. D. S. Griffith
10. T. S. Kress
11. A. W. Longest
12. R. A. Lorenz
13. A. L. Lotts
14. G. N. Miller
15. H. E. Trammell
16. ORNL Patent Office
17. Nuclear Safety Information Center
18. Central Research Library
19. Document Reference Section
20-21. Laboratory Records Department
22. Laboratory Records (RC)

External Distribution

23. Office of Assistant Manager for Energy Research and Development, DOE, ORO, Oak Ridge, TN 37830
24. R. Van Houten, Division of Accident Evaluation, Office of Nuclear Regulatory Research, NRC, Washington, DC 20555
25. T. M. Howe, EG&G Idaho, Inc., INEL, Idaho Falls, ID 83401
26. D. L. Hagrman, EG&G Idaho, Inc., INEL, Idaho Falls, ID 83401
27. R. R. Hobbins, EG&G Idaho, Inc., INEL, Idaho Falls, ID 83401
28. E. T. Laats, EG&G Idaho, Inc., INEL, Idaho Falls, ID 83401
29. C. L. Mohr, Battelle Northwest Laboratory, P.O. Box 999, Richland, WA 99352
30. H. Rininsland, PNS-Leitung, Kernforschungszentrum Karlsruhe, Postfach 3640, 75 Karlsruhe, FRG
31-32. Technical Information Center, DOE, Oak Ridge, TN 37830
33-347. Distribution as shown for NRC category R3 (NTIS-10)

☆U.S. GOVERNMENT PRINTING OFFICE: 1982-646-055/205